Point of Care Detection of Iron Metabolism Parameters Through Colorimetric Sensing

by

Michael Serhan

A Dissertation Presented in Partial Fulfillment
of the Requirements for the Degree
Doctor of Philosophy

Approved May 2020 by the
Graduate Supervisory Committee:

Erica Fozrani, Chair
Barbara Smith
Gregory Raupp
Tony Hu
Abhinav Acharya

ARIZONA STATE UNIVERSITY

August 2020

ABSTRACT

Abnormally low or high blood iron levels are common health conditions worldwide and can seriously affect an individual's overall well-being. A low-cost point-of-care technology that measures blood iron markers with a goal of both preventing and treating iron-related disorders represents a significant advancement in medical care delivery systems. Methods: A novel assay equipped with an accurate, storable, and robust dry sensor strip, as well as a smartphone mount and (iPhone) app is used to measure total iron in human serum. The sensor strip has a vertical flow design and is based on an optimized chemical reaction. The reaction strips iron ions from blood-transport proteins, reduces Fe(III) to Fe(II), and chelates Fe(II) with ferene, with the change indicated by a blue color on the strip. The smartphone mount is robust and controls the light source of the color reading App, which is calibrated to obtain output iron concentration results. The real serum samples are then used to assess iron concentrations from the new assay and validated through intra-laboratory and inter-laboratory experiments. The intra-laboratory validation uses an optimized iron detection assay with multi-well plate spectrophotometry. The inter-laboratory validation method is performed in a commercial testing facility (LabCorp). Results: The novel assay with the dry sensor strip and smartphone mount, and App is seen to be sensitive to iron detection with a dynamic range of 50 - 300 µg/dL, sensitivity of 0.00049 µg/dL, coefficient of variation (CV) of 10.5%, and an estimated detection limit of ~15 µg/dL These analytical specifications are useful for predicting iron deficiency and overloads. The optimized reference method has a sensitivity of 0.00093 µg/dL and CV of 2.2%. The correlation of serum iron concentrations (N=20) between the optimized reference method and the novel assay renders a slope of 0.95, and a regression coefficient

of 0.98, suggesting that the new assay is accurate. Lastly, a spectrophotometric study of the iron detection reaction kinetics is seen to reveal the reaction order for iron and chelating agent. Conclusion: The new assay is able to provide accurate results in intra- and inter-laboratory validations and has promising features of both mobility and low-cost.

DEDICATION

In loving memory of NJ Tao; a great scientist, rigorous mentor and exceptional person. Your legacy will stay with us forever.

In loving memory of Sayed Serhan and Hanna El-Sallack; My deceased grandparents whom I did not get the chance to say goodbye too.

Finally, I dedicate this work to my loving family and friends in Arizona and Lebanon. They have always provided me with unconditional love and support that was a critical for my success here at ASU.

ACKNOWLEDGMENTS

I am very thankful for the support of PLuS Alliance at Arizona State University (https://www.plusalliance.org/) and Ira Fulton School of Engineering at Arizona State University for a Dean's Fellowship, and my committee members for their guidance and expertise.

TABLE OF CONTENTS

Page

CHAPTER Page

CHAPTER Page

CHAPTER Page

LIST OF TABLES

Table Page

LIST OF FIGURES

Figure Page

Figure Page

Figure Page

Figure Page

Figure Page

Figure Page

Figure Page

CHAPTER 1

INTRODUCTION

Iron is essential in maintaining health in humans due to reliance on oxygen binding (heme), electron transport (energy production), and as a catalyst of hundreds of enzymes (redox and immune control)[1, 2]. Iron metabolism is guided by a complex set of genetically regulated processes for storage, transportation, and dietary uptake during feeding, thereby providing sufficient iron to all cells regardless of fluctuating dietary quantities, blood losses, or gains via transfusions[2, 3]. However, both iron deficiency and iron overload can result from a variety of dysfunctions, potentially leading to permanent damage of organ systems such as the liver and brain[4, 5] . Iron *deficiency* is a frequent concern for those with blood loss, including healthy menstruating females, and in all populations with limited access to proper nutrition via whole food diets or even with highly processed/refined foods with appropriate fortification[6-8]. On the other hand, iron *overload* is a threat, primarily to those (genetically) inheriting the so-called hemochromatosis genes from both parents, the recessive “High Iron” (HFE) C282Y allele with incidence of 1 in ~300 people of northern European decent[9]. This disease is difficult to screen due to vague symptoms (e.g., fatigue), but its progress leads to parenchymal damage in various organs and liver disease, pancreatic impairment (diabetes), heart arrhythmias or failure, and neurodegenerative disorders of the brain. In fact, over several years, the amount of stored iron in blood can reach 10+ grams (from a normal of 3-4 grams), saturating the iron transporters, and over-filling or "spilling-over" storage into an increasingly toxic labile intracellular pool[10, 11]. Thus, iron

distribution must be tightly regulated by medication or iron-removal strategies to avoid irreversible damage to the organs.

A well-cared for patient's annual physical exam should include determination of iron metabolism biomarkers, but unfortunately, due to cost, only two proxies for iron metabolism, hemoglobin and red blood cells, are commonly assessed, both poor markers for iron overload thereby leaving hemochromatosis as a disorder typically detected late in life when irreversible damage on organs is detected. Furthermore, prevention and interventions (e.g., supplementation) to address iron imbalances are costly, thereby leaving individuals at risk of prolonged state of deficiency or overload[9, 12, 13].

Total iron, i.e., total bound iron binding capacity (TIBC) or unbound (UIBC), and ferritin (iron storage protein) are clinically validated blood-derived biomarkers of iron deficiency or overload[14, 15]. The goal is to create a tool for globally screening of iron deficiencies or overloads. Measurement of all the clinically valid biomarkers is time-consuming, expensive, and painful requiring venous blood draw, temperature-controlled storage and shipping, and use of laboratory-based expertise and instruments such as spectrophotometry[16, 17].

Due to the above-mentioned limitations, a low-cost novel assay for detection of iron, TIBC, UIBC and percent iron saturation based on storable, dry, and disposable sensor strips and a smartphone mount and application to reduce the need of laboratory space and special instrumentation and to conduct all analyses at room temperature at a low manufacturing and end-user cost. A smartphone was chosen as a detection platform since the ever-increasing number of smartphone owners (3

billion+ as of 2020) opens the possibility to deliver low-cost detectors everywhere with proven capabilities of complex imaging algorithms for clinical applications[18-23].

Chapter 2 present the background and motivation of the work by introducing the physiology of iron metabolism as a set of complex protein-protein interactions that function to maintain daily iron homeostasis as well as introduces the main iron disorders (iron deficiency and overload) that result from dysregulation in iron metabolism that shift homeostasis and can result in depletion or build-up of iron stores. With the motivation of providing a cheap and user-friendly screening device for iron management, the main clinical biomarkers used for standard care as well as the rationale behind which biomarkers were included in the device are also described. Finally, methods for determining total iron and iron binding capacity are examined.

Chapter 3 discusses the methods that were used to design, test and validate the screening device and starts by examining the reference spectrophotometry method which was optimized resulting in an in-house optimized reference method that was used to conduct all future testing. Next, the design and testing methods for the novel design were explored and statistical agreement tools were used to compare the reference method to the developed sensors. This was followed by assessing the dispersion and performance of the mobile technology by comparing the app to a reference imaging software, ImageJ and measuring noise levels within the system to evaluate the performance of the sensing platform. Next, a novel optoelectronic reader was introduced as an alternative design for iron detection. Finally, methods for determining TIBC and percent iron saturation are examined with both the reference method as well as with the novel device.

Chapter 4 investigates the results of the methods described in chapter 3 by analyzing the reference spectrophotometric method from which an optimized method was validated as a reference method for all future testing by examining interference analysis, coefficients of variation, protein precipitation and kinetics. Next, results with the novel assay were analyzed and correlation plots and percent Bland-Altman plots were determined to compare serum measurements from both the liquid phase reference spectrophotometry method and the developed device. Next, the performance of the novel technology was evaluated by measuring inter and intra dispersion of the system as well as validating the smartphone app with a reference imaging software, ImageJ. An optoelectronic system was then introduced as an alternative detection platform with the hope of overcoming limitations obtained with the smartphone technology. Finally, total iron binding capacity and percent iron saturation were determined using both the novel device and the reference TIBC method with spectrophotometry and correlation plots and percent Bland Altman Plots were used to analyze the level of agreement between the two methods.

Chapter 5 summarizes the main findings of the described work and explores future work and limitations that need to be overcome to commercialize the device which include conducting a pilot study in vulnerable populations as well as modify the app to connect to a secured database where real time data acquisition enables a better assessment of a person's iron status and more detailed statistical analysis allows the development of new correlations that depend not only on iron levels but also on socio-economic factors.

CHAPTER 2

BACKGROUND AND MOTIVATION

Iron-binding species are essential components of human tissue as transporters of iron between cells, storage facilitators for short-term response to bacterial infection and medium-to-long-term considerations, such as red blood cell development or to store, even in the case of over-loading. Since “ironomics” continues to elucidate the identification, distribution, dynamics, role and impact of iron in biological systems, combined with proteomics (doing the same for iron-handling species), comprehension of iron metabolism has become strong enough to establish clear diagnoses and interventions for managing daily iron homeostasis for those at increased risk of morbidity and mortality from iron deficiency or overload[24]. Though this thesis focuses on **screening** and does not address diagnosis nor intervention per se, it is wise to understand at least a summary of the auto-regulation of iron processing; thus **section 2.1** (background) introduces the fundamental pathological pathways that govern iron metabolism and help maintain daily homeostasis as well as the main iron disorders that result from dysregulation in iron metabolism such as iron deficiency and iron overload. The known and accessible blood biomarkers of iron metabolism are also described as well as the methods used to detect these biomarkers.

In **section 2.2** (motivation), the need for a point of care screening device which entails the scope of this thesis is introduced. This chapter concludes by claiming that iron and total blood iron-binding capacity are both necessary and sufficient for screening for iron deficiency and iron overload. Further, a detailed development of a mobile and inexpensive screening tool of these two biomarkers is proposed to enable

millions of at-risk persons to both prevent disease as well as to monitor efficacy of interventions.

2.1 Background

2.1.1 Iron Overload Leading to Hemochromatosis

Hemochromatosis is a disorder that is caused by progressive iron deposition in tissues leading to liver damage, diabetes and bronze discoloration of skin. The primary cause of iron overload is genetic. It is associated with mutations in the HFE genes which encode a protein that is located on the surface of intestinal and liver cells and plays a pivotal role in iron regulation[25]. Mutations in these genes lead to an over-absorption of iron from diet which accumulates in body tissues and causes organ failure[26]. The most common mutations of this gene exist in two forms: replacement of the amino acid cysteine with tyrosine and is known as the C282Y mutation and the replacement of the amino acid histidine with aspartic acid and is known as the H63D mutation. These mutations cause an alteration in the three dimensional shape of the HFE protein and also, prevent the interaction of this protein with transferrin receptor 1 which results in a dysregulation of iron metabolism and an over-absorption of dietary iron[27]. This type of hemochromatosis is classified as type 1 hemochromatosis and is the most prevalent form of this disease [25, 28].

Hemochromatosis is mostly prevalent in Europe and North America with percent frequency of C282Y homozygosity and heterozygosity of 0.4% and 9.2% respectively for Northern European Populations (N= 6,203) and 0.5% and 9% in Northern American Populations (N=3,752) [25]. These numbers diminish significantly in Asian, Indian

subcontinent and African/ Middle eastern populations where the frequency of homozygosity was almost nil, and the frequency of heterozygosity was less than 0.5%[25].

Conventional tests include measuring serum transferrin saturation which represents the amount iron bound to transferrin and serum ferritin which reflects the amount of iron stored in the liver. Serum transferrin saturation greater than 45% and ferritin levels greater than 300 ng/ ml are considered abnormal and indicative of iron overload. Additional tests include liver function tests, MRI to measure the degree of iron overload, genetic testing to look for mutations in the HFE gene and liver biopsy to test for liver damage.

There are a few limitations with the current testing methods. To start with, the genetic test confirms whether the individual expresses the HFE mutation but does indicate whether abnormal iron behavior is expressed. In other words, are all individuals with the genetic mutation expressing complications of iron overload? A recent study showed that 75% of a homozygous population in Northern Europe expressed the biochemical symptoms represented by elevated serum ferritin and transferrin saturation. Of that population, 50% experienced increased liver iron which manifested into hepatic fibrosis and other iron overload diseases in 25% of that cohort[29]. This confirms that not all individuals with the genetic mutation express the biochemical indicators and even in sub-groups that present abnormal iron levels, clinical complications of hemochromatosis may not be expressed.

Another limitation is that elevated serum ferritin does not necessarily indicate iron overload since serum ferritin is also influenced by obesity, fatty liver and diabetes which result in inflammation of hepatic cells. Even though these populations display high serum ferritin, the cause is not due to iron overload; thus, phlebotomy in this case can lead to anemia before any drop-in serum ferritin is observed[30]. In addition, studies showed that

there are populations who express high ferritin levels and the cause is unrelated to iron overload[27].

Above all, the major drawback is that in individuals who express the biochemical abnormalities from an early age, clinical symptoms may not show up till mid 40's and 50's and is generally identified by liver problems and potentially liver cirrhosis[31], and even if clinical symptoms do show up early, they are usually vague for an accurate screening from a physician; consequently, the majority of people who are affected by this disease are asymptomatic up till iron levels have excessively built up in different tissues of the body and complications of liver failure are identified by the physician. Herein, a point of care screening device that measures iron biomarkers can enable early screening and prevention of complication of iron-related diseases.

The main treatment of hemochromatosis is through phlebotomy. This method is very effective since the regeneration of erythrocytes requires iron leading to a progressive depletion of iron stores. Even though patients who are undergoing phlebotomy may absorb up to 5 mg of iron daily (alarmingly high) as a response to blood loss, a negative iron balance can easily be maintained with repeated blood draws (note that every 450 ml of blood which is equivalent to one unit may remove up to 200 mg of iron). Iron chelation therapy is another treatment for patients with secondary hemochromatosis since phlebotomy may cause severe health complications[25, 28, 31]

2.1.2 Iron Deficiency Leading to Anemia

Anemia is caused by decreased levels of hemoglobin in red blood cells impeding oxygen transport to body tissues. The primary cause of anemia is iron deficiency where insufficient iron in blood streams results in ineffective erythropoiesis[32]. In developed countries, iron deficiency can be easily managed but is generally overlooked by physicians. However, in underdeveloped countries, this problem radically affects the population and appropriate management is not easily attainable[33]. To understand the severity of this problem, the percent of iron deficiency prevalence is usually extrapolated from the prevalence of anemia, which is a major health concern since it affects around 1.6 billion people according to the world health organization and is a serious health concern in children and women[34]. Since iron deficiency is considered the number one nutritional disorder in the world and contributes to 30%-50% of anemia, at least several hundred millions are affected by iron deficiency globally. **Figures 1 and 2** summarize percent prevalence of anemia and the total number of populations affected by this disease in different subgroups: preschool-age children, school age children, pregnant women, non-pregnant women, men and elderly. **Figure 3** displays the percent prevalence of anemia in different geographical areas: Africa, Americas, South-East Asia, Europe, Eastern Mediterranean and Western Pacific. **Figures 1-3** reflect data collected by the World Health Organization from 1993 and 2005 [13, 34].

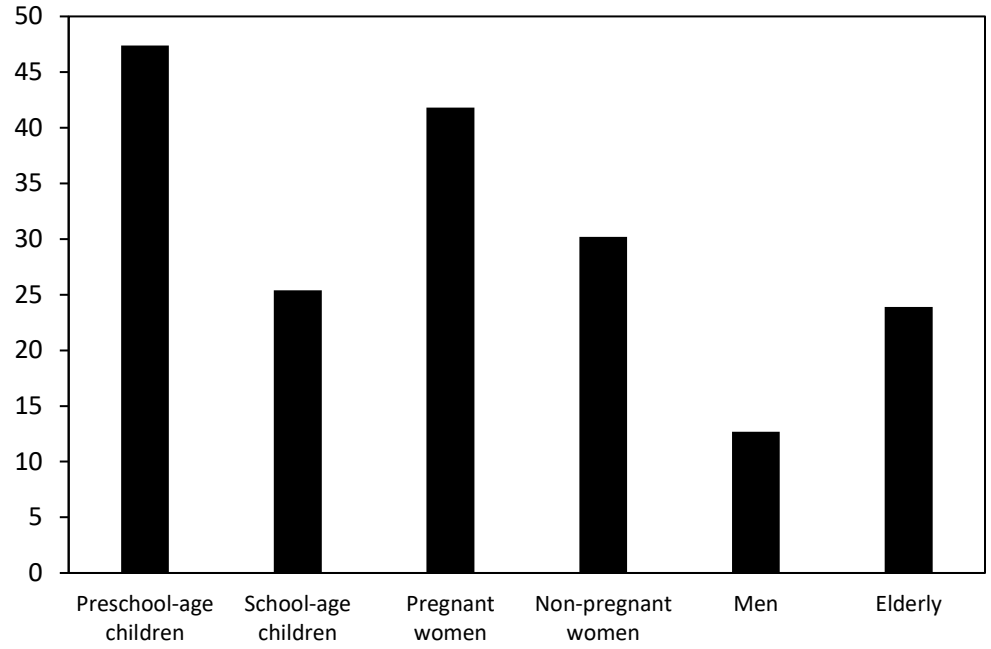

Figure 1: Percent Prevalence of anemia in different populations[34].

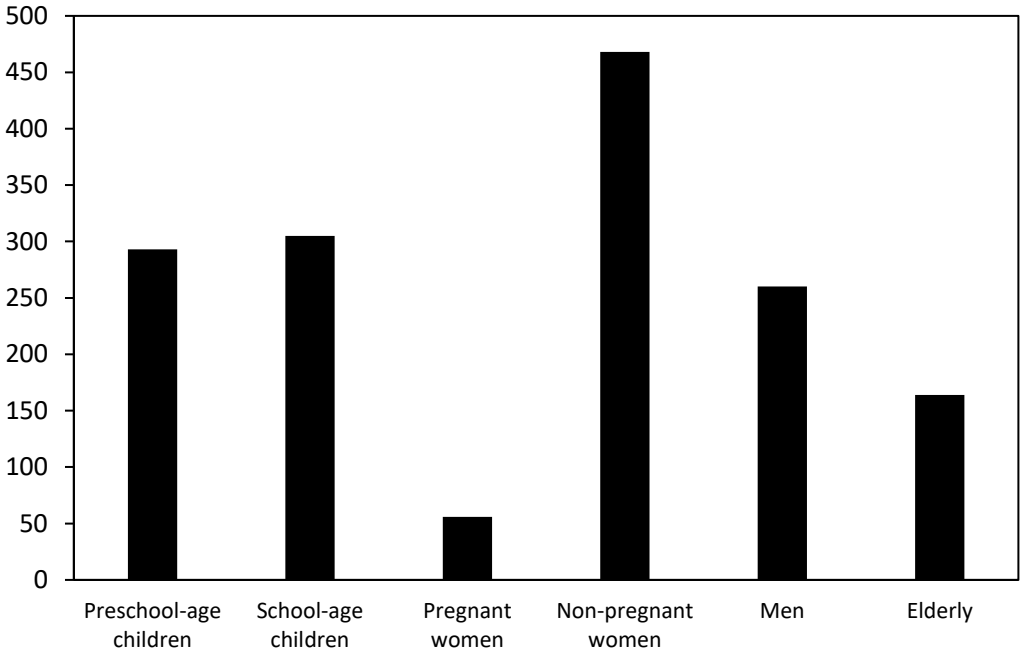

Figure 2: Number of individuals affected by anemia in different populations [34].

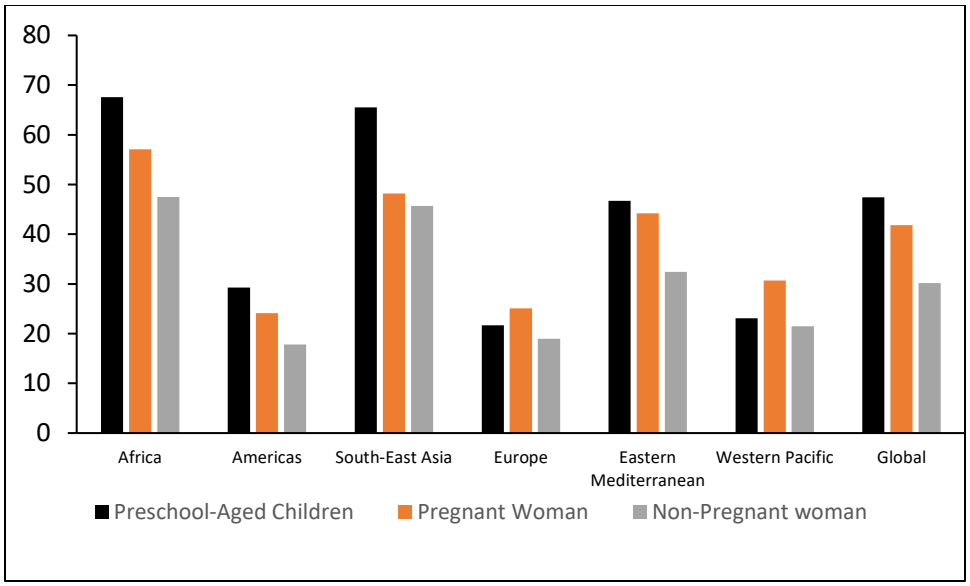

Figure 3: Percent prevalence of anemia in different geographical areas and in different population sub-groups[34].

Figures 1 to 3 reveal that iron deficiency anemia (IDA) is widely prevalent globally. It is most common in pregnant and menstruating women as well as in children. More importantly, these figures show that iron deficiency is primarily dependent on socio-economic factors since this disease affects more than 50% of women and children in Africa and South-East Asia while diminishes significantly in areas such as Americas, Europe and western pacific where standard of living is adequate.

Blood loss is a primary cause of iron deficiency. On average, the body absorbs 2 mg of iron daily to maintain iron homeostasis. However, with hemorrhage, the amount of red blood cells are diminished as well as the supplied amount of iron [35]. Therefore, there is an extra requirement to produce more red blood cells with a decreased amount of circulating iron resulting in an alarming iron negative balance. Therefore, menstruating and pregnant women are at high risk of developing anemia with iron losses of 7 mg/

menstruating cycle and 2000 mg of iron needed for birth during the pregnancy period). Another extreme example includes a combination of blood loss and auto-immune response which causes severe IDA. Malaria is widely prevalent in tropical regions of the world (Africa). This disease triggers the production of hepcidin to reduce amount of circulating iron in the blood; at the same time, one of the symptoms of malaria is intravascular hemolysis resulting in blood loss in the urine[36]. This complex dynamic between auto-immune response as well as iron regulation has led to a suppressed erythropoiesis (the body stores iron to fight infection while blood loss is causing an alarming iron net negative balance). Malnutrition is another cause of iron deficiency anemia and is critical with pregnancy and individuals who already have low iron stores. Heme iron, which is bioavailable in the form of meat is easily absorbed by the body while inorganic iron is more complex and involves more mechanisms before it be readily absorbed. It is also important to look at the ability of the gut to absorb iron. For example, in the presence of infections or inflammations, increased production of hepcidin will suppress gut absorption of iron[37].

Iron deficiency anemia is usually recognized via biochemical and clinical outcome assessment. Biomarkers such as low serum ferritin (<15 ug/L), low transferrin saturation (< 15%) as well as low hemoglobin levels (< 13 grams/ 100 mL) suggest the person has diminished iron stores as well as ineffective erythropoiesis and is an accurate indicator of iron deficiency anemia. Clinical indicators include poor mental performance, cold intolerance, fatigue, dizziness and cognitive dysfunction (very vital with kids since it may be long-lasting and impedes their growth) [38].

The challenge with IDA is the lack of healthcare facilities and clinics in areas where this disease is mostly prevalent. Socio-economic barriers that limit adequate healthcare

infrastructure combined with poor status of livings (wages< $4/hour) diminish the ability of acquiring proper diagnostics and interventions in these areas. In other words, households in under-privileged communities face more severe economic/ health burdens that they physically are unable to or are uninterested in getting their iron levels checked. Therefore, a cheap user-friendly device can help provide necessary diagnostics tools that are unattainable in these areas. Another challenge with iron deficiency is not directly associated with the problem itself but rather a complication of having this disorder that results when iron stores get depleted. In other words, patients with iron deficiency may be asymptomatic and healthy yet still experiencing progressive depletion of iron stores to accommodate for the negative iron balance. Only when iron stores get depleted, anemia is developed and clinical symptoms are observed raising concern in the patient and physician[13].

The primary treatment of iron deficiency anemia is through iron fortification. In general, menstruating women and children are more prone to be affected by this disease. Iron fortification is possible via supplementation, bio-fortification of grains and commercial food products as well as intravenous iron preparations for extreme cases [37]. Note that treatments should stop when anemia is resolved, and iron stores are back to normal levels. A serum ferritin level of 50-100 ug/L is an indicator that iron stores are replenished (400-800 mg of stored iron). Prolonged treatments may have a reversal effect such as iron overload which may potentially lead to hemochromatosis and organ damage[37].

2.1.3 Physiology of Iron Metabolism

In the past decade, an extensive comprehension of iron metabolism physiology has been established and a better understanding of protein-protein mechanisms that regulate daily iron homeostasis have been thoroughly described. In this section, a summary of the fundamental regulatory iron processes that maintain daily iron homeostasis as well as the processes that are activated when abnormal iron behavior is observed are described.

Even though several dozen proteins play a pivotal role in iron regulation, this section only focuses on the three most clinically and physiologically relevant biomarkers: transferrin, ferritin and hepcidin. To start with, transferrin is a glycoprotein produced in the liver and has high affinity towards ferric iron. Since all plasma iron exist in the ferric state, most of iron is bound to transferrin which functions the major transporter of iron to different tissues in the body[39]. In plasma, transferrin has two binding sites for Fe^{3+} with high affinity. Once iron is bound to the transferrin molecule, the protein binds to a surface transferrin receptor which channels a cascade of reactions that lower the pH to 5.5. At these reduced pHs, the transferrin loses its affinity towards ferric ions which are then released into the cell for storage or production of hemoglobin. At low pH, the transferrin molecule remains bounded to the receptor molecule and is recycled back to blood. At neutral pH, the apo-transferrin is dissociated from its receptor and goes back to circulation[39]. This entire cycle is considered a single turnover, and a transferrin molecule undergoes a turnover rate of 10 cycles per day to ensure sufficient iron is supplied for erythropoiesis.

In iron deficiency, increased production of transferrin takes place in the liver as a homeostatic response to increase the binding of iron to transferrin. With diminished plasma iron and an overproduction of transferrin, TIBC, plasma iron and percent iron saturation

become clinically relevant when screening for IDA. On the other hand, low transferrin levels are cause by liver damage or infection. While transferrin is responsible for iron transport in blood, ferritin is the primary storage of iron inside of cells. It is a large molecule that can sequester up to 4,500 iron atoms per molecule. Ferritin levels in the blood reflect iron stores in the body and are widely used in clinical assessment of an individual's overall iron status[40].

Transferrin and ferritin are considered the iron cargo in daily iron homeostasis (transport and storage) while hepcidin, the queen of 'ironomics', is the main regulatory protein in iron metabolism. The production of hepcidin is stimulated with elevated iron levels in plasma blocking both the intestinal absorption of iron from diet and the transport of iron from cellular stores to the blood. If plasma levels are low, hepcidin production is suppressed to increase both the intestinal absorption of iron as well as increase its transport from cellular stores to the blood. In addition, hepcidin activity is also influenced by the erythropoietic process which signals high iron consumption; as a result, hepcidin activation is suppressed and more iron is released onto the bloodstream from hepatic cells and macrophages and from the gut. These two pathological pathways which include the feedback loop between plasma iron levels and hepcidin activity as well as erythropoiesis and hepcidin levels are the major processes that govern iron metabolism and ensure iron homeostasis is maintained[41] .

However, with iron dysregulation (overload or deficiency), new pathological pathways become more dominant causing shifts in iron homeostasis. For example,. HFE is known to interact with both transferrin receptors 1 and 2 in hepatocytes. A competitive process takes place between the HFE protein and transferrin when binding to TFR1. If the

activity of the HFE-TFR1 is increased, iron overload develops due to a decrease in hepcidin production while a suppression in the HFE-TFR1 increases the expression of hepcidin causing iron deficiency. On the other hand, HFE does not compete with transferrin on binding with TFR2 receptor molecule. The HFE- TFR2 complex goes through a cascade of pathways which lead to active hepcidin expression. Hemochromatosis causes an alteration in the HFE structure which increases the activity of the HFE- TFR1 as well as alters the HFE-Tfr2 pathological pathways leading to an iron overload phenotype and a suppressed hepcidin production [42].

With iron deficiency anemia caused by blood/loss or malnutrition (most prevalent form of anemia), production of hepcidin is heavily suppressed due to low iron levels in plasma which triggers the iron-hepcidin feedback loop; therefore, intestinal absorption is activated as well iron transport from hepatic cells and macrophages to blood stream. Iron deficiency may also be of a genetic origin referred to as (Iron-refractory iron deficiency anemia) and is a genetically transmitted hypochromic microcytic anemia which stimulates the transcription of the Hamp gene stimulating the production of hepcidin and consequently, anemia is developed. Elevated hepcidin levels are also observed in infections, chronic inflammations and cancer since macrophages get stimulated and release a network of cytokines of which stimulate hepcidin expression; consequently, anemia is developed. In this case, it is no longer iron-hepcidin feedback loop that regulates iron absorption but rather the presence of inflammation-induced cytokines [43]

So far, this section showed how iron is generally regulated in healthy individuals and what pathological pathways are observed when abnormal iron behavior is developed. Next, a model was used to show how these pathways influence the rate of iron

accumulation. The purpose of representing iron metabolism with a model was three folds: observing the complex 'ironomics' and proteomics from a mathematical and engineering point of view, understand the main areas where iron is consumed or absorbed and finally show how changes in different mass transfer rates can influence the total net accumulation of iron. The simplest model that can be used to describe iron metabolism is shown in equation 1:

$$\frac{dm}{dt} = f * \dot{m}_1 - \dot{m}_2 \text{ [1]}$$

Where $\frac{dm}{dt}$ represents the daily rate of accumulation of iron in the body, $\dot{m}_1$ represents the daily rate of iron intake into the body through nutrition and/or supplementation. $\dot{m}_1$ is multiplied by an efficiency factor f which represents absorption efficiency since not all iron that is ingested is absorbed by the body and thus, the unused portion must not be accounted in the mass balance. Note that the amount of iron in a round healthy diet ranges between 10-15 mg/day and consequently, with absorption efficiencies of 10-15%, the average daily amount of iron that is absorbed from nutritional sources is between 1-2 mg/day which is sufficient to maintain iron homeostasis. $\dot{m}_2$ represents daily iron excretion rates which include shedding of epithelial cells and blood loss.

Next, the model was applied to study how external and internal stressors influence the accumulation of iron in the body. As aforementioned, the two main pathways that govern iron metabolism in healthy individuals include the feedback loop between plasma iron and hepcidin as well as erythropoiesis signaling suppressed hepcidin activity; consequently, absorption efficiency (f) is increased resulting in an increase in the daily accumulation of iron . If plasma levels are high, hepcidin production is activated decreasing

the absorption efficiency (f) resulting in a negative dm/dt to counterbalance any excess build-up of iron. These mechanisms ensure iron homeostasis is maintained. This shows that iron metabolism is tightly regulated by the absorption efficiency.

In menstruating women, additional blood losses of 5-10 mg/ cycle is observed (increase in $\dot{m}_2$). To compensate for this blood loss, hepcidin production is suppressed increasing the absorption efficiency (f). Similar mechanisms are observed with pregnant women where 2000 mg of iron are needed to cover losses to fetus, placenta and delivery blood loss. Absorption efficiencies can increase up to 50% if needed.

Another example includes homochromatic individuals where suppressed hepcidin production governs the main pathological pathway in iron regulation. A constant elevated absorption efficiency (f) of 30-40% cause a progressive positive daily net accumulation of iron. Consequently, the excess iron builds up in hepatic cells and spill to other bodily tissues. In extreme cases, daily accumulations of iron can spike up to 4-5 mg/day.

In remote areas and underdeveloped countries where malnutrition is one of the primary causes of anemia, the rate of iron intake is decreased significantly ($\dot{m}_1$) which triggers a suppressed production of hepcidin which results in an increase in absorption frequency (f). However, poor diets that exclude meats and green vegetables contain alarmingly low levels of iron that even with increased absorption efficiencies, the net accumulation of iron remains negative. This progressive iron deficit eventually leads to anemia.

In cases where inflammation stimulates the production of hepcidin, absorption efficiency is significantly diminished resulting in negative iron balance which leads to anemia, The main difference between inflammatory induced anemia and IDA is that in the former, hepcidin is heavily produced so plasma iron levels are alarmingly low since no iron is transferred to the blood; in this case, iron stores are slightly affected but ineffective erythropoiesis is quickly developed (anemia is developed without iron stores depletion); with the latter, since hepcidin production is diminished, plasma iron are constantly fed from iron stores and gut absorption to meet erythropoiesis requirements which leads to depletion of iron stores in hepatic cells and macrophages before the development of anemia. The limitation with this model is its inability to distinguish between cytokines-induced anemia and iron deficiency anemia.

An extreme case of anemia includes the combination of blood loss, malnutrition as well as inflammation. Malaria is widely prevalent in tropical areas especially in Africa. Not only does this disease cause an auto-immune response that increases hepcidin production to decrease intestinal absorption of iron (decrease in f), but it also causes urinal blood loss (increase in $\dot{m}_2$). Coupled with poor dietary intake (decrease in ($\dot{m}_1$)), the total daily accumulation of iron becomes alarmingly negative and extreme cases of anemia are rapidly developed and increased fatality rates are observed in these populations.

To sum up, the study of iron metabolism physiology also referred to as "ironomics" is quite complex and baffling and involves several protein-protein interactions where deviations in one process may lead to a shift from iron homeostasis. A model was developed to display how external and internal stressors may lead to deviation in iron absorption/ losses and consequently influence the daily accumulation of iron. With

progressive build up or depletion of iron stores, anemia or hemochromatosis may develop, and the individual's well-being becomes at risk.

2.1.4 Clinical Assessment of Iron

As previously discussed, in iron metabolism, several proteins play a significant role in iron transport and storage to maintain daily homeostasis. In this section, the clinically relevant biomarkers are only presented with their physiological relevance in patients with iron disorders which include: hemoglobin (Hb), mean corpuscular volume (MCV), total iron, total iron binding capacity, percent iron saturation and ferritin[42]. To start with, Hb and MCV are both specific for anemia and represent whether the quantity and size of red blood cells fall below the healthy clinical range. Hb and MCV levels lower than 12-13 g/dl and 90 Fl indicate the presence of anemia [44]. Total iron represents the concentration of iron in blood and acts as a first clinical indicator of a person's iron status. In general, patients with iron overload tend to have increased concentrations of serum iron which may spike up to values greater than 200 ug/dl. On the other hand, patients with iron deficiency exhibit low serum iron concentration and may creep down to less < 30 ug/dl. Most commonly, serum iron is coupled with total iron binding capacity (TIBC), a measure of the maximum amount of iron a blood sample can carry. In healthy individuals, 25%-35% of the transferrin is saturated while the remaining unbound transferrin is referred to as unsaturated iron-binding capacity (UIBC) also holds great clinical value. Serum Iron, TIBC, percent saturation and UIBC are related and are expressed as follows:

$$\%\, Saturation = 100 * \frac{Serum\ iron}{TIBC} \text{ [2]}$$

$$TIBC = UIBC + Serum\ iron \text{ [3]}$$

Another significant biomarker in iron metabolism is ferritin, the protein that is responsible for iron storage. Ferritin levels in blood are 100 folds lower than the concentration of transferrin. Ferritin levels are high in individuals with iron overload (>200-300 ng/mL) and low in patients with iron deficiency (<30 ng/mL). **Table 1 summarizes** the healthy clinical ranges of these iron-biomarkers in males, females and children[45].

Table 1: Clinical ranges for four major iron biomarkers: total iron, TIBC, transferrin saturation and ferritin.

Iron Biomarker	Males	Females	Children
Total iron	80-180 µg/dl 14-32 uM	60-160 µg/dl 11-29 uM	50-120 µg/dl 9 uM- 22 uM
TIBC	250-450 µg/dl	250-450 µg/dl	200-400 µg/dl
Transferrin saturation	20%-50%	15%-50%	27%-44%
Ferritin	24-336 ng/mL	11-307 ng/mL	7-140 ng/mL

In addition to the biomarkers identified in **Table 1,** additional tests may be required for a more accurate screening and are shown in **Table 2.**

Table 2: Clinical Tests to Screen for Iron Deficiency Anemia and Iron Overload.

Iron Deficiency Anemia Tests	**Hemochromatosis Tests**
Hemoglobin levels	Genetic testing
Hematocrit levels	Liver Biopsy
Serum iron	Serum iron
Total iron binding capacity	Total iron binding capacity
Ferritin levels	Ferritin levels
Percent transferrin saturation	Percent transferrin saturation

Even though some subtle nuances exist between tests recommended by one physician and the other, there is a general consensus on the order of tests and the rationale of this sequence. The standard approach when screening for iron deficiency anemia comprises of three phases. The first phase includes conducting a complete blood count test that measures hemoglobin levels in blood and the mean corpuscular volume. Hemoglobin levels lower than 12-14 ng/L or a MCV lower than 90 Fl confirms the development of

anemia. A healthy CBC suggests that the person is non-anemic. Next, a ferritin, total iron, total iron binding capacity and percent iron saturation tests are recommended. If ferritin levels are below 30 ng/L, the cause of anemia is iron deficiency while ferritin levels greater than 100 ng/L suggests that anemia is non-iron related. For ferritin levels between these two cutoff values, an increased TIBC, decreased total iron and decreased percent iron saturation indicates that iron deficiency is the cause of anemia. Otherwise, anemia is non-iron related. **Figure 4** illustrates the chronological steps for an accurate screening of iron deficiency anemia.

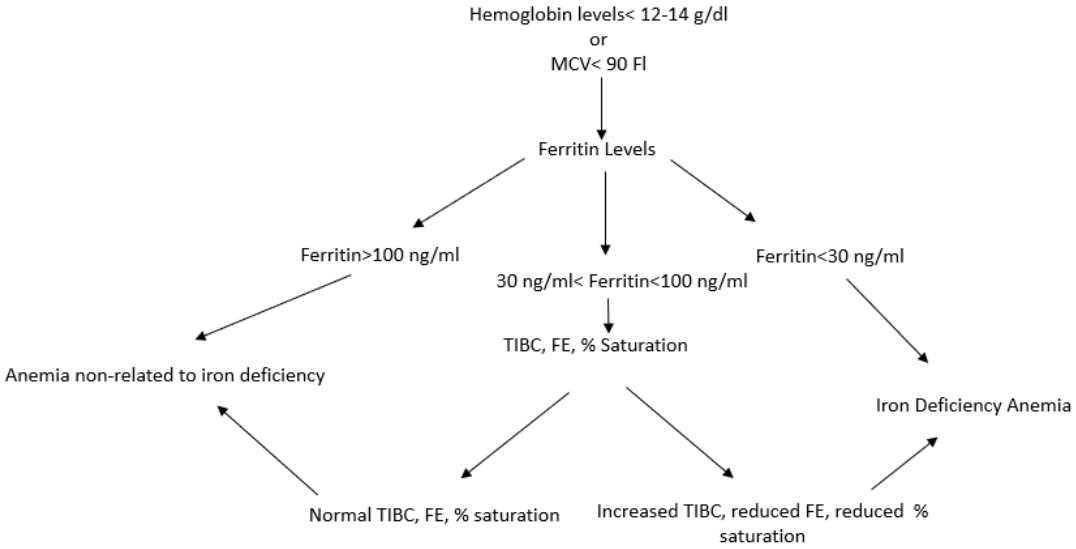

Figure 4: Screening of iron deficiency comprising of three steps: step 1: complete blood count, step 2: ferritin levels, and step 3: TIBC, total iron (FE) and percent iron saturation.

The standard approach when screening for hemochromatosis comprises of two steps. An initial assessment of ferritin and percent transferrin saturation. Ferritin levels> 200-300 ng/L or transferrin saturation levels greater than 40% signify that the person is at risk of developing hemochromatosis. Next a genetic test is performed and a homozygous genotype (C282Y: C282Y) confirms the presence of hemochromatosis and phlebotomy is

required to reduce iron stores. With a (C282Y: H63D) genotype, the physician would recommend a liver biopsy. If the latter reveals high iron stores, phlebotomy is recommended. Finally, a heterozygous or a non C282Y genotype indicate that the cause of elevated iron markers is not due to a genetic mutation in the HFE gene**.** The standard tests for iron overload are shown in **Figure 5.**

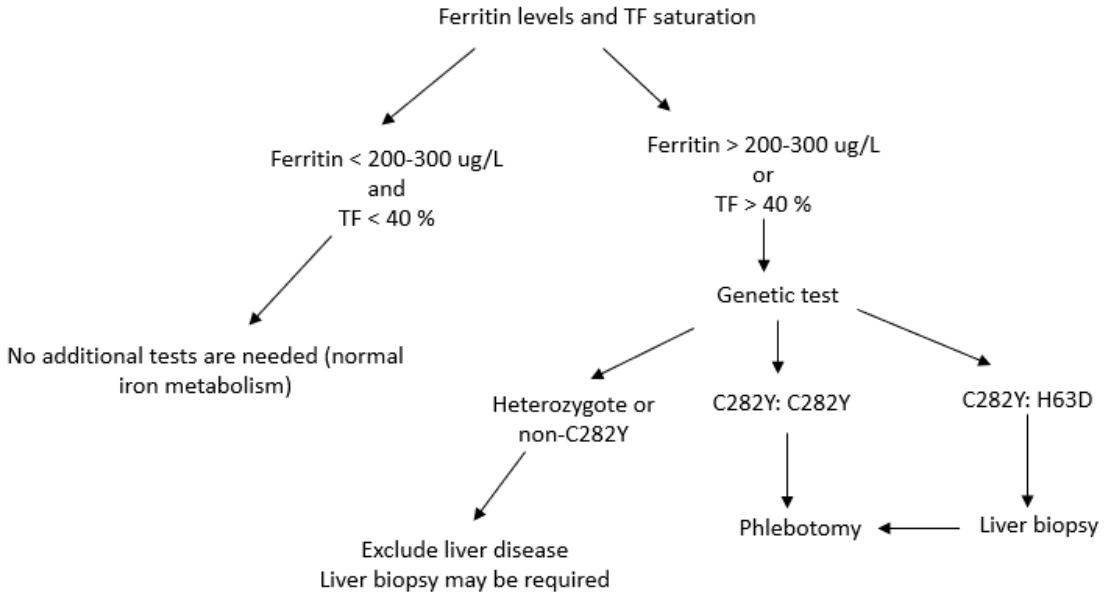

Figure 5: Screening of hemochromatosis comprising of two steps: step 1: Ferritin and percent iron saturation, step 2: genetic test.

2.1.5 Methods to Determine Total Iron

Since the late 19th century, chromatic iron chelators have been investigated as means to quantify iron concentrations in human samples. The core of these molecules relies on exploiting certain atomic configurations that form highly sensitive ligands with ferrous ion such as 1,10- phenanthroline, 4-7-diphenyl-1,10-phenanthroline, 2,2$^{'}$-bipyridine, 2,6-bis(2-pyridyl)-pyridin[46]. However, many of these ligands were tedious to produce, unstable in normal conditions, produced weak signals and can only form in very small

window of pH. However, in 1970 and 1982 two revolutionary iron ligands were discovered: ferrozine and ferene S respectively[47, 48]. Both of these reagents were more sensitive, stable, and easier to synthesize (hence, reducing cost) and played a pivotal role in the future iron detection[49].

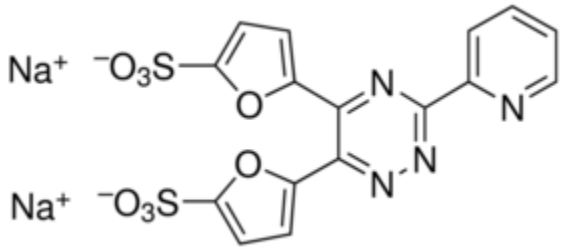

Figure 6: Chemical Structure of Ferene-disodium salt

The main difference between these two ligands is the introduction of the furyl group to the chelating molecule of the ferene S structure which is believed to lead to chromophoric enhancements. The main problem with all iron-sensitive ligands is the interference of cuprous ions that may lead to a 30% overestimation in absorbance measurements. Three different copper masking chelators were discovered to eliminate cuprous interferences: thiourea, thioglycolic acid and neocuproine[49]. Since plasma iron is in the ferric state, its reduction is necessary prior to chelation. At a pH<5, iron (III) is reduced to iron (II) in the presence of ascorbic acid.

For the reference method, ferene was chosen as the iron sensitive ligand for two reasons. On one hand, ferene produced the highest sensitivity among the different chelating agents with a molar absorptivity of 34,500 L, cm^{-} mol^{-1} and exhibited linear behavior over the dynamic clinical range of iron metabolism[50, 51]. On another hand, the most recent

iron-related protocols or research publications produced in the past twenty years recommend utilization of ferene as the chelating agent. In specific, the in-house method was narrowed down to a protocol produced by Weiner Laboratories[52]. In that protocol, two different reagents were described: reagent A and reagent B. Reagent A is the reducing reagent and consists of 200 mM citric acid to create the acidic medium, 34 mM of ascorbic acid to reduce iron (III) bound to transferrin, 100 mM of thiourea to quench cuprous interferences and finally, surfactant (unknown concentration). Reagent B, on the other hand is the chelating agent and consists of ferene with concentrations> 3 mM. The protocol specifies a volume ratio of 5:1:1 of reagent A to reagent B to sample and an incubation time of 35 minutes[52].

2.1.6 Methods to Determine Iron Binding Capacity

Serum iron concentration on its own is not sufficient for accurate screening for iron deficiency or over-load, so, additional tests, such as total iron-binding capacity is considered part of the standard of care. TIBC is defined as the total amount of iron that can bound/transported by the transport proteins. Patients with iron deficiency may show increased TIBC in conjunction with low iron levels, whereas iron-overloaded predictably have unusually low TIBC[53]. In addition to total iron binding capacity, the unsaturated iron binding capacity and percent iron saturation are clinically significant when screening for iron disorders. Protocols to determine iron binding capacity date back to 1960's and 1970's and may be looked at from two different approaches: TIBC method and UIBC method[54, 55]. The TIBC method involves three steps: saturating the serum sample with iron such that all transferrin binds to iron in both available spots; precipitating the excess iron with magnesium carbonate because it has a high affinity for free iron but relatively

low affinity if iron is bound to transferrin and finally, perform the same spectrophotometric test described previously for iron detection (i.e chelating the reduced iron with the chromogen). The UIBC method, on the other hand consists of only two steps: saturation of transferrin at a pH>8 with a known concentration of iron (III) and chelating the excess iron with the chromogen[56]. Even though both methods exhibit some common steps, the target analyte of each method is different. For the TIBC method, the chelated iron represents the total iron binding capacity with the UIBC method, the target analyte is the excess unreacted iron that can be used to determine the unsaturated iron binding capacity. **Figures 7 and 8** depict a more visual representation of the given methods[57].

Both methods have their own limitations, unspecific binding of iron to other serum proteins may lead to an over-estimation of TIBC by up to 20% with the TIBC method. Some standardized guidelines are used to reduce these systemic errors, but they cannot be avoided. In the purpose of screening for iron disorders, these errors can be tolerated. On the other hand, the main problem with the UIBC method is the competition reaction that takes place between the reduction of iron (III) and the working reagents and the hydrophilic polymerization of iron (III) at an elevated pH. Without any modification, this method is generally not accepted due to a significant under-estimation of TIBC[55].

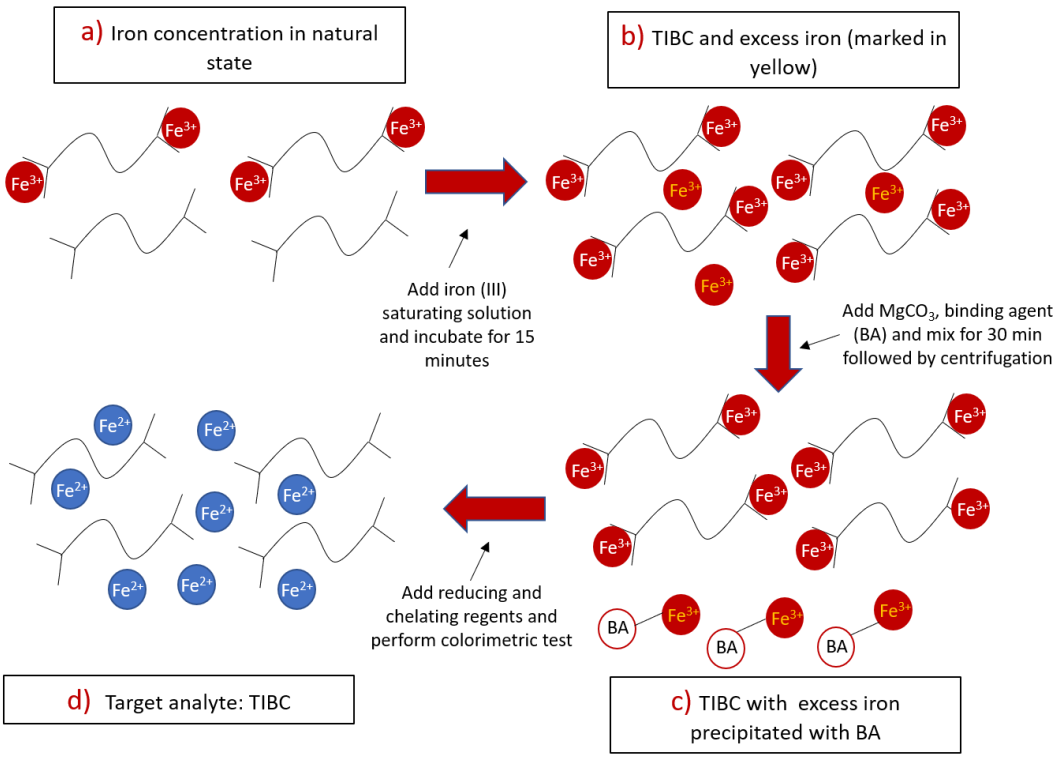

Figure 7: TIBC approach: a) represents the natural state of transferrin and iron (III) in a volume faction of plasma b)saturating the serum sample with iron (III) solution resulting in a state of TIBC with excess iron (III) c) adding magnesium carbonate to precipitate excess iron d) reduction and chelation of iron (III) and a colorimetric measurement is obtained to quantify the target analyte: TIBC.

Figures 7 and 8 show chronological steps of the TIBC and UIBC Methods. Both start with the addition of iron (III) saturating solution; the amounts added must ensure that all unbound transferrin molecules become saturated. With the UIBC method, the added amount must be quantified. At this stage, samples of both methods contain saturated transferrin in addition to excess free iron (III) ions. Next, with the TIBC method, $MgCO_3$ is added to bind specifically to the excess iron (III) which are precipitated; while, with the UIBC approach the reducing agent (ascorbic acid) as well as the chelator (ferene) are added at a pH>8 where transferrin has high affinity towards iron (III) ions and a colorimetric measurement is obtained (2 step process). Finally, the same reducing and chelating agents

are added to the supernatant of the TIBC method and a measurement is obtained (3 step process).

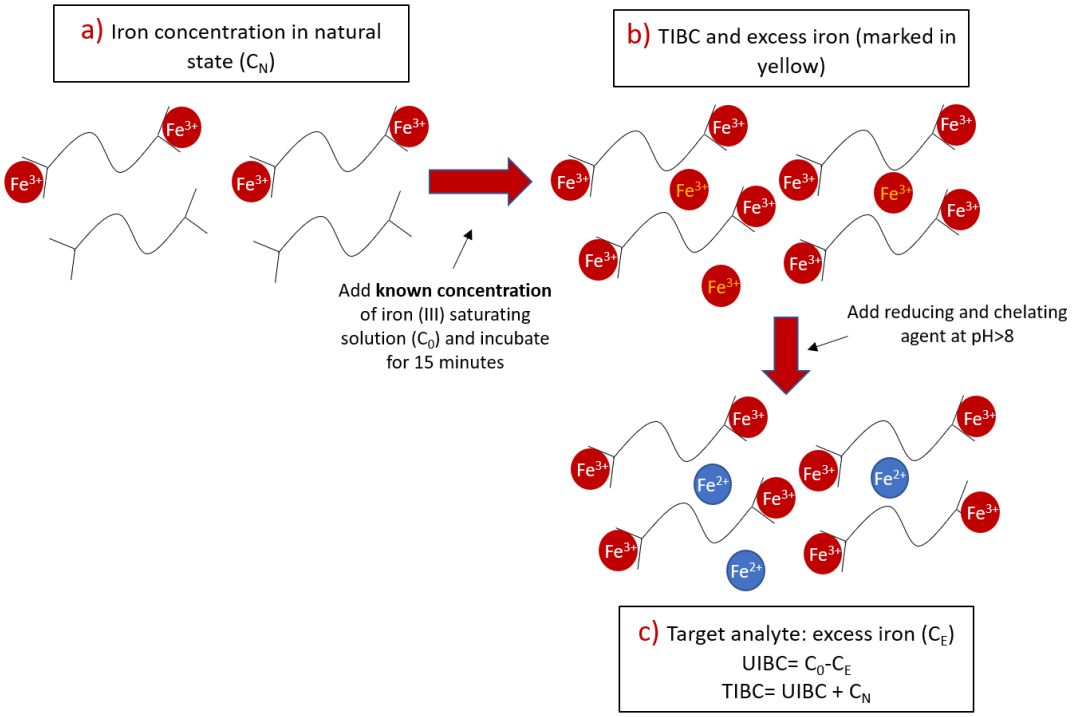

Figure 8: UIBC approach: a) adding a known concentration of iron (III) saturating solution b) reduction and chelation of the excess iron at a pH >8 and c) Colorimetric measurement with target analyte the excess iron.

2.1.7 Statistics

Throughout this thesis, several statistical methods were used to measure data dispersion, agreement and correlation regression and are introduced in this section. To start with, the percent coefficient of variation (C.V %), shown in equation 4, was used to study the dispersion of a data set by assessing inter and intra assay variations.

$$C.V\% = 100 * \frac{standard\ deviation\ of\ sample}{average\ of\ sample} [4]$$

Even though the same equation is used for both inter and intra assay dispersions, the data set represent different entities. Intra-assay dispersion represents data variation within the same assay while inter-assay dispersion represents data dispersion from different assays.

Next, to study the agreement of two different methods (validating the experimental method with the reference method), two different plots are used: a correlation plot as well as a percent Bland-Altman plot. The former represents plotting the experimental data as a function of the reference data and then fitting the curve with a linear line. The better the agreement, the closer the model converges to the identity line (y=x). In a percent Bland Altman Plot, percent difference, percent bias, lower limit of agreement and upper limit of agreement were calculated as follows:

$$\%\ difference = 100 * \frac{experimental\ data - reference\ data}{reference\ data} [5]$$

$$\%\ bias = \frac{\sum_{i=1}^{n} \%\ difference}{n} [6]$$

$$\%\ Std.s = \frac{\sum_{i=1}^{n} (\%\ difference - \%\ bias)^2}{n-1} [7]$$

$$LLOA = \%bias - 1.96 * \%Std.s [8]$$

$$ULOA = \%\ bias + 1.96 * \%Std.s [9].$$

Finally, a power law was utilized to determine the sample size needed to validate the device. The power law includes four different statistical tools: an expected difference between two different populations (an example is moving from a clinical iron level of 100 ug/dl to an iron deficiency mean of 50 ug/dl or to an iron overload mean of 150 ug/dl). The second parameter is the group standard deviation which was calculated via taking the standard deviation of a given sample. The third parameter represents the size or level of

statistics alfa and was chosen to be 0.05. The final parameter was considered to be the power of the test that represents the probability of rejecting the null hypothesis and that the two data sets statistically have different means. In this work, the number of samples was chosen initially and a power > 0.8 confirms that the selected number of samples is adequate to statistically discriminate between the two data sets.

2.2 Motivation

In section 2.1 (Background), a summary of the main iron regulatory proteins, the main iron disorders that are prevalent globally as well as the standard clinical tests to screen for iron disorders were introduced. The purpose of the background information was to show that iron metabolism 'ironomics' and 'proteomics' are well defined physiologically and clinically. The motivation of this work is then to integrate this knowledge with innovative design strategies to bring a new accurate, user-friendly and inexpensive device for timely intervention of patients with poorly functioning iron metabolism and sustain human performance in healthy normal vulnerable populations from a broad range of socio-economic societal conditions.

2.2.1 Rationale of Biomarker Selection

The biomarkers that were included in the proposed design were: serum iron, total iron binding capacity and percent transferrin saturation. The rationale behind this decision is based on the tradeoff between device feasibility and accuracy of screening. To elaborate, TIBC, serum iron and percent transferrin saturation are common blood biomarkers for both iron deficiency anemia and hemochromatosis screening and have proved to be robust testing parameters. They also exhibit concentrations of the same order of magnitudes and

can be determined using the same chelating agent, thus, simplifying device requirements and complexity. Quantification of serum ferritin improves screening accuracy; however, the concentration of serum ferritin is 100 folds lower than that of serum transferrin and protocols for ferritin detection involves different detection mechanisms increasing the complexity of the device down the road.

The question is now, how accurate, and specific is the screening process if the aforementioned biomarkers were only utilized? Since the device is not developed at this stage, the decision was based on two factors: the current standard clinical tests as well as previous publications that have studied the specificity and accuracy of these biomarkers in screening for both iron deficiency anemia and iron overload. Regarding iron overload and hemochromatosis, **figure 5** shows that the first stage in screening for hemochromatosis is determining transferrin saturation; hence, it is expected that the selected biomarkers must have high accuracy and specificity; otherwise, it wouldn't be a standard primary test recommended by physicians globally. In fact, a study (HEIRS) conducted by PC Adams revealed that transferrin saturation >45% and UIBC < 150 µmol/L have a sensitivity of 75% and 79% as well as a specificity of 93% and 95% in predicting the homozygosity genotype. Another test showed that transferrin saturation greater than 50% in men and 40% in women showed a sensitivity of 92%, specificity 93% and a positive predictive value of 86%, and overall, there is this general consensus that percent transferrin saturation is sufficient for accurate screening of iron overload.[42]

On the other hand, with iron deficiency anemia, **figure 6** shows that a complete blood count and ferritin levels are more vital biomarkers while TIBC, percent transferrin saturation come at a later stage in the screening process. A test was conducted on 101

patients (41 were iron deficient) and 60 were iron sufficient. Transferrin saturation < 0.2 had a sensitivity of 60.5% and specificity of 48.1% while total iron binding capacity > 45 umol/L had a sensitivity of 71% and a specificity of 75%. Another test conducted on 627 anemic patients of whom 54% were African American, the sensitivity and specificity of TIBC > 406 ug/dl of 80.3% and specificity of 61.5% and the sensitivity and specificity of TS< 10.4% were 80.3% and 78.8% respectively[58]. The overall consensus is that ferritin is the golden standard iron biomarker to screen for IDA, yet some publications suggest that transferrin saturation is the best alternative biomarker while others claim that TIBC is the second-best biomarker for screening. There still exists some nuances regarding whether the selected biomarkers are sufficient to accurately screen for IDA. Note that data collected in these publications reflect at most two measurements per patient; therefore, with dynamic data collection (daily, or weekly), new correlations can be established and better judgements regarding the accuracy of these biomarkers as screening tools can be recognized. In addition, anemic individuals from different geographical areas or ethnic origins might demonstrate different biochemical changes and therefore, a set of specific criteria that has high screening accuracy in one area may demonstrate poor predictive capabilities in another region.

In addition, the major limitation with the golden standard test is that the actual patient must initially show clinical symptoms of anemia such as fatigue and cognitive impairment before a full diagnosis is provided. Biochemically, these symptoms translate into diminished Hb and MCV measurements. In fact, based on the current standard tests, screening of IDA comes in a later stage when anemia was already diagnosed. However,

with the point of care device, if screening of iron deficiency precedes that of anemia and proper interventions are taken accordingly, the complications of anemia can be avoided.

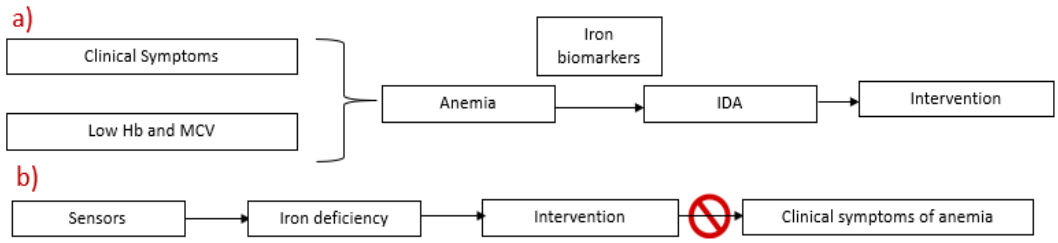

Figure 9: Two different pathways to manage IDA: a) current standard tests where an individual displays the symptoms of anemia and the diagnosis of IDA comes in a later stage, b) Iron deficiency is initially identified before the development of IDA.

To summarize, the purpose of this section was to explain the rationale of the biomarker selection process which include: TIBC, total iron, transferrin saturation and UIBC. The primary reason to selecting these biomarkers is the similarity in their detection methods and sensitivities; thus, device design and operation becomes feasible. The drawback is by excluding other biomarkers such as ferritin, the sensitivity of the device and specificity in screening for iron deficiency and overload may be impaired. The general consensus is that percent transferrin saturation is required and necessary to screen for iron overload (promising for the device) while there is a debate whether transferrin saturation or TIBC can actually replace the golden standard marker, ferritin in screening for IDA. Some publications state that TIBC is highly specific and accurate in screening for iron deficiency, others believe that transferrin saturation is the best alternative to ferritin while other publications state that TIBC and transferrin saturation do not bring any added value[59]. Hopefully, with multiple measurements per individuals as well as geographically dispersed users, new correlations can be established between these iron biomarkers and the device's ability to screen for IDA.

2.2.2 Rationale of Utilizing Smartphone Technology

Despite the remarkable scientific discoveries that have been made in healthcare, disease continues to spread at an alarming rate, raising the need for accurate and rapid diagnosis[60]. Although early detection and accurate diagnoses have led to more effective treatment and prevention of disease, most detection methods are time-consuming and require costly procedures and instrumentation. Additionally, healthcare costs in the U.S. are projected to account for 30% of the GDP by 2040, and the rising cost of healthcare has led to a push for the development of low-cost sensing technologies[61]. To combat these problems, numerous diagnostic tools have been developed for use at the point of care (POC). POC devices tend to be portable, cost-effective devices that provide users with rapid and reliable test results. The emergence of POC devices has allowed patients in remote areas and resource-limited settings to receive quick and reliable healthcare while also reducing the costs and time required for specialized medical testing. Thus, POC devices have the potential to provide more effective care for diseases by limiting the cost and time needed for accurate diagnosis and being accessible for use around the world despite the medical conditions of a geographic area[60].

Due to the emergence of digital electronics, many POC devices utilize smartphones as a graphical user interface to conduct and display test results to users. Since smartphones are being widely used by individuals of all age groups and income levels, they are the most optimal platform for a POC device. Currently, over 3 billion individuals utilize smartphones and that number is consistently increase each year. Hence, due to the development of mobile applications and the widespread adoption of smartphones,

smartphones could be used as a potential tool for the clinical diagnosis of disease as a POC device[62, 63].

Past research has shown that cell phones have been utilized to diagnose numerous diseases and conditions by detecting the levels of specific biomarkers that are related to the disease or condition in question. For example, smartphone apps have been used to detect Ovarian Cancer by measuring the levels of the He4 biomarker in urine and sense dehydration by quantifying biomarkers present in saliva and sweat[64]. They are also used to detect vitamin D levels in serum samples by measuring brightness difference with a smartphone camera[20]. Additional applications include cholesterol testing, DNA detection, ELISA substitution, and the detection of several other blood derived biomarkers[65-68]. The purpose of designing these point of care mobile technologies is three folds: to replace golden standard methods that require qualified personnel and bulky equipment, to provide cost-effective and rapid sensing platforms for early diagnostics and consequently early interventions for better healthcare management and finally, provide convenience by eliminating unnecessary trips to clinics and reduce waiting time to obtain an accurate diagnosis report[63].

In addition, the mechanism of iron detection involves chelating iron (III) with a chromogen that exhibits an excitation wavelength at 590 nm. The resulting complex produces a color in the visible spectrum and thus, utilizing the smartphone camera to perform some color deconvolution to quantify the signal formed by the specific color complex proves to be a promising tool.

2.2.3 Device Use Case

2.2.3.1 Screening of Iron Deficiency Anemia

The sub-groups who are mostly at risk of iron deficiency anemia are pregnant and menstruating women in underdeveloped communities. In fact, according to the world health organization (WHO), 58% of pregnant women are estimated to be anemic in third world countries which leads to fatigue, increase in perinatal mortality, low birth weight as well as increased risk of death[34]. The major causes of anemia in these areas are malnutrition and blood loss. Therefore, there exists policies to provide daily iron supplements to all pregnant women without any screening. The amount of iron in these daily supplements range between 50-100 mg. Even with these protocols, there was not any significant reduction in the prevalence of anemia. This is because women were not adhering to these supplementation programs due to gastrointestinal upset and additional side effects. In addition, the quality, quantity, and infrastructure to adequately supply these pills are lacking significantly. This means even if the devices were deployed in these areas and were accurately screening for iron deficiency and identifying the risk of anemia, there is an inadequate supply of pills and other iron-management procedures so, it is not only the lack of diagnostics that is causing the prevalence of this disease but also a lack of infrastructure to meet the basic healthcare requirements[37, 69].

Even though it is recommended for pregnant women to adhere to these protocols without any prior diagnostics, the device can be used as a monitoring tool for proper iron management. This can be observed in three different ways. With the assumption that these women are taking the recommended pills daily, the device can be used on a weekly basis to verify that the quality of the pills is adequate by measuring the different biomarkers (e.g low plasma iron, low percent iron saturation and high TIBC) and ensure that no

alarmingly low iron stores are observed. On another hand, with women who are not affected by anemia or are experiencing mild iron deficiency but are still blindly adhering to these iron management protocols, these devices can be used to detect iron overload and potential hemochromatosis which will induce a set of other complications. Therefore, upon measuring the same biomarkers, appropriate management can be taken such as reducing the dosage of these pills or even completely eliminating them. Finally, this device can play a pivotal role in monitoring iron levels and stores for kids between ages 1 and 7 where proper iron homeostasis is critical for the child's mental development[70].

Another major problem observed in developing countries is the lack of access to health-care facilities. In fact, in several areas, there are no ambulances or alternative means of transport to transfer patients who need immediate medical attention. Coupled with minimal wages (<4$/hour) and minimal hygiene other concerns such as fever, infections and diarrhea are prioritized in lieu of screening for iron disorders. In addition, not only are healthcare facilities lacking in quantity but also in the quality of their services. In fact, a lot of these medical facilities lack basic equipment and medical supplies and in extreme cases, some needles are reused, and proper disinfecting procedures are not followed. In this myriad of complications, the developed device can provide a good solution to screening iron disorders without the need for a medical facility or professional[71].

In developed countries, the prevalence of iron deficiency is significantly less than that in underdeveloped communities (12-15 folds less in males and 5-7 folds less in females). This is because of easy access to adequate diagnosis, therapeutics, interventions as well as improved nutritional diets that host an array of nutrients and minerals. With this said, the device can still be used in these communities to further improve iron management.

However, even in developed countries, there are socio-economic barriers that restrict certain populations or minority groups to purchase expensive fruits and meats. These groups are more likely to develop iron deficiency and potentially anemia. In addition, iron deficiency can be associated with certain age groups such as: infancy, childhood and adolescence. In general, due to easy healthcare access, these groups are capable of getting appropriate diagnosis and therapeutics, but the device can provide a more cost-effective alternative for a quick and accurate screening[72].

2.2.3.2 Anemia of Inflammation and Chronic Disease

In many diseases, complications such as iron deficiency anemia might develop and therefore, the ability to test for iron at the point of care might help screen for these diseases on one hand and also help mitigate the symptoms of these diseases. For example, a study showed that 77% of cancer patients develop anemia[73]. In some cases, more than 60% of these affected groups do not receive anemia treatment since they might associate fatigue with their primary disease or not even report it. The main causes of anemia in cancer patients are nutritional deficiency, erythropoietin suppression and iron metabolism impairment. Recent studies showed that the risk of death increased by 60% if cancer patients are anemic since these patients exhibit more fatigue, reduced ability of work as well as feel more socially isolated. In times, where mental fortitude is critical for the patient's well-being, anemia can exacerbate cancer symptoms[73].

Anemia can also be associated with chronic kidney disease (CKD) and is more common in patients who are not undergoing dialysis. In the U.S, 10% to 20% of individuals with CKD have anemia which is caused by ineffective erythropoiesis, iron deficiency and inflammation. Anemia prevalence was also recorded to increase with a decline in

glomerular filtration rate. In these patients, anemia can lead to cognitive disfunction, sleep deprivation, fatigue and an increased cardiovascular risk.[74].

Anemia is also linked with several other diseases such as HIV/AIDS, cardiovascular disease, inflammatory bowel disease, pulmonary disease and diabetes and studies indicate that individuals diagnosed with a certain disease have an increased risk of fatality if anemia is developed at a later stage. The cause of such increased mortality rates lies in the complications that manifest from anemia such as fatigue, cognitive impairment and lack of energy which exacerbate the person's health to deal with their underlying disease.

In addition, not only can a point of care device help mitigate the symptoms of anemia-induced by chronic diseases, but it may potentially help screen these diseases from an early stage. To elaborate, since anemia caused by chronic diseases leads to diminished plasma-iron levels (cytokines signal hepcidin production), sudden drops in iron levels would be an indicator of anemia of inflammation or chronic disease as shown in **Figure 10**.

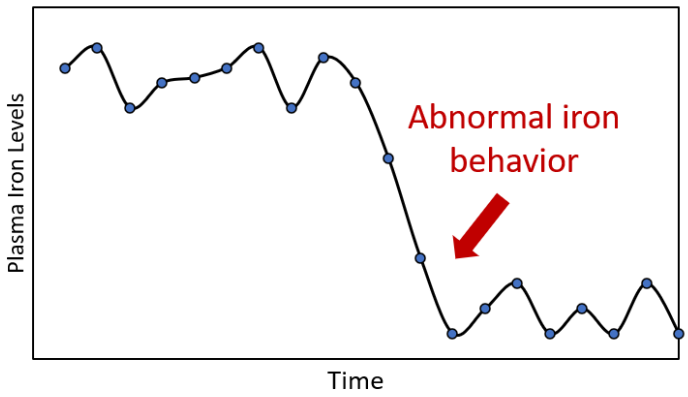

Figure 10: Dynamic data for iron levels. Abnormal iron behavior may indicate anemia of inflammation or chronic disease.

2.2.3.2 Iron Overload and Hemochromatosis

Since hemochromatosis is mostly prevalent in developed countries, diagnostics and therapeutics and appropriate managements are widely available. The aim of a point of care device would be to reduce cost on individuals with hemochromatosis as well as encourage more people who are prone are at risk of developing this disease to assess their biochemical stigma prior to displaying clinical symptoms.

The major challenge is that one would think that a person who is born with this genetic disease leading to an over-absorption of iron would experience progressive iron overload, yet correlations between age and liver iron are not clear. In fact, not all individuals who are homozygous with the disease represent the phenotypic complications. With moderate penetrance, many homozygous maintain healthy biomarkers even without phlebotomy. Another risk associated with hemochromatosis is that it is mostly asymptomatic; thus, most people tend to avoid getting tested since no clinical symptoms are experienced.

A point of care device can revolutionize screening of hemochromatosis in these areas. Since these sensors are cheap, user friendly and minimally invasive, they can be distributed to all households that might be at risk of iron overload raising general awareness and curiosity. Since the genetic test itself does not convey whether the person's iron stores are high, an accurate screening can be realized at-home eliminating the need for genetic testing or, the genetic test can be conducted as secondary screening upon consultation with the physician. In addition, these sensors enable more frequent measurements providing a better understanding of the dynamics of these biomarkers (transferrin, ferritin, total iron) and may enable better management procedures such as the frequency of phlebotomy as

well as the volume of blood drawn. In addition, it is also cost-effective to screen and manage hemochromatosis at an early stage before liver damage takes place.

2.2.3.4 Dynamic Changes in Iron

Another advantage that the point of care device can potentially provide is real time data collection. Currently, there is a lack in knowledge in fluctuations of iron levels (daily, weekly, monthly…). How do iron levels correlate with different stimuli such as stress, sudden life changes (positive or negative) or with other blood biomarkers? How do these correlations vary between country, age, gender or ethnicity and above all, how do they help screen or predict the development of iron-related diseases?

There are three major reasons why there is this fundamental gap in knowledge of dynamic changes in iron levels exists. On one hand, conducting these frequent tests is expensive and inconvenient. Not only does each test cost approximately $25-50, but the patient must also visit a clinic and undergo a tedious venous blood draw prior to each measurement limiting the ability of conducting extensive studies. In addition, there is a general lack of interest of collecting iron data and other biomarkers are considered to be more essential. Above all, from a patient's perspective, there are three reasons why an individual decides to get their iron level checked. The most common cause is when clinical symptoms are displayed and consequently, the patient decides to visit a medical professional (constant fatigue, bronzing and extreme cases of liver cirrhosis). The problem is that at this stage, iron stores are either alarmingly low (still manageable by taking iron supplementation over the course of six months) or alarmingly high (extreme case where patients display symptoms of liver cirrhosis) and management of the disease becomes more difficult. The second cohort includes individuals who are more wary about their well-being

and get their iron levels tested just for a regular check-up or in case of genetic history with an underlying iron disorder. The advantage here lies the ability to screen for iron deficiency or overload before displaying any symptoms and appropriate interventions can be taken to circumvent complications caused by iron-borne diseases. Finally, in the most extreme case, a third group of individuals who are already diagnosed with iron deficiency anemia or hemochromatosis and are taking appropriate measures (supplementation or phlebotomy) would get their iron levels checked 3-4 times a year at for monitoring purposes; thus, frequent measurements of iron levels are not necessary to ensure the well-being of a person. However, with these devices, further studies become increasingly feasible with cheaper materials, faster feedback from measurement with analysis turnaround rates of 15 minutes and lower risk of damage due to a finger-prick sample as opposed to a venous blood draw; thus, gaps in the knowledge in dynamic changes in iron levels are abridged.

CHAPTER 3

METHODOLOGY

3.1 Characterization of Iron Detection with Reference Spectrophotometry

3.1.1 Absorption Spectrum

Initial tests to find the absorption spectrum of the ferene complex were conducted using the spectrophotometer, the industry standard (Section 4.4, Figure 11). The absorbance spectrum showed that the excitation wavelength of iron is 590 nm which agrees with literature values. All future tests were conducted at that specified wavelength.

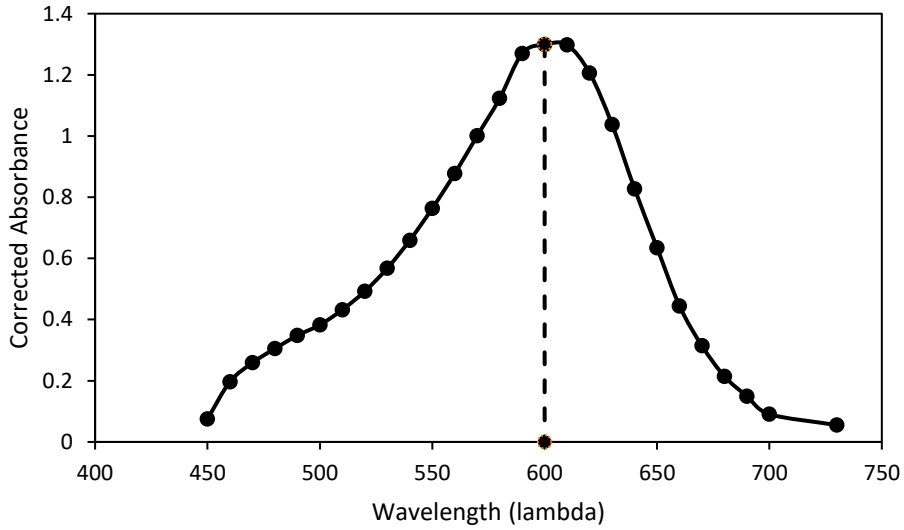

Figure 11: Absorption spectrum for the iron (II)-ferene complex which exhibited an excitation wavelength at 590 nm.

3.1.2 Reference Method for Iron Detection

A reliable certified laboratory reference method for iron quantification is a spectrophotometric assay that includes a “reagent A”, containing 200 mM citric acid, 34 mM ascorbic acid, 100 mM thiourea, and surfactant; “reagent B”, containing ferene at >3 mM, and the tested sample with final volume ratios of 5:1:1 **[52]**. The lab protocol begins with whole blood samples processed to isolate serum

or heparinized plasma, then processed with “reagent A” to strip Fe (III) from transferrin with citric acid, followed by reducing Fe(III) to Fe(II) with ascorbic acid, and finally the addition of “reagent B” to chelate Fe(II) to the chromophore ferene[52]. The recommended incubation time for the final reaction is thirty minutes. Ferene is chosen because of the direct proportionality of iron concentrations to absorbance values from the ferrous complex and high absorptivity at 575-600 nm range. Thiourea is included to quench Cu(II), a known interferent in blood iron detection. A surfactant is used in order to contribute to reaction homogeneity.

3.1.3 Optimized Method for Iron Detection in Serum

Two issues with the current reference method encouraged us to optimize it: 1) a need to avoid apparent protein precipitation during the incubation of serum samples, and 2) a need to increase sensitivity to assure accuracy of detection for low iron concentrations. To address these issues we: 1) removed the surfactant causing sample turbidity and unusual high absorbance values and 2) reduced the volume of “reagent A” to a ratio of 3:1:1 to increase relatively higher iron and ferene concentrations (see chapter 4.1) The changes resulted in the creation of an “optimized reference method”. **Table 3** shows the resulting final molar ratios of the original reference method versus optimized reference methods for use in the spectrophotometer. Detailed rationale for sensor strip chemistry ratios is given in experimental methods.

Table 3: Comparison of Molar Concentration Ratios of Reagents to Iron for the Three Analytical Methods Used.

Reagent	Orig. Ref. Method	Opt. Ref. Method	Sensor Method
Ascorbic acid	9.5×10^3	5.7×10^3	2.7×10^3
Citric acid	55×10^3	34×10^3	16×10^3
Thiourea	28×10^3	17×10^3	8.0×10^3
Ferene	2.2×10^2	2.2×10^2	3.2×10^2
Iron	1.0	1.0	1.0

Note for Table 3: Ascorbic acid, citric acid, and thiourea are far in excess (2,700-55,000 times larger than the iron concentration), whereas the ferene is in excess rendering ~1:220-320 ratio. The calculations were for practical examples, e.g., 50 μL of iron standard (100 μg/dL) added to 200 μL of total assay reagents in the optimized method, 36 μL of the same iron standard was added to 214 μL of total assay reagents in the original method. 30 μL of 100 μg/dL iron sample was delivered to the dry sensing channel in the sensor strip method.

3.1.4 Common Spectrophotometric Features and Test Sample Sources

All spectrophotometric measurements for the original and optimized reference methods were performed with 96-well plate in a Spectra Max M5 spectrophotometer at 590 nm, using 250 μl final test volumes, which rendered a path length of 0.6 cm. Iron standards were made fresh from Fe(III) nitrate nonahydrate crystals in 0.5 M nitric acid solution using high-intensity shakers for 15 minutes to ensure iron crystals were completely dissolved. Calibration curves for spectrophotometric measurements (original and optimized refence methods) and new sensor strips measurements were obtained from analysis of iron standards: a

blank, 25, 50, 100, 150, and 300 μg/dL, covering the physiologically relevant total iron levels.

In addition, eight venous blood samples were obtained via consent (from each subject via Arizona State University's IRB study protocol (STUDY00008255). All the samples were processed for serum and used for intra-laboratory validation. Two of the eight samples were sent to LabCorp for inter-laboratory validation.

All experiments were conducted by the same technician, on the same instrumentation over the course of several months.

3.1.5 Specificity of the Iron Detection Reaction

In order to study the selectivity of the iron detection reaction, the response to several potential serum interferent analytes using the optimized reference method was tested. The interferents' analytes included glucose (140 mg/dl), creatinine (1.2 mg/dl), uric acid (7 mg/dl), potassium chloride (20 mg/dl), sodium chloride (333 mg/dl), and urea (20 mg/dl). The concentration of interferents was chosen to be the highest concentration values that could be found in a healthy human body blood [75-78]

3.1.6 Kinetic Investigation of the Optimized Method

In order to obtain the iron (II)- ferene complex, two reactions are involved: the reduction of iron (III) with ascorbic acid (AA) and the complex formation between the reduced iron and ferene. In the protocols, the concentration of ascorbic acid is in excess relative to the other chemical species. To simplify the number of variables, the concentration of ascorbic acid will remain constant and will be factored in with the rate constant. In this case, the rate law is reduced to the following:

$$\frac{d[COM]}{dt} = k'[Fe^{3+}]^{\alpha}[Ferene]^{\beta} [4]$$

$$k' = [AA] * k \ldots [5]$$

An initial slope analysis was conducted to determine the rate orders α and β and the following assumptions and approximations were used:

At t=0, concentrations of reactants are equal to initial concentrations

$\frac{dC}{dt} = \frac{(C_{i+1} - C_{i-1})}{2\Delta t}$ for all points other than t=0

$\frac{dC}{dt} = \frac{(C_1 - C_0)}{\Delta t}$ for t=0

An initial slope analysis was performed by fixing the concentration of one reactant constant while varying the concentration of the other reactant, and so:

If iron [III] concentrations are held constant:

$$\frac{\left.\frac{d[COM]}{dt}\right|_{t=0,[Ferene]1}}{\left.\frac{d[COM]}{dt}\right|_{t=0,[Ferene]2}} = \left(\frac{[Ferene]_1}{[Ferene]_2}\right)^{\beta} [6]$$

By taking logarithmic on both sides, the above equation can be reduced to the following:

$$\ln\left(\frac{\left.\frac{d[COM]}{dt}\right|_{t=0,[Ferene]1}}{\left.\frac{d[COM]}{dt}\right|_{t=0,[Ferene]2}}\right) = \beta \frac{[Ferene]_1}{[Ferene]_2} [7]$$

Similarly, if ferene concentrations were held constant, the following mathematical equation is obtained to determine α:

$$\ln\left(\frac{\left.\frac{d[COM]}{dt}\right|_{t=0,[iron\,]1}}{\left.\frac{d[COM]}{dt}\right|_{t=0,[iron]2}}\right) = \beta \frac{[Iron]_1}{[Iron]_2}$$

Once the rate law powers are approximated, the rate constant was determined by evaluating the following expression at different instances.

$$\frac{d[COM]}{dt} - k'[Fe^{3+}]^{\alpha}[Ferene]^{\beta}[8]$$

Since the data collected is absorbance measurements, a series of stoichiometric balances were necessary to convert absorbance values to concentration. Since the complex-formation is irreversible at pH<5, equations 16 and 17 become valid.

$$\frac{d[COM]}{dt} = -\frac{d[Fe^{3+}]}{dt} = -\frac{d[Ferene]}{3dt}[9]$$

$$[COM] = [Fe^{3+}]_0 * (\frac{Abs_t}{Abs_\infty})[16]$$

$$[Fe^{3+}] = [Fe^{3+}]_0 * (1 - \left(\frac{Abs_t}{Abs_\infty}\right))[10]$$

$$[Ferene] = [Ferene]_0 - 3[Fe^{3+}]_0 \left(\frac{Abs_t}{Abs_\infty}\right)[11]$$

Once absorbances are converted to concentrations, a linear solver was used to determine the value of the rate constant by minimizing the square of the error.

$$\min (\sum \left(\frac{d[COM]}{dt} - k'[Fe^{3+}]^{\alpha}[Ferene]^{\beta}\right)^2)[12]$$

With this in mind, two 50 and 100 μg/dL iron standards in combination with 2 and 4 mM ferene concentrations were used and time profile of absorbances and their corresponding numerical derivatives were obtained to determine the reaction order and rate constants. This analysis enabled the rational selection of the iron detection reaction times, which were critical for the development of iron detection on the dry sensor strips which will be discussed in the next section.

3.2 Iron Characterization in Mobile Technology

3.2.1 Sensor Strip Designs

The focus of this work is on iron analysis from serum with the goal of developing a novel assay for accurate, sensitive, and reproducible detection of iron. The assay consists of an accurate, storable, and robust dry sensor strip in a vertical flow design with the aim of iron detection time of five minutes. **Figure 13** shows the 3D sensor design, indicating the sample delivery port and the sensing side, as well as assembly. The sensor strip has a sensing area and a reference area (**Figures 12 and 13**). The sensing pad is made of a dry, porous, and absorbent nitrocellulose blotting filter paper impregnated with all reagents, which resulted in a built-in capacity to drive a 30 μL sample by capillary forces without spilling, and rapidly separating large components such as proteins from soluble ions . Reagent A strips Fe (III) from transferrin, reduces Fe (III) to Fe (II), and chelates potential interferents such as Cu(II), whereas reagent B (ferene) chelates Fe (II) to form the coloured complex. The reference pad comprises the same (white) material as the sensing pad but has no reagents. In summary, the sensing pad facilitates processing of iron, containment for chemical reactions, and production of color change, whereas the reference pad does not accept sample and is present for reference lighting conditions during the measurement. The color change is read via reflection of light resulting from the white LED incident light on the sensor surface. The sensor housing was designed in collaboration with SolidWorks. The sensor was 3D printed using an Ultimaker 3 printer requiring Polylactic acid (PLA) feed polymer.

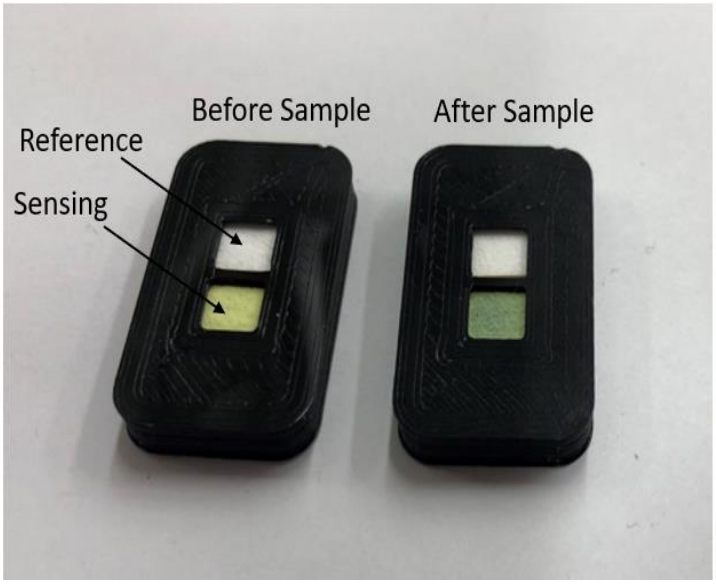

Figure 12: Sensor strip sensing and reference pads before (left) and 5 min after (right) delivering a 30 µL sample.

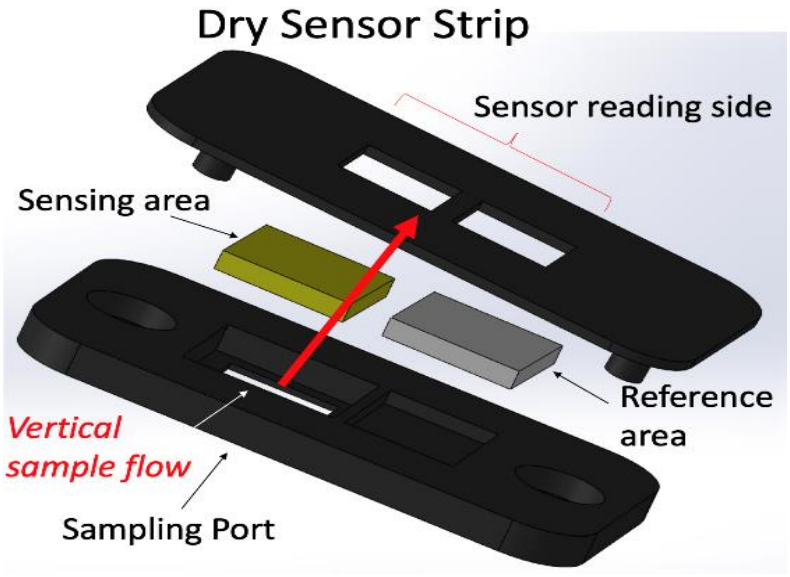

Figure 13: 3D printed design and assembly of the sensor strip.

In order to estimate the final reagent concentration ratios in the dry sensor strip, 14 dried sensing channel blotting filter papers were weighed prior to and after reagent impregnation, calculating weight differences to determine the weight of reagents. Assuming the reagents in total (ascorbic acid, citric acid, thiourea, and ferene) were

absorbed maintaining their solution mass concentration ratio, the reagents' concentrations once rehydration occurred upon wetting with 30 µL samples were estimated. The results of the final local concentrations in the sensor are shown in **Table 3**.

3.2.2 Smartphone Mount

To secure the position of the sensor strip and to consistently control the smartphone camera's exposure to lighting, a chamber and mount were also designed to host an iPhone and the sensor strip. As shown in **Figure 14**, the iPhone is mounted an appropriate focal distance from the sensor strip. A battery-powered LED light source was mounted inside the chamber, requiring strategically placed lighting diffusers.

Figure 14: :iPhone mounted appropriate distance from sensor strip. All material is 3D printed to control position and LED lighting, for very little cost. The image shows the user inserting the sensor strip into the chamber.

Note that all sensor components: strip, mount and chamber sensor strips were designed and 3D-printed using SolidWorks and Ultimaker3 respectively. CAD designs of both the sensor strip and iPhone mount are shown below.

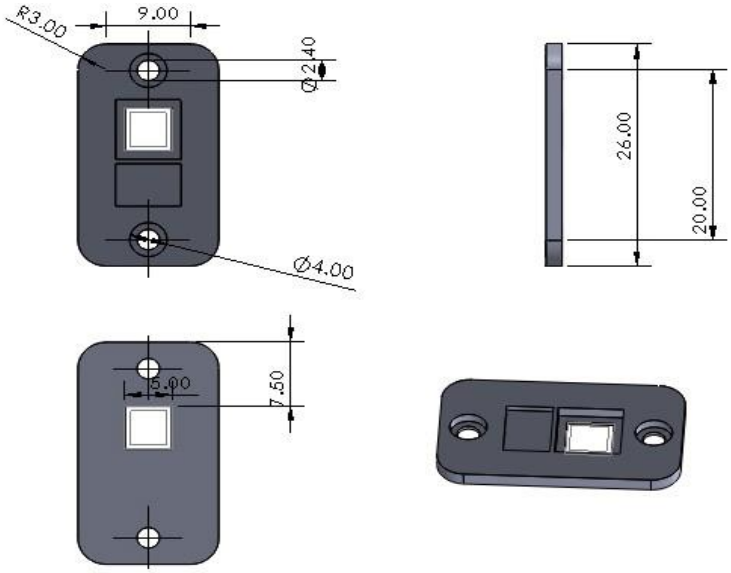

Figure 15: SolidWorks 2D Cad Design of sensor strip (bottom strip).

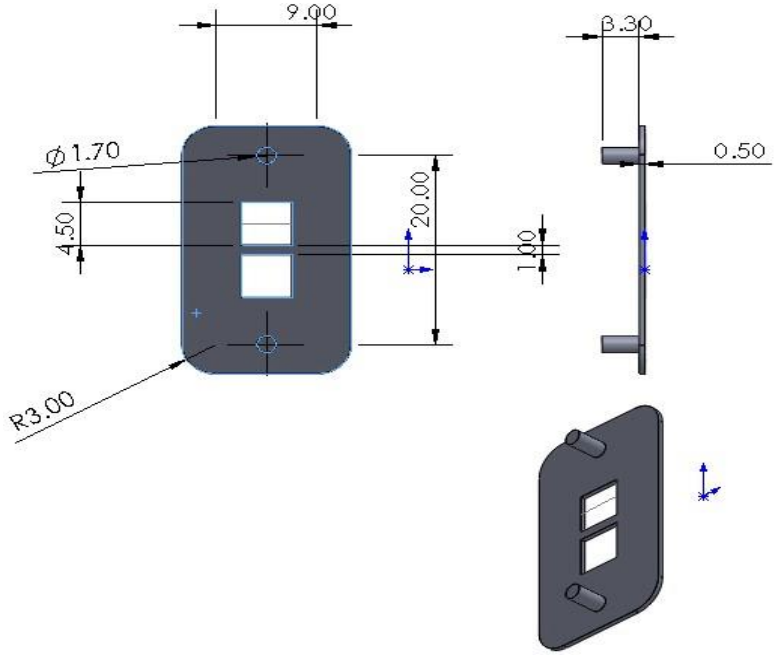

Figure 16: SolidWorks 2D Cad Design of sensor strip (top strip).

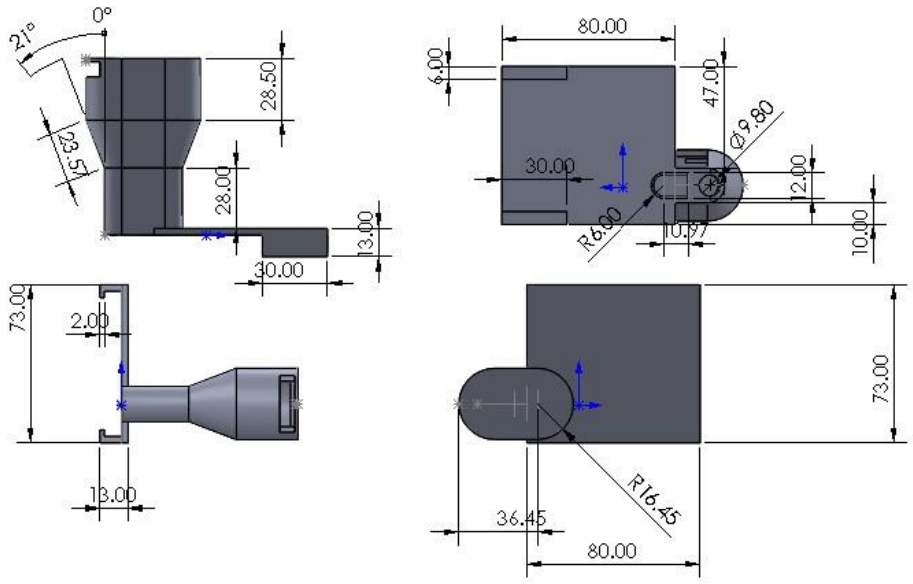

Figure 17: SolidWorks 2D Cad Design of chamber and mount.

Besides assumed ownership of a 2yr old or newer iPhone, the device materials were inexpensive to obtain or 3D-printable at $13 to build a prototype, whereas the cost of sensor strip components was near $0.07. In the future, the sensor strip will accommodate whole blood from human capillary puncture, but the minor changes in sensing pad material does not change the seven cents per use estimation. Therefore, a reduced cost of CLIA lab-based total iron measurements at $25.00 toward under $0.10 per measurement was achieved.

3.2.3 Smartphone Measurement of Iron on the Sensing Strip

Apple's iPhone provides high quality imaging hardware and software useful in precision colorimetry, offering at least an 12-megapixel iSight camera at 1.5µm pixels, autofocus, $f/2.2$ aperture, hybrid IR filter, exposure control, with the flash turned OFF[79]. Color changes from the sensing pad and white values from the

reference pad were electronically captured (images) and analysed utilizing an in-house iOS App developed for the iPhone and device (mount, chamber and strips). , iron standards (25 μg/dL to 300 μg/dL) were used to generate a calibration curve, followed by human serum samples with sensing and reference pads read by both technologies and absorbance signals calculated using the following equation:

$$\textbf{Absolute absorbance} = -\log\left(\frac{\mathbf{I}_{\textbf{sensing channel}}}{\mathbf{I}_{\textbf{reference channel}}}\right) [\mathbf{20}]$$

where I = intensity rendered from RGB component deconvolution of the colors.

3.2.4 Sensor Strip Stability to Heat Exposure

In order to explore the stability of the sensor to heat exposure, accelerated tests were performed by placing experimental sensors in an oven at 50 ^{o}C versus control sensors at room temperature of 20 ^{o}C for 2 days. Based on a predicted accelerated test algorithm, the accelerated aging factor (AAF) defined as the ratio of the room temperature estimated time and the accelerated aging time was as follows[80]:

$$\mathrm{AAF} = 2^{\mathrm{X}} \; [21]$$

with

$$\mathrm{X} = \frac{\mathrm{T_{heat}} - \mathrm{T_{room}}}{10} \; [22]$$

representing 16 days of accelerated aging with no loss in sensitivity.

3.2.5 Environmental Conditions' Effect on Sensitivity

The sensitivity of the sensor strips were studied at low and high temperature and relative humidity conditions ranging from 10^{o}C to 51^{o}C and 10% to 72%.

3.3 Mobile Technology Performance Evaluation

3.3.1 RGB Standards

Accuracy and speed/performance in deconvoluting a color surface was explored by testing the experimental iPhone App's RGB outputs when scanning 13 colors over the RGB spectrum. The 13 chosen colors (**Figure 18**) sufficiently represent the color spectrum with an aim of validating the hardware/software accuracy in the iPhone.

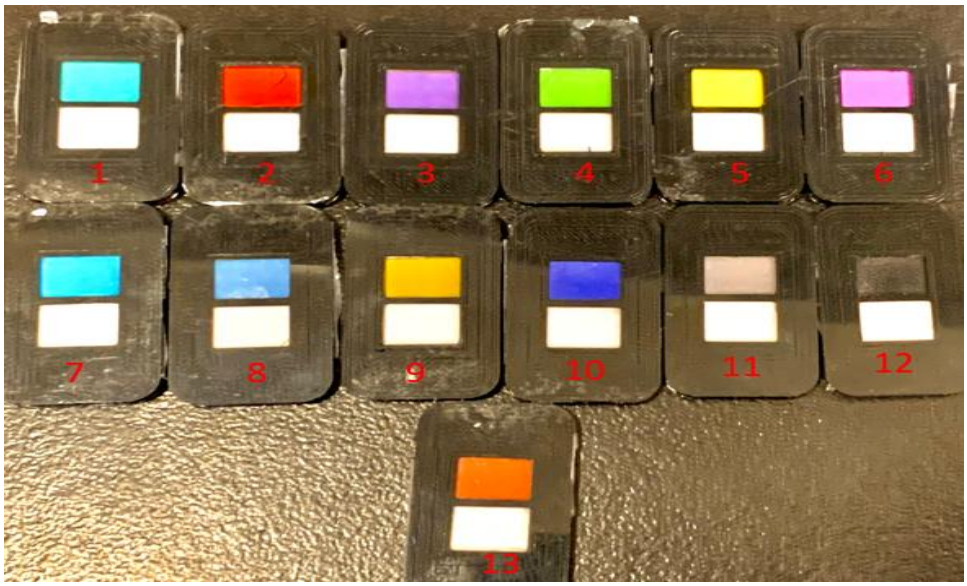

Figure 18: Thirteen sensors comprising of known RGB standards to be used for device validation.

3.3.2 Validation of Smartphone App with ImageJ

Correlation plots between the iPhone App's RGB output and ImageJ, a public image processing software developed by the National Institute of Health and the Laboratory for Optical and Computational Instrumentation were compared to determine the accuracy of the smartphone device. Twenty images per sensor (**Figure 18)** were analyzed with both methods.

3.3.2 Inter and Intra App Dispersion of Smartphone Device

In order to assess the dispersion of the smartphone device, inter and intra assay dispersions were calculated for each sensor in **Figure 18.** The former was determined by calculating the coefficient of variation of 20 consecutive images per sensor without modification of sensor position or lighting. This represents the systematic variations within the same assay. The latter is determined by taking coefficient of variation of ten cycles where each cycle represents the average RGB value of four images followed by removing the sensor strip, turning off the LED, and then turning it on again. This enables the assessment of systematic errors between different assays.

3.3.3 Rationale of Utilizing A White Reference

All sensors described in this work comprised of a sensing and a reference window. The rationale of using a reference window is a secondary control/ correction parameter. Since the phone and sensor strip positions were fixed and the sensing chamber was designed to isolate all external lighting interferences, then the same RGB signals should be obtained upon deconvoluting the reference area with intrinsic variability similar to the noise levels of the device if the same reference material was used in all of the sensors. This enables a more accurate measurement with the app in case, chamber sensing conditions abruptly change such as slipping of the sensor strip, burning of LED or unexpected perturbation to the system.

3.4 Design and Performance Evaluation of Optoelectronic Reader

3.4.1 Optoelectronic Chamber Design

The limitation with the smartphone technology is in the hardware and software changes that are implemented to smartphones every year (size of phone, camera position, number of cameras, focal length of each lens). Therefore, to accommodate these changes, modification of the chamber design and app algorithm are required. In addition, even though the novel mobile-based technology is very promising for point of care applications, the end-goal is to produce a device that resembles a glucometer-like device that relies on converting an electronic signal to a concentration reading. Herein, an alternative detection platform is presented that relies on a circuit board comprising of an LED at a specific wavelength centered equidistantly between two photodiodes. The mechanism of detection involves measuring the reflected light from both the senor and reference windows. Each window reflects a fraction of the light intensity to the corresponding photodiode where a potential difference is obtained. A circuit schematic as well as the CAD designs of the chamber are shown below.

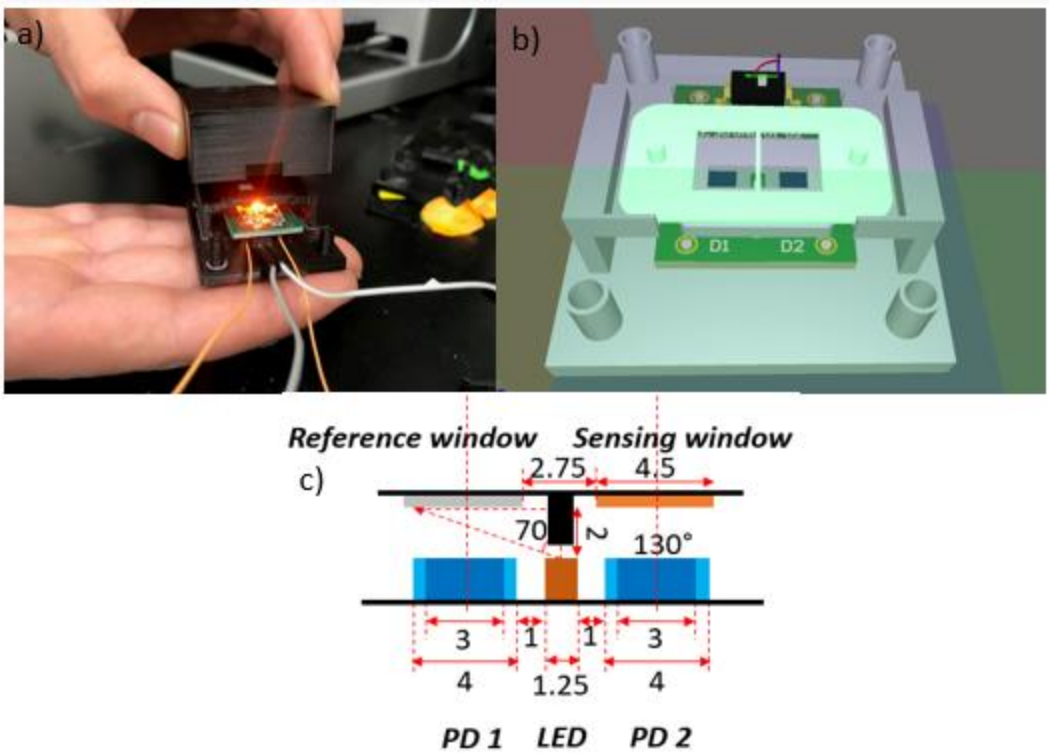

Figure 19: Optoelectronic reader design with a) 3D-printed prototype in operation b) CAD design of assembly c) schematic comprising of the two photodiodes and LED.

3.4.2 Assessment of Optoelectronic Noise Levels

Noise levels were assessed by determining the coefficient of variation of the sensing and reference photodiodes.

3.4.3 Calibration curve with Iron Standards

Finally, the same iron standards that were used to build the smartphone app calibration curve were used with he optoelectronic reader. The same mathematical analysis was performed, and absorbance values were calculated from potential difference readings from both photodiodes. The LED wavelength that was selected was 610 nm which emits an orange light. The rationale for selecting this specific wavelength is that the ferene complex has a maximum excitation wavelength between 590 nm and 610 nm.

3.5 Iron-binding Capacity Methodology

3.5.1 Optimized Protocol for TIBC Measurements with Ferene

The method developed in the lab is based on the protocol designed by Ramsay and is devised to accommodate the extreme cases where an iron-overloaded blood donor might present with 100% transferrin saturation, and so the measurement protocol adding of iron (III) should end with all additional iron being unbound. In the other extreme, an iron-deficient blood donor might present below 15% saturation. According to literature, the concentration of unsaturated iron can range between 0 (iron overload patient demonstrating high transferrin percent saturation) and 5 ug Fe/ml (iron deficient patient demonstrating low percent saturation) and thus, a sufficient yet conservative amount of iron was added (to a 1 ml serum sample, 2 mL of 500 ug/dl iron (III) standard was added as well as 200 mg of $MgCO_3$ as described in the original paper). This should yield a molar ratio of $MgCO_3$ to iron of 13,100 :1 respectively ((absurdly high). To reduce the amount of $MgCO_3$ dissolved, the amount of magnesium carbonate was reduced from 20,000 ug of $MgCO_3$/ ug of added iron (III) to 4000 ug of $MgCO_3$/ ug of added iron (III). It is also recommended to add 0.5 volume of a 2000 ug/dl standard/ volume of sample to operate at higher concentrations of iron even though the same amount was added. The chronological steps of TIBC procedure is shown below:

- To one volume of sample, add 0.5 volumes of 2000 ug/dl iron (III) standard solution Mix them sample for 15 minutes.
- Add 4000 ug of $MgCO_3$ / ug of added iron. Use high intensity shakers for 30-50 minutes to mix the samples followed by centrifugation at 3000 rpm for five minutes.

- Apply the same optimized protocol discussed in chapter to the supernatant fluid.
- Note that the dilution factor of 1.5 must be factored in due to the addition of iron (III) saturating solution in step 1.

3.5.2 Validation of Specific Binding of Magnesium Carbonate

In order to validate the specific binding of magnesium carbonate to free iron, 5 mg of $MgCO_3$ were added to both a 500 ug/dl standard as well as a serum sample with known iron concentration and the same reference method for TIBC was applied (mixing for 30 minutes followed by a 5 minute centrifugation). Control samples were also prepared by conducting the same procedure on exact replicates of the samples without addition of magnesium carbonate. Two outcomes are expected: a decrease in iron concentration with the standard sample due to specific binding of magnesium carbonate and no changes in absorbance readings with the serum sample to due to poor specificity of $MgCO_3$ to iron (III) bound to transferrin.

3.5.3 TIBC and Percent Iron Saturation in Serum samples

Similar to the agreement tests that were analyzed between total iron measurements with the developed assay and the reference method, similar strategies were implemented to test the accuracy of measuring TIBC, percent iron saturation and UIBC with the novel assay. Each serum sample was divided into four different volume samples. One volume sample was used for iron measurements using the spectrophotometric optimized reference method**.** The second volume was utilized to measure iron levels using the novel sensors**.** The modified protocol for TIBC measurement was applied to the third and fourth sample volumes. However, the supernatant of the third sample volume was detected via spectrophotometry and was considered as the reference method while the fourth sample

volume was applied to the same novel sensor previously discussed. A clear illustration of all methods is displayed in **Figure 20** for reference and experimental TIBC, UIBC and percent iron saturation are obtained:

Reference TIBC = C

Reference UIBC = C-A

Reference percent saturation= A/C

Experimental TIBC = D

Experimental UIBC= D-B

Experimental percent saturation = B/D

Correlation plots and percent Bland Altman plots were used to analyze agreement between the experimental and reference method for total iron binding capacity.

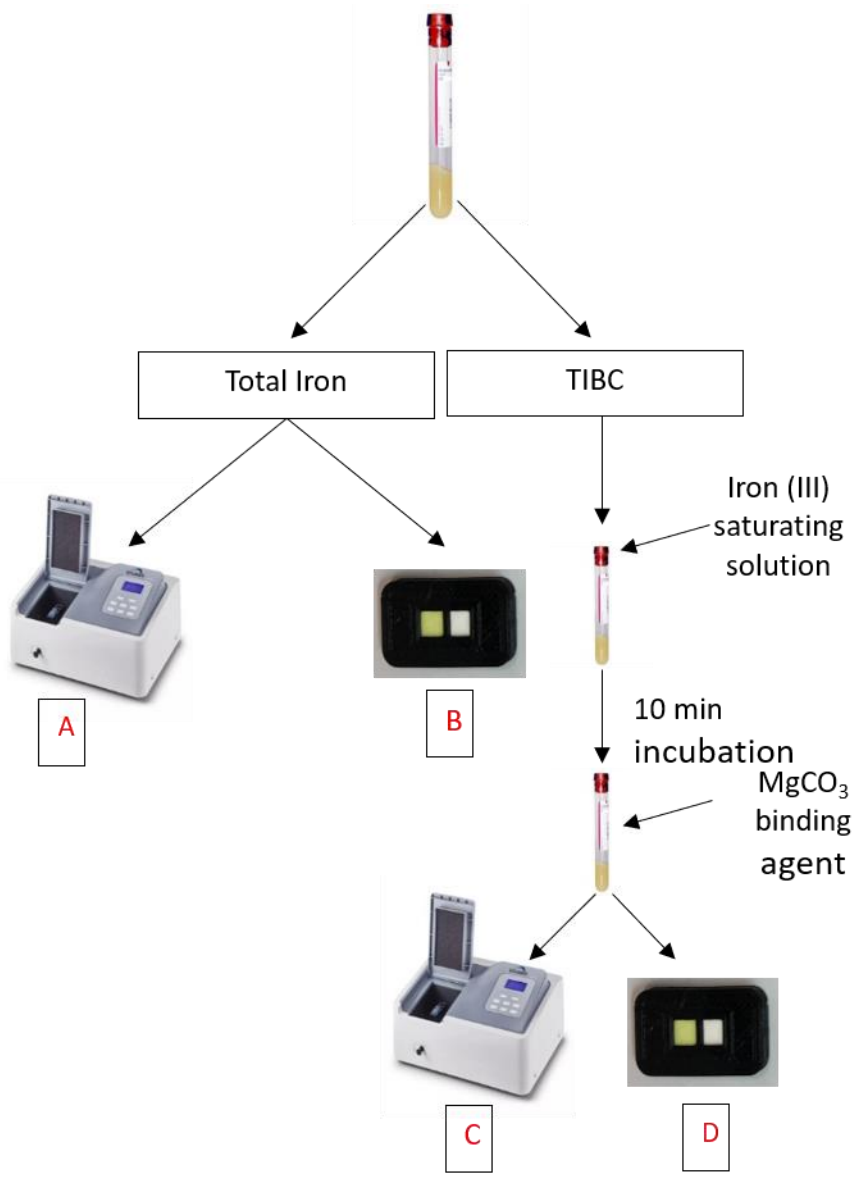

Figure 20: Methods for determining reference and experimental total iron, TIBC, UIBC and percent iron saturation.

3.6 Detection of Total Iron from Whole Blood Samples

3.6.1 Generation 2 Sensor Strip Design

For point of care application, the final assay should host whole blood samples and output accurate measurements without any sample modification. With this said, Various

research groups and private companies have tried to isolate serum at the point of care with various paper membrane arrangements, volume increasing approaches, or even utilizing pressure differentials to enhance the capillary wicking effects of paper. However, challenges such as low rates of retained volume, slow capillary wetting, slow color development and above all, weak recovery rate of analyte in the filtered plasma were observed. To overcome these challenges, the sensor strip comprised of four unique membranes that were tightly squeezed together as a stack (vertical flow of sample). The first layer was chosen to be highly porous and thin at 0.1 mm thick. It is hydrophilic nylon, functioning to capture the entire sample volume and attract it evenly onto the surface. No filtration takes place with this membrane. The second layer comprised a fiberglass membrane of pore size 3.1 μm and 1.0 mm thick whose function is to filter out the bulk of the red blood cells. The third layer was asymmetric in porosity, from 17 μm down to 1.3 μm and 330 μm thick polysulfone membrane designed to trap the remaining red blood cells. Finally, the fourth layer was a hydrophilic nylon membrane of 0.45 μm porosity and 2 mm thickness, embedded with the working reagents to receive the filtered plasma where iron is stripped from the transferrin molecule, reduced to iron (II) and chelated with ferene resulting in a color change. A reference window comprising of a white reference blotting paper was used. This reference area is not embedded in any reagent and functions for control of lighting within the chamber. A detailed schematic of the sensor device is shown in **Figure 21.** Several important features of the sensor strip include a compressed height and a groove. The compressed height ensures mechanical compression of the membranes enhancing capillary action between the layers. Without membrane compression, non-consistent wetting as well as build-up of fluid on the sampling port are observed. In addition

a a bottom groove enhances the trapment of the fluid within the confined membrane area. The Sensor strips were designed using SolidWorks and then 3D-printed with Ultimaker 3 using PLA filament.

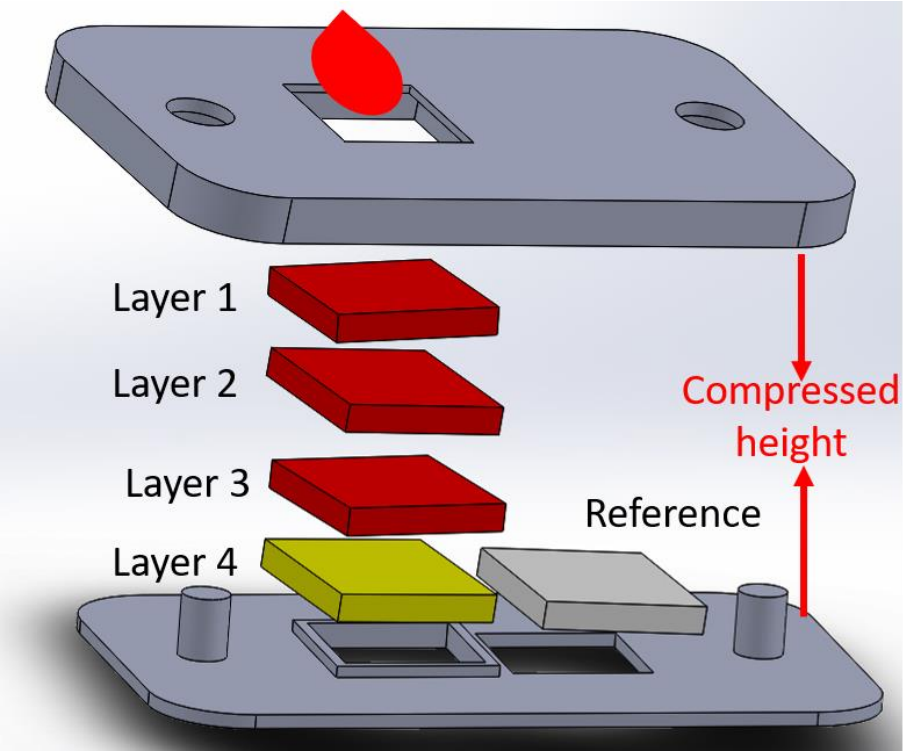

Figure 21: vertical flow sensor strip design comprising of four layers tightly squeezed with a compressed height as well as a groove. Layers 1,2 and 3 function to accept blood and filter cellular component from plasma while layer 4 contains the working reagents

3.6.2 Characterization of Whole Blood Separation

Two different methods were used to characterize whole blood filtration. After applying 50 ul of sample to the sensor strip, the sensor was disassembled once the fluid has dried and camera images of layers 1 to 3 were obtained. The same membranes were also imaged with a scanning electron microscope.

3.6.3 Sensor incubation time

To determine the optimal incubation time of measurements, eight replicates of one whole blood sample were tested at 2 minutes, 5 minutes and 7 minutes. To imitate current

POC devices, incubation times greater than 7 minutes were ignored. The absolute signal magnitude as well as the signal to noise ratio at these three instances were compared.

3.6.4 Testing Conditions and Sample Preparations

Fourteen venous blood draws were obtained through Arizona State University's IRB protocol (STUDY00008255). 50 ul of each sample was applied to the sensor strip and a smartphone measurement was obtained five minutes after sampling. The same whole blood sample was then processed via centrifugation and a 96- well plate spectrophotometric measurements was conducted (the optimized reference method) on the supernatant with the following operating conditions: Spectra Max M5 instrument, endpoint analysis at 590 nm wavelength and a total volume of 250 ul per well rendering a path length of 0.6 cm.

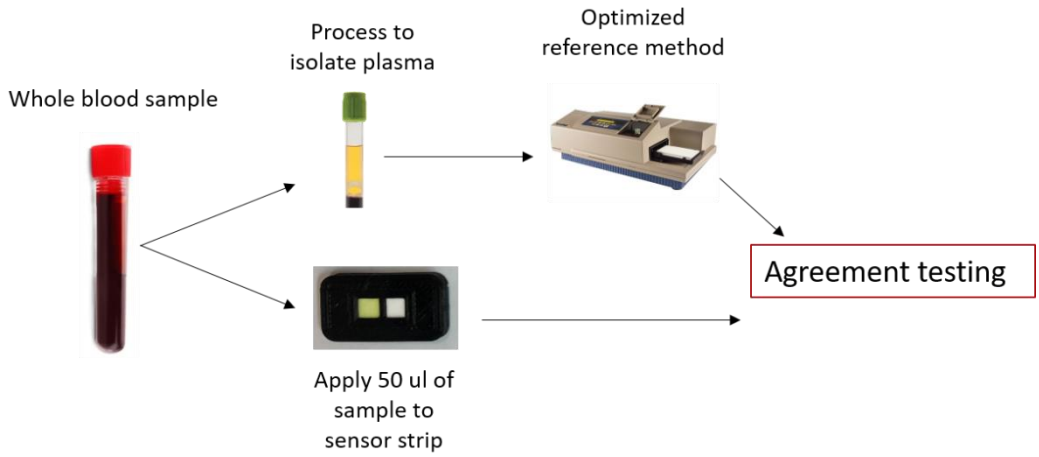

Figure 22: Schematic of experimental design. 50 ul of whole blood sample is applied onto the sensor strip and a measurement is taken after five minutes. Simultaneously, the. Blood sample is processed, and the obtained plasma is analysed with the optimized reference method

CHAPTER 4

RESULTS AND DISCUSSION

4.1 Validation of Reference Methods for Total Iron Measurement

4.1.1 Optimized Method for Iron Measurement

Calibration curves based on the absorbance changes at 590 nm as a function of the iron standard concentrations were made, presenting a linear dependent signal as a function of the known iron concentration. The sensitivities of the optimized (and original reference methods were 0.00093 and 0.00072 a.u./µg/dL) respectively, with a regression coefficient of 0.99 for both methods (**Figure 23**). The CVs of the optimized and original methods for the iron standards were 2.2%, and 3.7%, respectively. Thus, the sensitivity of the optimized method was 30% greater than the original method while the CV of the optimized method was 40% smaller than the original, giving a higher-quality method against which to test the results of smartphone analysis of total iron in human subjects' serum samples.

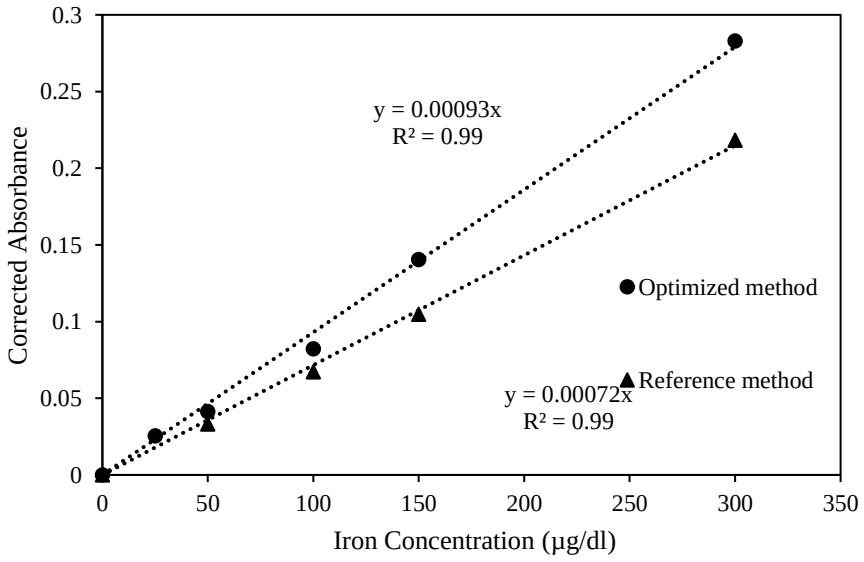

Figure 23: Calibration curves compared. The reference spectrophotometric method is a 5:1:1 volume ratio (reagents A to ferene to iron standards) and without surfactant, giving a slope of 0.00072. Optimized method with 3:1:1 volume ratio, increased sensitivity by 30%, providing a slope of 0.00093.

4.1.2 Measuring the Effect of Protein Precipitation

While the original reference method performs well on iron standards, it is highly variable with serum samples, resulting in unpredictable fluctuations throughout 60 minutes incubation. **Figure 24** shows an example profile of iron detection absorbance changes at 590 nm vs time for a known serum sample of 231 μg/dL total iron, for both the original reference and optimized reference method. At minute 10, the original method (circles) is already four times greater (and growing) than that of the optimized method (squares). To investigate whether the turbidity in the original method's solutions contributed to the unpredictable and greater absorbance values, measurements at a non-absorbing wavelength for the iron complex, 730 nm (triangles) were conducted. These non-zero absorbance values and high fluctuations were indeed indications of interfering turbidity. As a result, surfactant was removed for all future use as a reference method, as well as for the sensing strips design. For inter-laboratory validation, two of the venous blood samples were sent to LabCorp and reported to be 231 μg/dL and 203 μg/dL respectively. The same samples were analysed with the optimized method which resulted in 238 ± 18 μg/dL and 206 μg/dL ±10μg/dL , which confirmed the decision to eliminate the surfactant. In addition to sensitivity improvement, removing the surfactant shortened the detection time from 30 minutes (as indicated in the protocol of the original reference method) to 2 minutes.

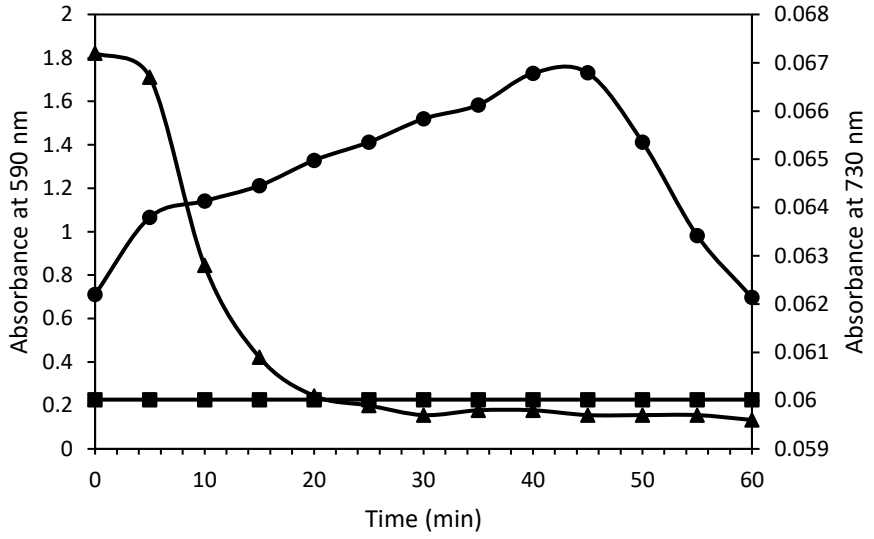

Figure 24: Left y-axis: Known serum sample with 231 μg/dL total iron absorbance change at 590 nm over time using a) the original reference method (•) and b) the optimized method (squares). Right y-axis: Same known serum sample (231 μg/dL iron) at 730 nm.

4.1.3 Specificity of the Optimized Method

The optimized method's iron detection response to 50 μg/dL of iron at 590 nm was compared to potential interferents, each concentration representing the high end of "normal" in otherwise healthy adults. **Figure 25** shows that interfering signals from these most common and abundant molecules in blood, that is, from glucose, creatinine, uric acid, potassium chloride, sodium chloride, and urea, were sufficiently low to proceed.

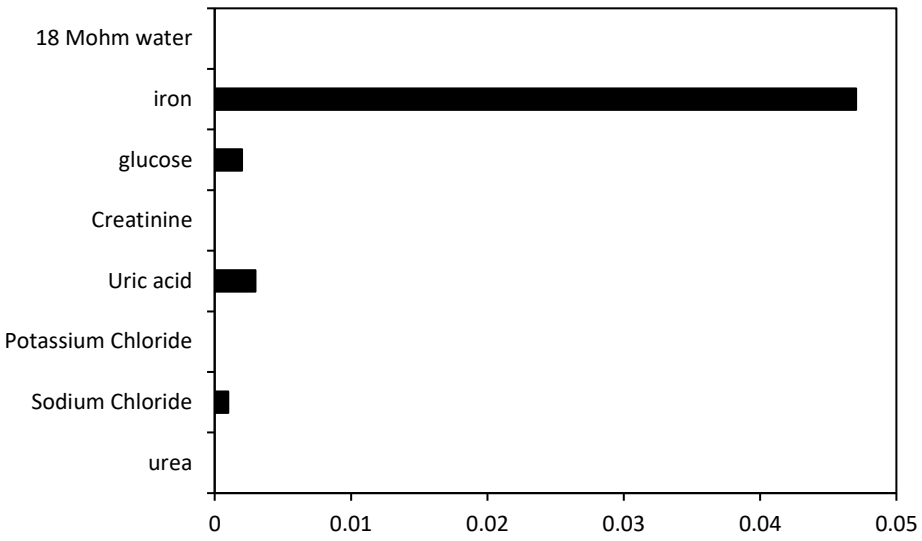

Figure 25: Specificity test (optimized method). Comparison of the corrected absorbance values of 18 MΩ water and iron standard (0.05 mg/dL) to: glucose (140 mg/dl), creatinine (1.2 mg/dl), uric acid (7 mg/dl), potassium chloride (20 mg/dl), sodium chloride (333 mg/dl).

4.1.4 Kinetics results With Optimized Method

Spectrophotometry was used to measure the changes in color for the optimized method, with the slope of the calibration curve, a known path length of 0.6 cm, and the Beer-Lambert law used to provide kinetic analysis. A molar extinction coefficient for the Fe(II)-ferene complex (COM) of 33,366 $L.cm^{-1}.mol^{-1}$ was found, comparable to published results (34,500 $L.cm^{-1}.mol$) [23]-[24]. The rate of the Fe(II) - complex (COM) formation in presence of ascorbic acid (AA), oxidizing to dehydroascorbic acid (DAA) (k) is as follows:

$$2Fe(III) + H\text{-}AA\text{-}H + 6ferene \xrightarrow{k} 2[Fe(II) - 3ferene] + AA + H_2$$

Considering that the AA concentration was in excess, the overall reaction rate (k') was simplified to:

$$\text{Fe(III)} + 3\text{ferene} \xrightarrow{k'} \text{Fe(II)} - 3\text{ferene}$$

AA in excess

Under the above-described conditions, the reaction order for iron (α), and ferene (β) was determined according to the following rate law:

$$\frac{d[COM]}{dt} = k'[Fe^{3+}]^{\alpha}[\text{ferene}]^{\beta}$$

Absorbance time profile as well as their derivatives were obtained via spectrophotometry for two different cases: ferene concentrations were held constant while iron concentrations were varied and the second case where iron concentrations were held constant and ferene concentrations were varied and the plots are shown below:

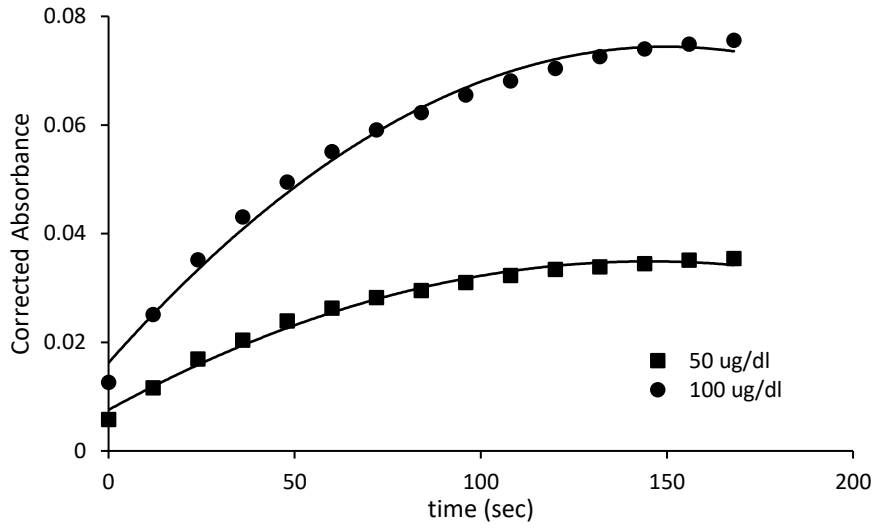

Figure 26: Absorbance profile for two iron standards: 50ug/dl and 100 ug/dl respectively at a ferene concentration of 4 mM.

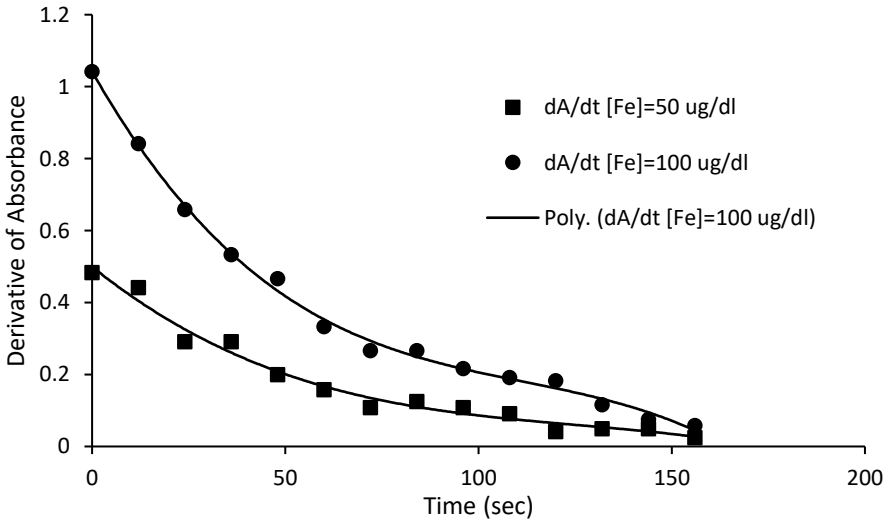

Figure 27: Derivative absorbance profile for two iron standards: 50ug/dl and 100 ug/dl respectively at a ferene concentration of 4 mM.

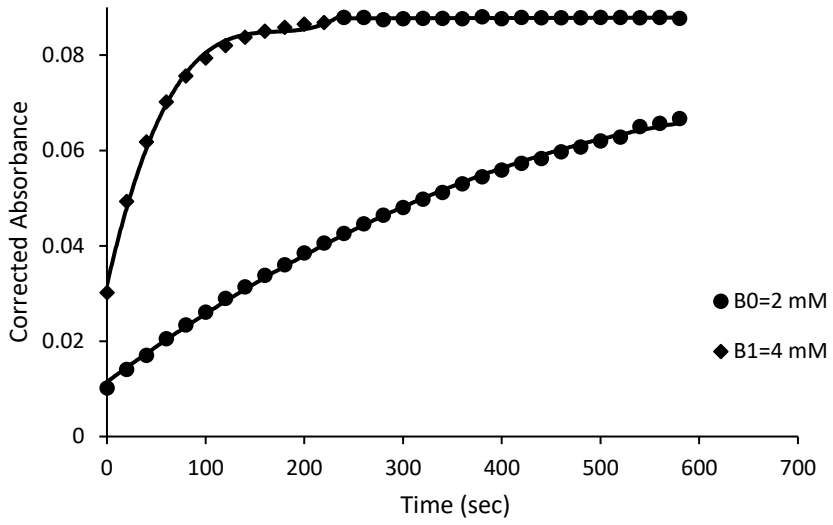

Figure 28: Absorbance profile for two ferene concentrations: 2 mM and 4 mM respectively at an iron concentration of 100 ug/dl.

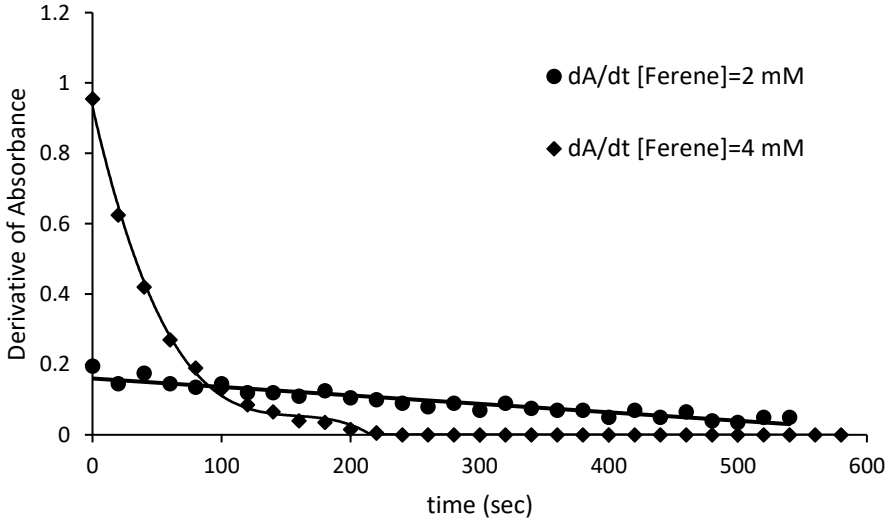

Figure 29: Derivative absorbance profile for two ferene concentrations: 2 mM and 4 mM respectively at an iron concentration of 100 ug/dl described in the numerical section, points at 10, 20 and 30 seconds were used to determine the rate orders as well as the rate constant and the modified rate constant.

Table 4: Kinetic Parameters of Reaction rates (k, k') and Reaction Order for Iron (α), and Ferene (β) from Studies of the Ferrous Complex Formation in Presence of Ascorbic Acid (AA) in Excess.

Parameter	Value
Alpha (α)	1.2
Beta (β)	2.3
k' ($mM^{-1.47}s^{-1}$)	0.089
k ($mM^{2.47}$ s^{-1})	0.0044

4.2 Total Iron Characterization with Mobile Technology

4.2.1 Smartphone Calibration Curve and Dry sensor Strip

The same iron standards used to construct the calibration curves of liquid phase methods were applied to the sensing strip and processed by the iPhone App and ImageJ. **Figure 30** describes screenshots of the iPhone App display, (a) upon receiving a sample on the (yellowish) sensing pad in comparison to the white reference pad and (b) results following RGB analysis. **Figure 31** provides a striking color comparison between 50 – 1000 µg/dL concentrations of iron standards, including the blank and a human serum sample.

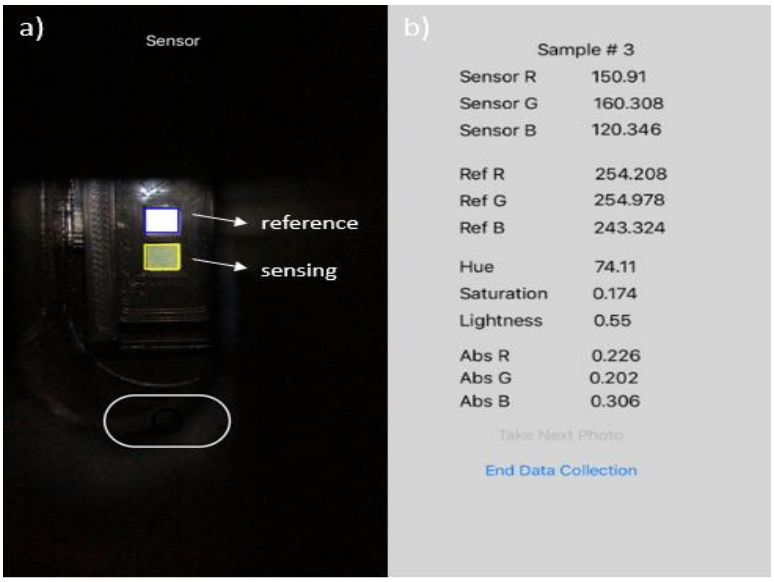

Figure 30: Smartphone application user interface showing a) camera's view of the sensing and reference channels on the dry sensor strip and b) iOS app output screenshot after sensor strip image is taken.

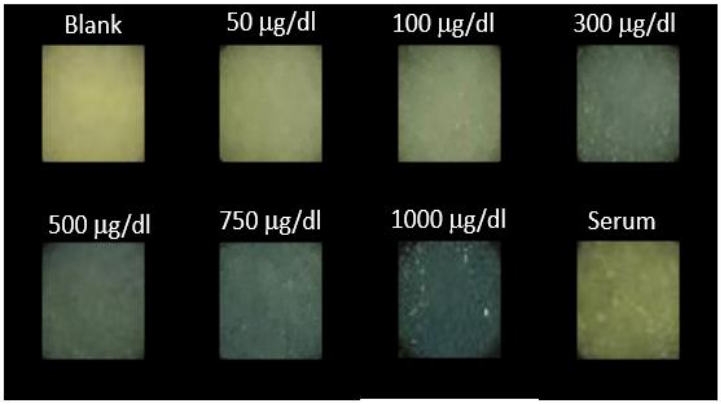

Figure 31: Smartphone application's images of the sensor strip's sensing area upon exposure to increasing iron ion standard concentrations and to serum.

those obtained with ImageJ processing, revealing negligible differences. The Red component consistently produced the most sensitive data, with a slope of 0.00049, r^2 = 0.96, and CV of 10.5%, compared to Green (0.00032, r^2 =0.97), whereas Blue was not sensitive to the iron concentrations. Red was thus chosen as the sole sensing signal for producing the calibration curve from the iPhone App (example shown in **Figure 30**). Furthermore, the smartphone's outputs were verified

by the reference method of ImageJ, giving confidence to move forward with blood serum sample analyses and comparison to spectrophotometry. (Refer to chapter 2). Last, in development of a calibration curve from the iPhone, an estimated detection limit (LoD) of 16.5 µg/dL total iron concentration was calculated from the assessed sensitivity, and by assuming a signal equal to 3 times the noise level from 30 blank samples (marked with a red asterisk at 16.5 µg/dL in **Figure 32**) [81, 82].

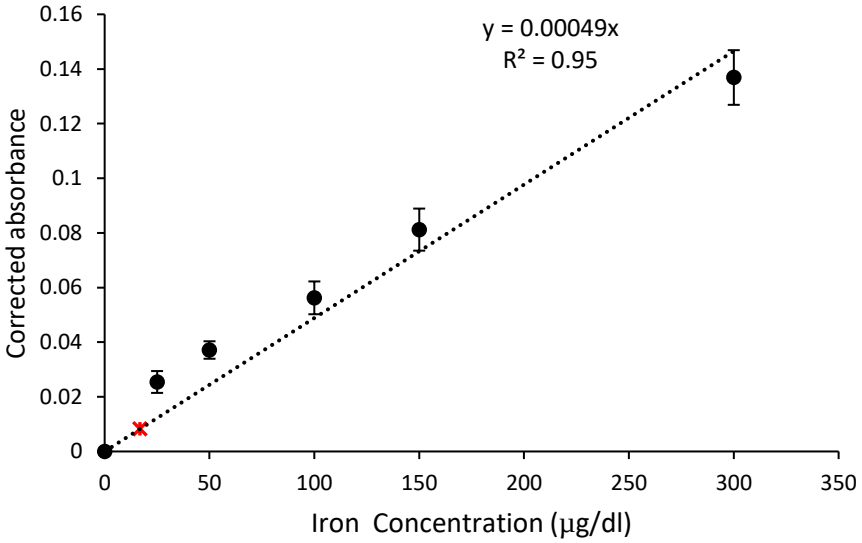

Figure 32: iPhone-produced calibration curve from 25-300 µg/dL resulted in a slope of 0.00049, comparable to the spectrophotometric 0.00093 in **Figure 21**. Average values are marked with +/- 1 standard deviation. The estimated limit of detection was 16.5 µg/dL, marked with a red asterisk.

4.2.2 Specs Analysis of Reference Method and Sensor Device

Table 5: Specs Comparison of Optimized Reference Method and Novel Device. The Following Parameters were Investigated: Sensitivity, Incubation Time, Reproducibility, Limit of Detection, Dimensions, Cost and Sample Volume.

Specifications	Optimized Reference Method	Smartphone Device
Sensitivity	0.00093 a.u/ ug/dl	0.00049 a.u/ug/dl
Incubation time	5 minutes	5 minutes
Reproducibility	C.V= 2.2%	C.V = 10.5 %
Limit of detection	2.2 ug/dl	15 ug/dl
Dimensions	Bulky instrument (100 cm by 50 by 30 cm)	Reader: 5 cm by 3 cm by 8 cm Sensor strip: 2.5 cm by 1.7 by 0.3 cm
Cost	Cost of instrument ($ 5,000) Cost of operation: ($30)	Cost of reader: $ 13 Cost of operation < 10 cents
Sample volume	10 ml venous blood	50 ul blood sample

We start by comparing the specifications of the optimized reference method to the novel sensor system. Both methods exhibit linear behavior over the clinical dynamic range of iron metabolism; however, the sensitivity of the novel system is almost half that of the optimized reference method and exhibits higher dispersion as shown in **Table 3**. While the reference optimized method, the golden standard method for iron detection is the more robust instrument for iron detection, the novel sensor is cheaper (cost of one sensor is less than 10 cents while the approximate cost of a single a measurement with a spectrophotometer is approximately $30). In addition, the cost of a spectrophotometer is approximately $5000 while the cost of full operating sensor chamber is $13. Integrated with slick and portable designs, these sensors can be deployed globally. Above all, the major advantage of this device is no sample processing is required while whole blood process in required prior to testing with the spectrophotometric approach.

4.2.3 Environmental Operational Conditions of Use

The study of the sensitivity of the sensor strips and device at different environmental conditions allowed to conclude that while environmental relative humidity does not influence changes in sensitivity, the temperature affects sensitivity at 5 x 10^{-5} a.u / (μg/dL) / ºC. All results shown above were assessed at 23-25 ºC. However, with a parallel temperature sensor, the correct calibration factor could be applied to assess iron concentration at any temperature with the calibration temperature range between 10ºC – 50ºC (tested environmental operational conditions).

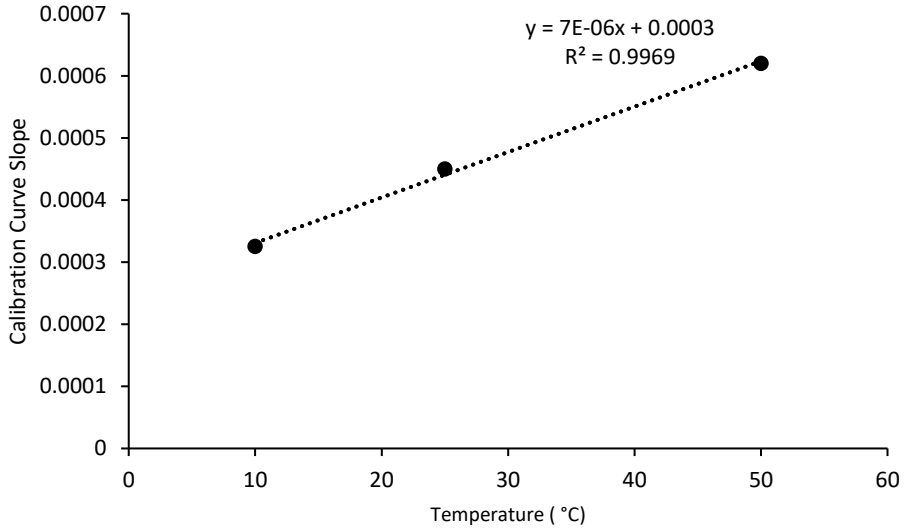

Figure 33: calibration curve sensitivity plot with temperature for the following ranges (10 ºC – 50 ºC).

4.2.4 Intra-laboratory Validation

Intra-laboratory validation: **Figure 34** shows the correlation analysis between the output iron concentration values from serum samples between the novel assay and the modified reference method with a slope of 0.95 and regression coefficient

of 0.98. Further, **Figure 35** shows the corresponding Bland-Altman plot that revealed a bias of -4% with lower and upper limits of agreements (95% CI) of 20%.

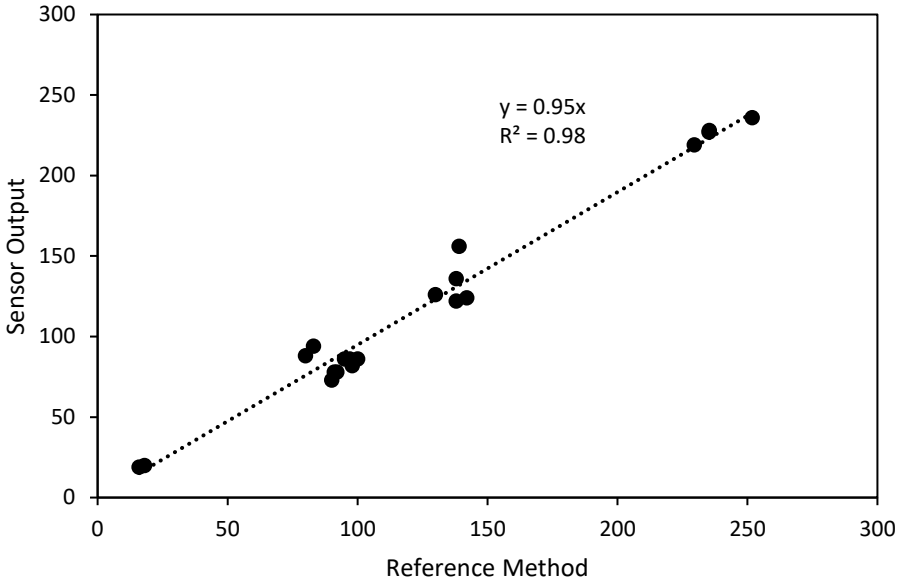

Figure 34: iPhone readings of dry sensor strips (x-axis) versus internal "optimized" reference method. (n=20).

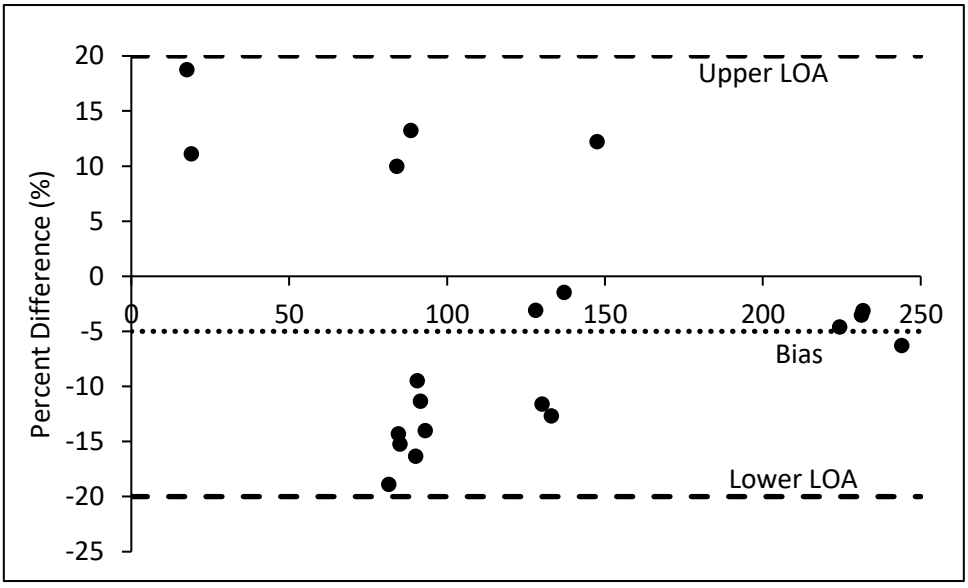

Figure 35: Percent Bland-Altman plot showed a bias of -4% and limits of agreements of 20% and -20% respectively. (n=20).

The Bland-Altman plot showed two important features. On one hand, a negative bias of 4% indicates that the device output is generally lower than the reference method, and thus, appropriate corrections can be taken to compensate for this difference. Second, the highest mismatch between the experimental and reference methods were recorded for low iron concentrations with maximum percent differences of 20% while this difference creeps down to 5% at high iron concentrations. For screening purposes, these mismatches can be overlooked. For example, in the extreme case where a person's serum iron is 20 ug/dl, the device output will range between 16 ug/dl -24 ug/dl; and thus, will accurately predict that the person is at risk of iron deficiency.

4.3 Evaluation of Mobile Technology Performance

4.3.1 Intra-laboratory Validation

As afore-mentioned, ImageJ was used as a reference imaging software to validate the accuracy of the app. Thirteen known RGB standards were printed and ten images were taken and analyzed with the app and ImageJ simultaneously. The resulting red, green and blue signals were analyzed by plotting correlation plots.

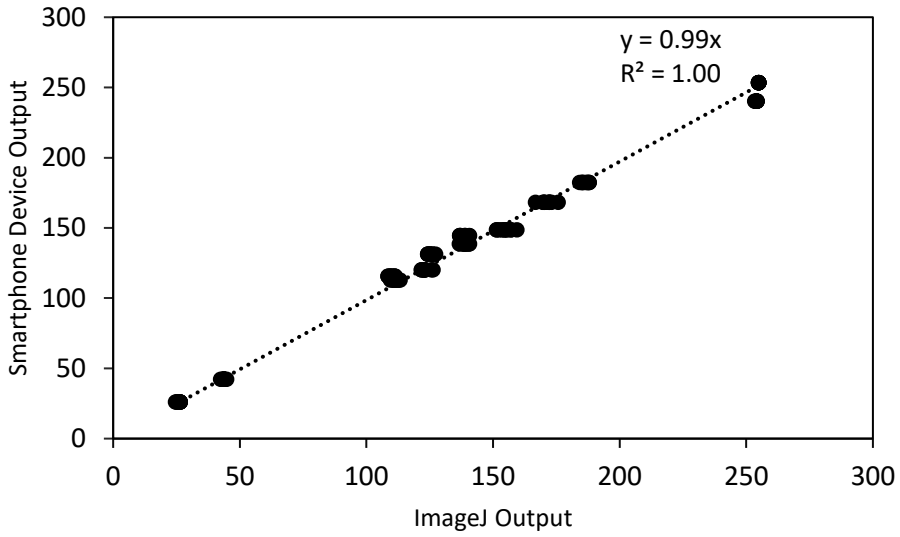

Figure 36: Correlation Plot between smartphone app and ImageJ for the red signal. The best fit curve is a straight line with slope of 0.99 and regression Coefficient of 0.99.

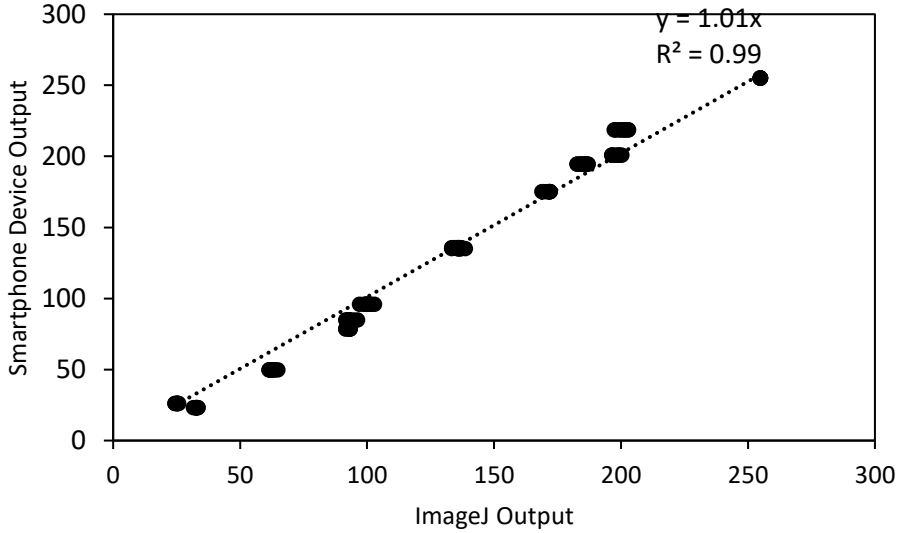

Figure 37: Correlation Plot between smartphone app and ImageJ for the green signal. The best fit curve is a straight line with slope of 1.01 and regression Coefficient of 0.99.

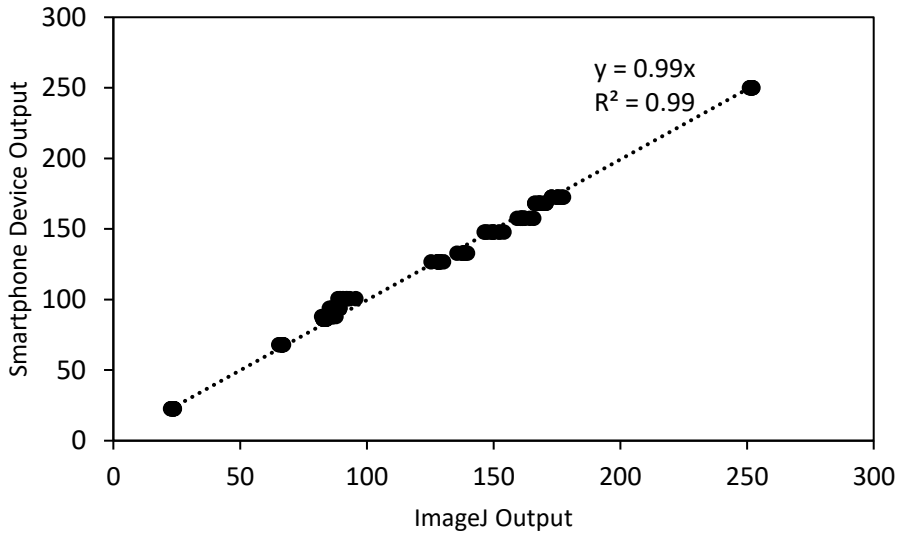

Figure 38: Correlation Plot between smartphone app and ImageJ for the blue signal. The best fit curve is a straight line with slope of 0.99 and regression Coefficient of 0.99.

For the three signals, the best fit curve was similar to the identity line with slopes between 0.99 and 1.01. This indicates that the app output agrees with the output of ImageJ and that the three deconvoluted signals accurately predict RGB color coordinates of the surface of interest.

4.3.2 Inter and Intra Dispersion Analysis

To assess the dispersion of the smartphone device, inter and intra coefficient of variations were determined for each sensor and are shown in the bar graphs below.

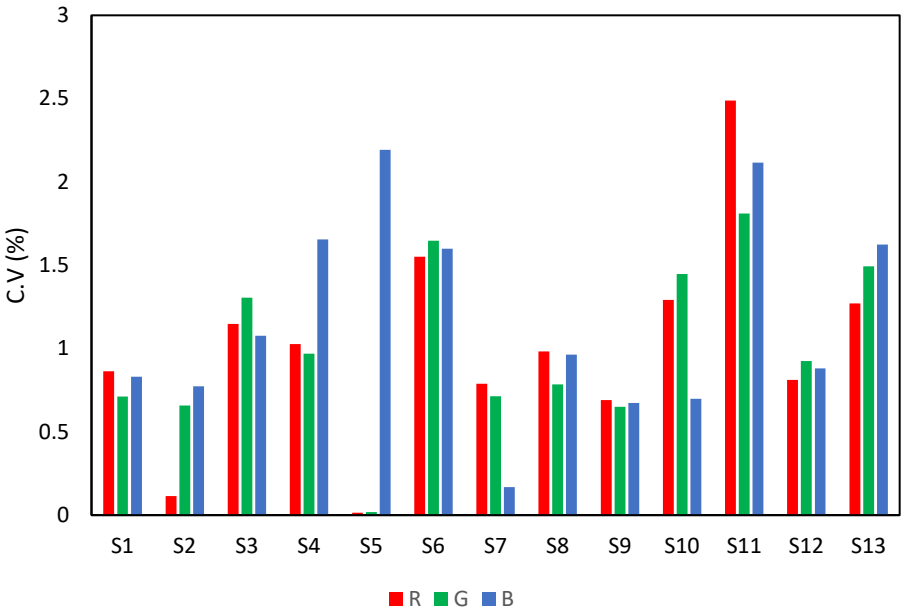

Figure 39: Intra-assay dispersion coefficient of variation of 13 RGB standards.

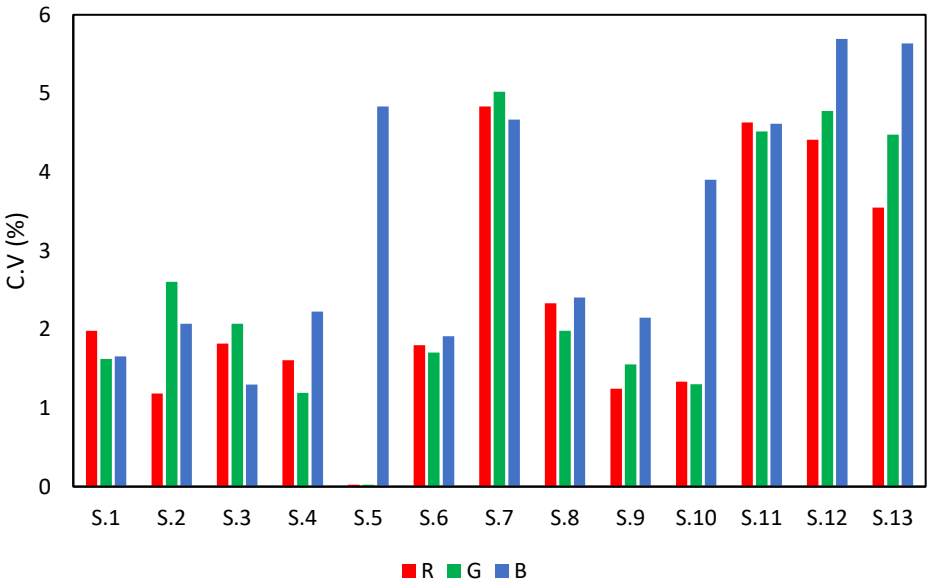

Figure 40: Inter-assay dispersion coefficient of variation of 13 RGB standards.

Two important features can be observed from these plots. On one hand, the device showed great reproducibility with an average intra-coefficient of variation of 1%. This indicates that the signal magnitude is a 100 - fold higher than the systematic noise in the app. With maximum coefficient variations of 2.5%, the system is quite robust and

reproducible. Note that these values reflect only intra assay-dispersion when no removal of sensors is done. In other words, these variations are caused by the phone (heating of device, inherent errors from iPhone 6s camera and app algorithm). With inter-assay dispersion, the average coefficient of variation was 2.73% which was almost 3 times that of the intra-coefficient of variation. This was expected since, this value reflects dispersion from different assays. To be exact, four images were taken at each cycle and between each cycle, the LED was turned off and back on and the sensor strip was removed and reinserted. Inter-assay dispersion was assessed by repeating the cycle ten times for each sensor. In addition to errors that caused intra-assay dispersion, errors from positioning the sensor and/or errors from LED intensity have led to a decreased signal/noise. However, even with this observed increase in dispersion levels, a signal to noise ratio of 40 was obtained with these sensors.

4.4 Validation of Optoelectronic Reader

4.4.1 Noise Assessment of Optoelectronic Reader

After introducing the electronic device design and its method of operation**,** the noise level was measured by calculating the coefficient of variation of the same 13 sensors used to assess the performance of the smartphone app**.** The CV(%) was determined by taking 10 different measurements per sensor and the results are shown in the graph below.

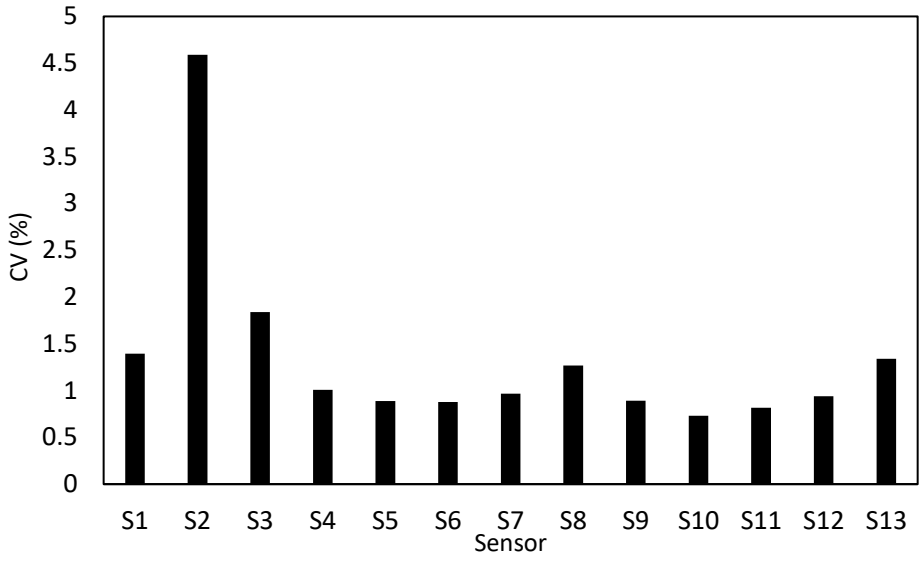

Figure 41: Evaluation of noise levels by calculation coefficient of variations of thirteen different sensors.

With an average coefficient of variation of 1.35%, the signal to noise ratio is 74 indicating that the device is highly reproducible.

4.4.2 Calibration Curve with Iron Standards

Next, calibration curves were determined using iron (III) standards that represent cutoff values for iron deficiency and iron overload with the following concentrations**:** 50 ug/dl, 150 ug/dl and 300 ug/dl.

4.5 TIBC Results

4.5.1 Validation of Specific Binding of Magnesium Carbonate

Upon the addition of magnesium carbonate to both a standard and a serum sample followed by mixing, centrifuging and addition of the working reagent as well as the chelating agent, the following concentration changes were measured and displayed in **Figure 42.**

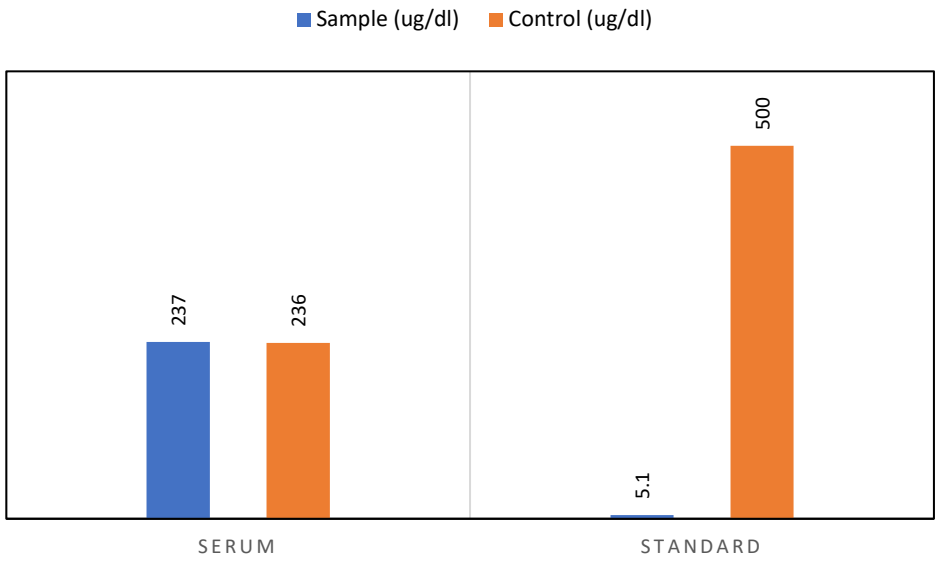

Figure 42: Validation of specific binding of magnesium Carbonate by performing the TIBC method on a Serum Sample and standard.

As hypothesized, iron concentrations with standard samples dropped from 500 ug/dl to 5.1 ug/dl indicating the precipitation of all free iron (III) ions as opposed to a 500 ug/dl with the control standard. No difference was recorded between the serum sample and control; thus, confirming that magnesium carbonate has high affinity towards free iron only.

4.5.2 TIBC and Percent Transferrin Saturation

In addition to total iron, TIBC and percent transferrin saturation were determined by plotting the total iron concentration from the sensor versus that of the optimized reference method (**Figures 43 and 44)** with TIBC correlation slope of 1.04 and regression coefficient of 0.91 and transferrin saturation correlation slope of 0.96 and regression coefficient of 0.82.

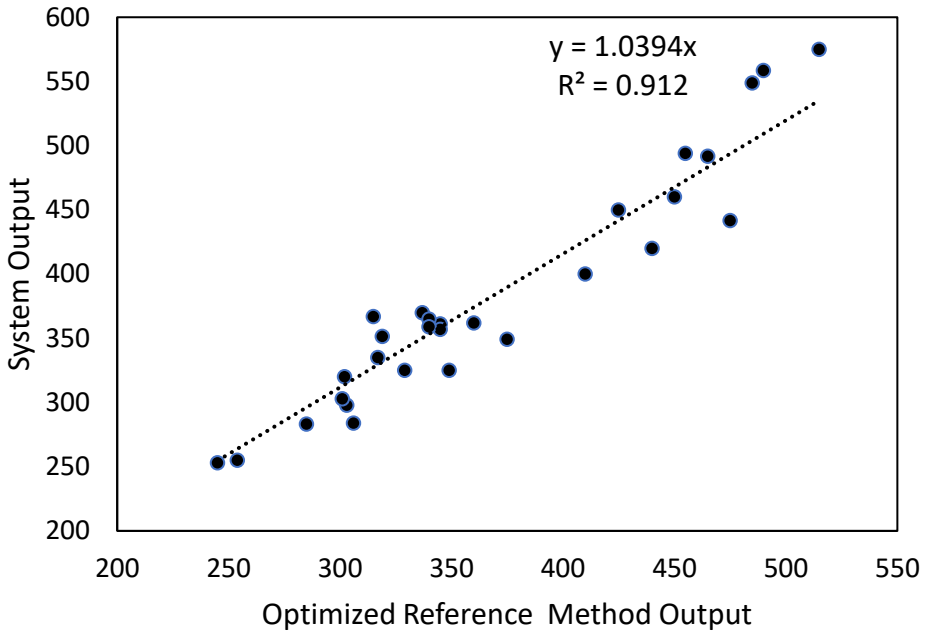

Figure 43: illustrates a correlation plot for TIBC measurements with plasma samples between system and optimized method with correlation slope of 1.04 and regression coefficient of 0.91

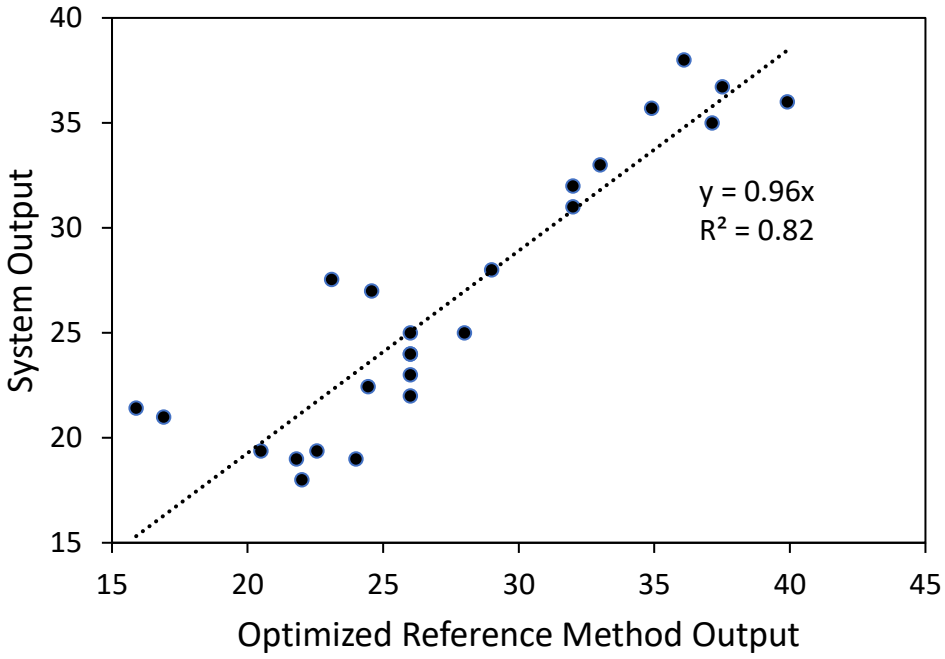

Figure 44: illustrates a correlation plot for transferrin saturation percentage with correlation slopes of 0.96 and regression coefficient of 0.82.

4.6 Total Iron Detection from Whole Blood Samples

4.6.1 Membrane Characterization for Whole Blood Separation

After sample application onto the sampling port of the sensor strip, the sensor was disassembled and images of layers 1, 2 and 3 were analyzed. Two interesting features is observed with the current membrane configuration. On one hand, it is obvious that the fiberglass membrane (image b in **Figure 45**) acts as the major red blood cells separating component as compared to the other two membranes. On another hand, the bulk of the filtered component is trapped in the area centered by the groove pressing on the membrane surface to ensure proper capillary action and prevent leakages from the edges.

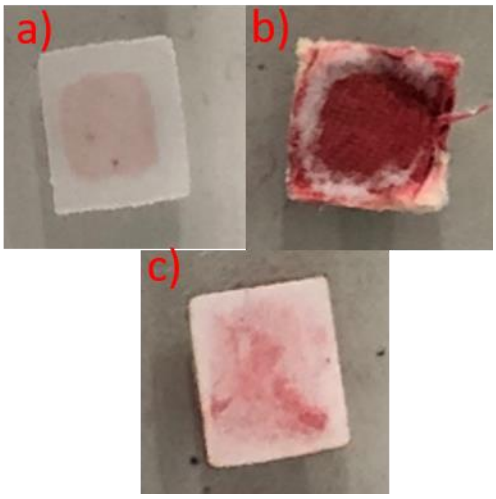

Figure 45: Macroscopic images of the membranes after sample application and drying with a) nylon sampling membrane, b) fiberglass membrane and c) polysulfone membrane

After the initial assessment of these membranes, a scanning electron microscopy (SEM) was conducted for further characterization of the fiber-glass and asymmetric polysulfone membrane since they act as the main filtration components in this system. **Figure 46 (a)** represents a cross-sectional SEM of the polysulfone membrane and shows varying pore size with thickness. The mechanism of separation involves a progressive

capturing of red blood cells where any unfiltered cellular components initially wet the coarse surface (large pore size) and gradually flow through the asymmetric structure of this membrane trapping any remaining red blood cells. Finally, at the fine surface, the only remaining sample is the filtered plasma. Images (c) and (d) are top-down SEM images of the fiber-glass membrane which shows its effectiveness in capturing red blood cells.

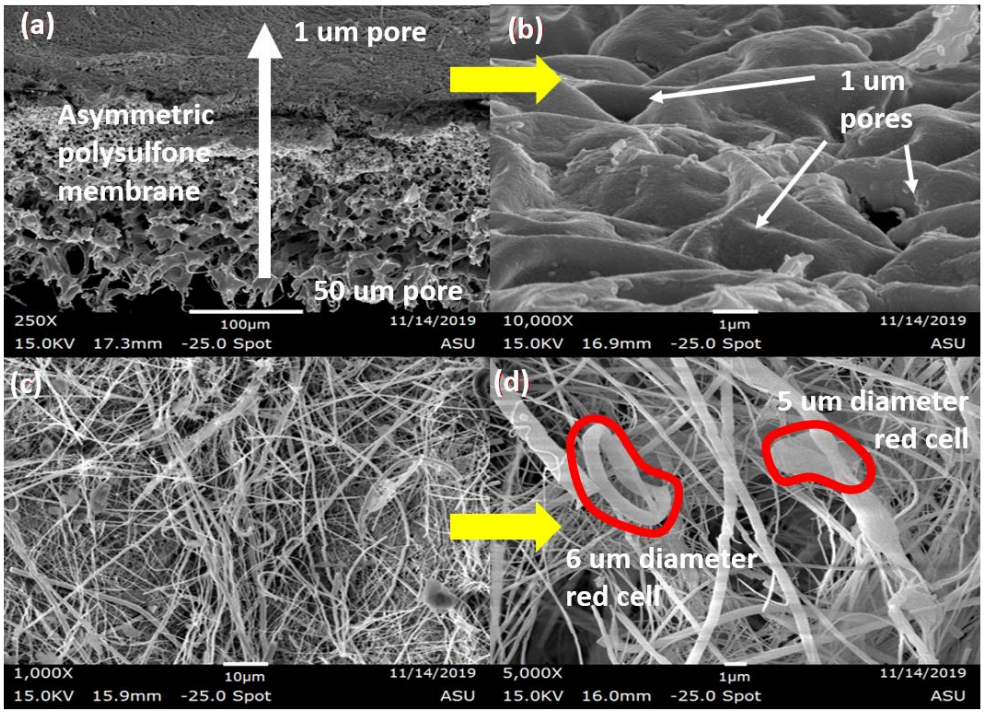

Figure 46: (a) and (b) represent cross-section and top down SEM images of the polysulfone membrane respectively and (c) and (d) represent top-down SEM images of the fiberglass membrane

4.6.2 Sensor Incubation Time

Eight replicates of one whole blood sample was measured at three different instances: 2, 5 and 7 minutes. To imitate current point of care devices, incubation times greater than 7 minutes were ignored. Two parameters were investigated: reproducibility by comparing coefficients of variations and sensitivity by comparing signal strengths at these three instances. The signal obtained at 5 minutes yielded the most reproducible

output with C.V (%) of 10.6% and a maximum absorbance output of 0.153 as shown in **Figure 47**. Therefore, all measurements conducted in further tests were obtained after 5 minutes of incubation.

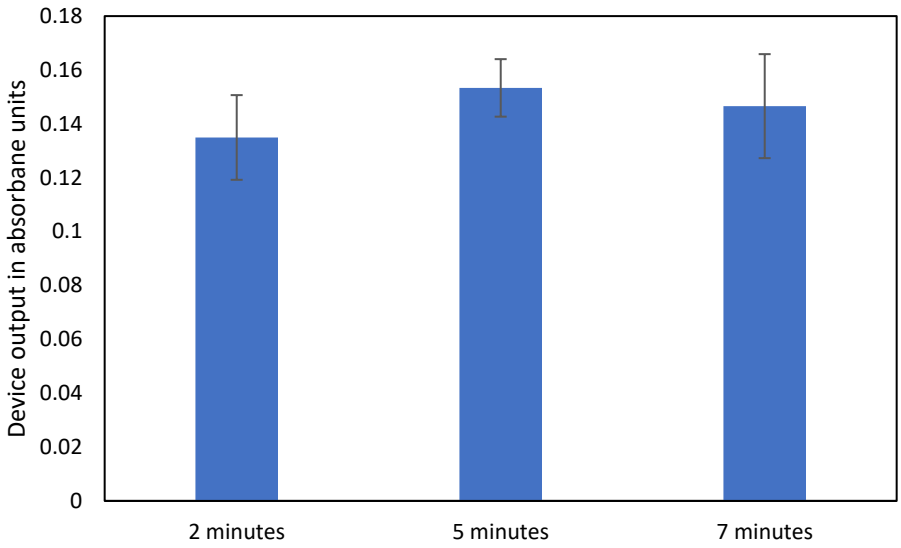

Figure 47: Absorbance output of eight replicates at two, five and seven minutes.

4.6.3 Analysis with Whole Blood Samples

A calibration curve between the system output reading with whole blood samples and optimized reference method (**Figure 48)** with a regression coefficient of 0.95 and sensitivity of 0.0004 absorbance unit/ ug/dl. With this calibration curve, several independent samples were utilized to interrogate the new system's iron concentration, and a correlation plot between the output readings from the new system and the optimized reference method was determined with slope of 1.09 and regression coefficient of 0.95, indicating that the novel system is in good agreement with the optimized reference method (**Figure 49).**

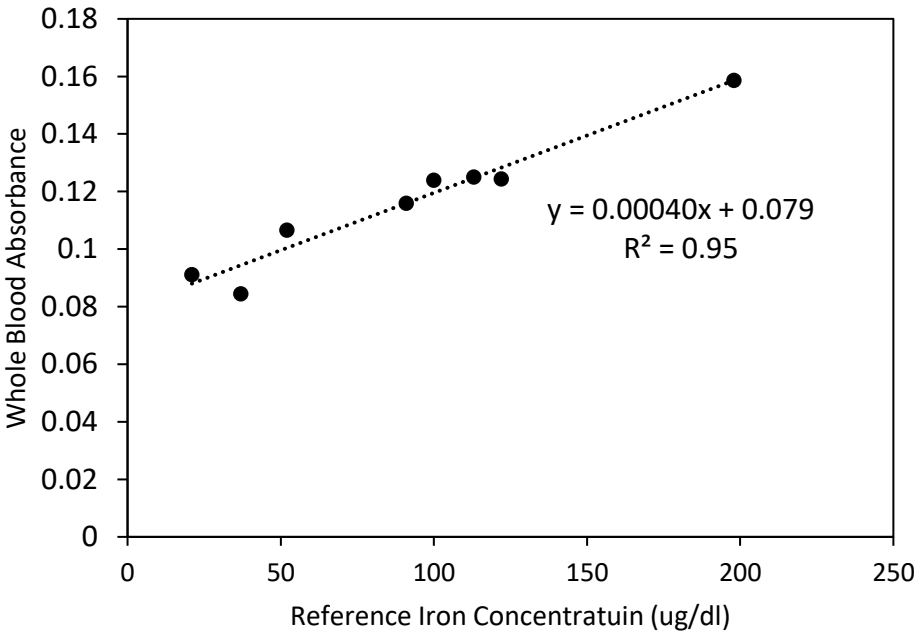

Figure 48:Calibration Curve between sensor absorbance output from whole blood samples and the optimized reference method with calibration slope of 0.0004 and regression coefficient of 0.95

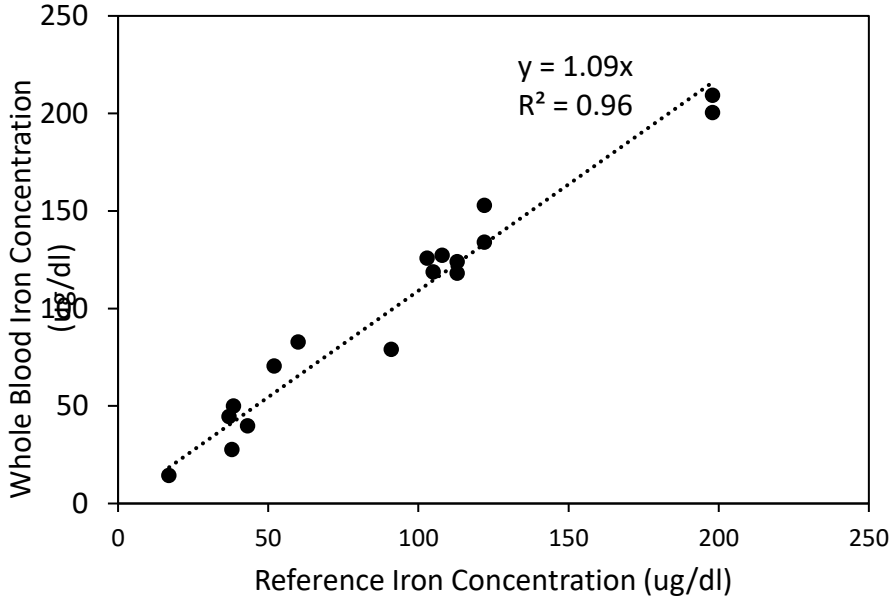

Figure 49: correlation plot between system absorbance output from whole blood samples and the optimized reference method with correlation slope of 1.09 and regression coefficient of 0.96

An alternative analysis method was used for screening application. Based on measurements obtained with the optimized reference method (reference spectrophotometer), the data was separated into three different categories: risk of iron deficiency (< 60 ug/dl), healthy iron levels (60 ug/dl -150 ug/dl) and iron overload (> 150 ug/dl). Then, a power law test was conducted with the corresponding data from the novel sensor system to validate whether the new system can statistically distinguish between the different means. For example, a power of 1.0 for 24 samples indicated that the system can discriminate between the healthy and iron deficient ranges (FIG. 50).

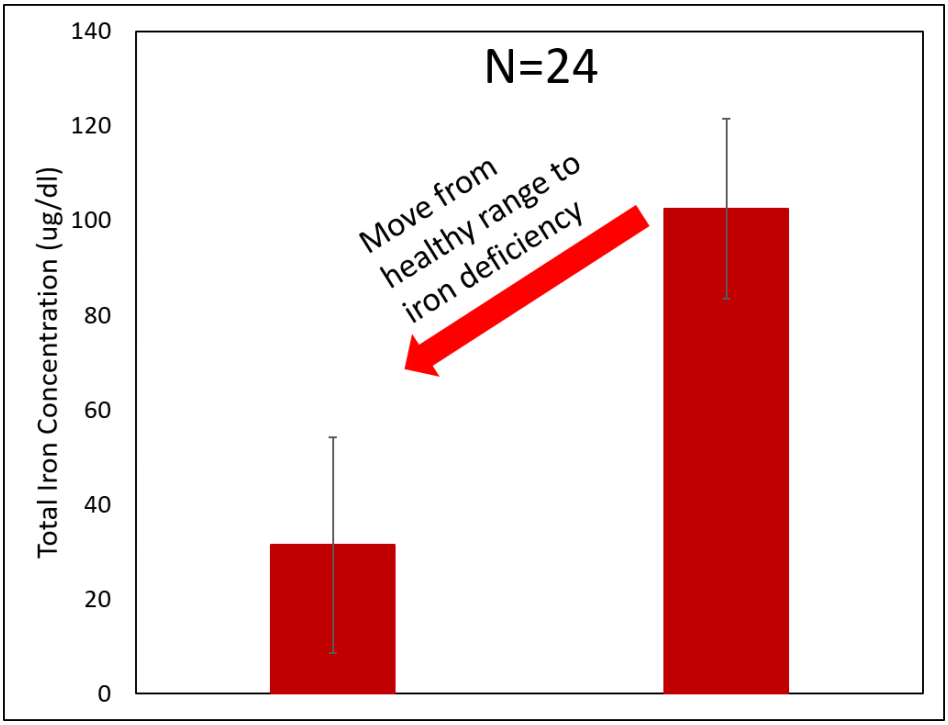

Figure 50: illustrates a power law test for screening purposes. A power of 1.0 indicates that the system can distinguish between healthy and iron deficiency clinical ranges

CHAPTER 5

SUMMARY AND PROPOSED WORK

5.1 Summary

In summary, the development of a new device is presented which includes a dry sensor, a smartphone mount, and an app. This device has similar detection accuracy as the in-house modified reference spectrophotometric method, and a third-party laboratory (LabCorp). Given the strong need for inexpensive, less invasive, and rapid screening and monitoring of iron levels in humans at risk for iron deficiency or overload, the new assay is a significant contribution to the solution[69].

Inspired by successful glucose control for management of diseases (Type I and Type II diabetes) and by former experiences of implementing technologies at the point of care[83, 84]. several steps toward creating a new point-of-care device to measure clinically relevant iron biomarkers for prevention or intervention in human iron deficiency or toxicity are completed. First, reference methods that can be used to validate iron, TIBC and percent iron saturation were created; second, the iron chemistry was tested for serum processing in an inexpensive dry sensor strip; third, an in-house smartphone mount and an App has enabled rapid reading of the sensor strip chemistry for testing accuracy and reproducibility; and last, the methodical approach to optimizing chemistry and color change processing has led to knowledge of the detection reaction kinetics. The experimental data confirmed the new assay offered a linear relationship between serum iron and absorbance in physiologically normal ranges.

The novel assay with the dry sensor strip and smartphone mount, and App was sensitive to iron detection with a dynamic range of 25 – 300 μg/dL, sensitivity of 0.00049 a.u/μg/dL, coefficient of variation (CV) of 10.5%, and estimated detection limit of ~15 μg/dL. These analytical specifications are useful for predicting iron deficiency and overloads. The optimized reference method had a sensitivity of 0.00093 a.u/μg/dL and CV of 2.2%. The correlation of serum iron concentrations in the intra-laboratory testing between the optimized reference method and the novel assay rendered a slope of 0.95, and a regression coefficient of 0.98, suggesting that the new assay is accurate. Last, spectrophotometric validation of the iron detection reaction kinetics for the test conditions was performed to reveal almost a first order reaction for iron ion, and almost a second order reaction order for ferene.

In summary, the new assay provided satisfactory accuracy results in intra- and inter-laboratory validations and provided promising features of mobility and low-cost manufacturing for global healthcare settings. Future work is oriented to full integration of the on-sensor strip with whole blood processing capabilities[85-88].

5.2 Future Work

5.2.1 Improve App Algorithm and User-Interface

Currently, the app outputs raw absorbance values. After a measurement is conducted, the user must access the history page and select the data that needs to be exported which is sent as an excel spreadsheet and sent via email to the designated destination. With previous calibration data, the user can then convert these absorbance values to an iron measurement. Therefore, the next step is to modify the current app algorithm so that the final exported data demonstrates final iron concentrations. Another important modification that is required at a later stage is a wireless communication between the app and a cloud- based network or data-base where each measurement is stored under the user's account where he/she is able to identify trends in his/her iron biomarkers. With the vision of deploying these sensors globally, the app must take in additional inputs such as: country, gender, age and ethnicity which enables a more detailed statistical analysis and perhaps a predictive model that predicts whether the user is at risk of developing anemia or hemochromatosis based on input parameters and biomarker readings.

ID	Age	Gender	Country	Ethnic Group	Total Iron	TIBC	% TF.S
A01	28	Male	U.S	Caucasian	100	350	29
A02	NA	Female	U.S	African American	35	480	7
A03	55	Female	Ireland	NA	120	370	32
An	34	NA	U.K	NA	210	285	74

Figure 51: Modification of current App-user interface to include input parameters such as gender, age, country, and ethnic group. The app output is stored in a secured database where a user can access his/her dynamic measurements and observe trends in their iron levels.

5.2.2 Pilot Study in Vulnerable Populations

The main findings obtained from this work is that the developed device's output statistically agrees with reference methods for total iron, TIBC, and percent saturation. In addition, the device is capable of discriminating between cut-off values for each of these biomarkers. However, this does not indicate that the device is capable of screening IDA or hemochromatosis but rather demonstrates the device's ability to accurately measure parameters that are needed to conduct a successful screening.

Therefore, the next pivotal step is to conduct a pilot study (200 sensors) in a remote area where iron deficiency anemia is widely prevalent such a (Africa, Asia South America) where 50% of the selected population are already screened with the disease (CBC or bone

marrow test) while the remaining test subjects are healthy, and a second pilot study to be conducted in Northern Europe (Ireland or U.K) where the same experimental design is adopted, but instead, the experimental objective is to screen for iron overload.

5.2.3 Approach to design Ferritin Sensor

Even though ferritin was introduced extensively in chapter 2 as an essential clinical biomarker to screen for iron deficiency anemia or iron overload, the 1st generation sensor device that was developed and explored throughout chapters 3 and 4 did not include ferritin detection. The sensor for ferritin detection will be developed and integrated into a 3rd generation sensor device prototype. The detection of ferritin will consist on a novel method that combines the selectivity of antibodies, with the electrochemical and magnetic properties of Ferritin for high sensitivity detection[89, 90]. The electrochemistry of ferritin has been previously well characterized[90] displaying a large irreversible cathodic wave ascribed to the ferritin electrochemical reduction. Ferritin reduction is then accompanied by Fe(II) release which can undergo subsequent oxidation/reduction to Fe(III)/Fe(0) respectively. Fig. 52A shows a schematic representation of the use of the above ferritin redox activity for the electrochemical detection of ferritin contents. The setup consists on a microfluidic channel in contact with an array of metal electrodes (left panel), each electrode holding independent potentiostatic control. The top channel slid (right panel) will bring the integrated counter electrodes in contact to the serum electrolyte to close the electrochemical cell circuit. The electrochemical detection will be done through a sequential anodic stripping procedure: electrodes 1 and 2 will be conjugated to two different monoclonal antibodies to selectively capture ferritin via different protein outer fragments[91]. The electrochemical potential of electrodes 1 and 2 will be set at the specific

cathodic reduction potential to reduce the absorbed ferritin on the electrodes' surface, and the corresponding charge will be integrated. Electrode 3 will serve as a second detection stage of the released Fe(II) resulting from ferritin reduction. Electrode 3 surface will be functionalized with mercaptoalkanoic acids known to effectively chelate Fe(II) and provide well-defined redox potentials to oxidize/reduce Fe ionic species[92]. The integrated currents from all three electrodes will be calibrated against well-defined standards.

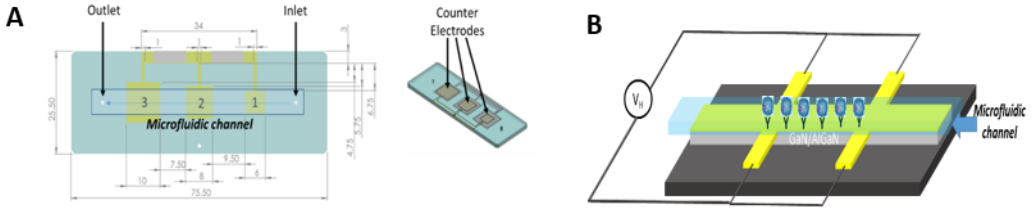

Figure 52: Sensor #3 – Ferritin. A) Multipotentiostatic electrodes array for sequential anodic stripping in ferritin detection. B) Spin-dependent part of the electrochemical setups with electrodes 1 and 2 shown in part A).

A more advanced stage in ferritin detection will consider ferritin magnetic properties[93] in the detection scheme shown in Fig. 52B, which considers the microfluidic channel on an electrochemical Hall Voltage (VH) device[92] to be implemented at electrodes 1 and 2 shown in Fig. 52A. Simultaneous to the anodic stripping of ferritin at these electrodes, the magnitude of the VH will be also used to monitor ferritin absorption due to the ferritin's characteristic magnetic moment[92]. The array of electrodes represented in Fig. 52 will be preserved, including last free Fe(II) electrochemical detection stage occurring at electrode 3[93]. Such multiplex detection system will bring ways to more reliably quantify ferritin levels in a target sample. Microfluidics, electrode pads, Hall devices and potentiostatic controls can be all designed in a miniaturized chip to allow portability of the final device (enabling point-of-care application). The above magneto-

electrochemical detection scheme will be integrated into the sensor #3 for ferritin of the sensor device. This requires working on sensor microfabrication, electrochemical characterization of antibody-functionalized metal electrodes, calibration of the main parameters for optimal sequential anodic stripping in the multi-potentiostatic electrodes array against well-defined test samples and plasma samples, and integration of the electrochemical circuit, and calibration of the Hall effect voltage signal into a 2nd generation sensor device prototype..

5.2.3 Beyond Iron Metabolism

In this work, a point of care device was developed to detect different iron biomarkers to screen for iron disorders. The device comprised of a 3D-printed chamber+ phone mount as well as a sensor strip specific for iron detection. Since all sensor components are independent from the membrane that is embedded with iron-specific working solutions, the sensing platform can be used to host other biomarkers to screen for other diseases as long as detection mechanism is based on color gradient. The ability to screen for several diseases increases the device's value for point of care testing. With this said, a QR scan can be added to the app to scan a bar-code that is specific to the desired biomarker. Once the bar-code is scanned, the appropriate calibration curves are loaded onto the app and the patient can proceed with the measurement. On the other hand, with the optoelectronic reader (glucometer-like), each biomarker has a specific chip that must be inserted onto the device prior to detection. The chip loads the appropriate calibration curves prior to taking a measurement.

Figure 53: QR scanning of specific biomarker with smartphone device. Corresponding calibration curves and threshold values are loaded.

Figure 54: A chip associated with a specific biomarker is inserted into the glucometer like device and the corresponding calibration data and threshold values are laoded.

REFERENCES

[1] R. Gozzeline, and P. Arosio, The Importance Of Iron In Pathophysiologic Conditions, 2015.

[2] L. A. Kaplan, and A. J. Pesce, "Iron, Porphyrin, and Bilirubin Metabolism," Clinical Chemistry Theory Analysis and Correlation, St. Louis: Mosby, 1996.

[3] Z. I. Cabantchik, "Labile iron in cells and body fluids: physiology, pathology, and pharmacology," Front.Pharmacol, vol. 5, no. 45, 2014.

[4] S. W. Abramowski, G. Waeber, C. Gassner, A. Buser, B. M. Frey, B. Favrat, and J.-D. Tissot, "Physiology of Iron Metabolism," Transfus Med Hemother, vol. 41, pp. 213-221, 2014, 2014.

[5] M. Worwood, "The laboratory assessment of iron status--an update," Clin Chim Acta, vol. 259, pp. 3-23, 1997.

[6] D. Chiabrando, F. Vinchi, V. Fiorito, S. Mercurio, and E. Tolosano, "Heme in pathophysiology: a matter of scavenging, metabolism and trafficking across cell membranes," Front. Pharmacol, vol. 5, no. 61, 2014.

[7] E. Beutler, and A. V. Hoffbran, "Iron Deficiency and Overload," ASH Education, vol. 1, pp. 40-61, 2003.

[8] R. Black, C. Victora, S. Walker, Z. Bhutta, P. Christian, M. de Onis, M. Ezzati, S. Grantham-McGregor, J. Katz, R. Martorell, and R. Uauy, "Maternal and child undernutrition and overweight in low-income and middle-income countries," Lancet, vol. 3, pp. 427-451, 2013.

[9] P. C. Adams, and J. C. Barton, "How I treat hemochromatosis," Blood, vol. 116, no. 3, 2010.

[10] B. M. N. de Graff, A. Neil, K. Sanderson, Y. Kristy, K. C. Yee, and A. Palmer, "Costs associated with hereditary haemochromatosis in Australia: a cost-of-illness study," Australian Health Review, vol. 41, pp. 254-267, 2017.

[11] A. Merryweather-Clarke, J. Pointon, Shearman JD, and K. Robson, "Global prevalence of putative haemochromatosis mutations," J Med Genet, vol. 34, no. 4, 1997.

[12] P. C. Adams, "Hemochromatosis and Iron-Overload Screening in a Racially Diverse Population," The new england journal of medicine, vol. 352, 2005.

[13] World Health Organization, "Nutritional anaemias: tools for effective prevention and control," 2017.

[14] P. C. Adams, J. C. Barton, and G. D. McLaren, “Screening for iron overload: Lessons from the Hemochromatosis and iron Overload Screening (HeirS) Study,” Study Can J Gastroenterol, vol. 23, no. 11, pp. 769-772, 2009.

[15] R. J. Stoltzfus, “Iron deficiency: Global prevalence and consequences,” Food and Nutrition Bulletin, vol. 24, pp. 99-103, 2003, 2003.

[16] T. Hirayama, and H. Nagasawa, “Chemical tools for detecting Fe ions,” Journal of Clinical Biochemistry and Nutrition, vol. 60, pp. 39-48, 2017.

[17] M. Nejad, A. M. Wabler, H. Zhou, J. Mihalic, C. Gruethner, T. DeWeese, and R. Ivkov, “An optimised spectrophotometric assay for convenient and accurate quantitation of intracellular iron from iron oxide nanoparticles,” International Journal of Hyperthermia, vol. 34, no. 4, pp. 373-381, 2018.

[18] S. Knowlton, A. Joshi, P. Syrrist, Coskun, Ahmet F. , and S. Tasoglu, “3D-printed smartphone-based point of care tool for fluorescence- and magnetophoresis-based cytometry,” Lab on a Chip, vol. 17, 2017.

[19] B. Coleman, C. Coarsey, and W. Asghar, “Cell phone based colorimetric analysis for point-of-care settings,” Analyst, vol. 144, pp. 1935-1947, 2019.

[20] S. Lee, V. Oncescu, M. Mancuso, S. Mehtac, and D. Erickson, “A smartphone platform for the quantificationof vitamin D levels,” Lab on a Chip, vol. 14, 2014.

[21] D. Lee, W. Pin Chou, S. Hwei Yeh, P. J. Chen, and P. Hei Chen, “DNA detection using commercial mobile phones,” Biosensors and Bioelectronics, vol. 26, pp. 4349-4354, 2011.

[22] S. Wang, X. Zhao, I. Khimji, R. Akbas, W. Qiu, D. Edwards, D. W. Cramer, B. Yed, and U. Demirci, “Integration of Cell Phone Imaging with Microchip ELISA to Detect Ovarian Cancer HE4 Biomarker in Urine at the Point-of- Care,” Lab on a Chip, vol. 11, no. 20, pp. 3411-3418, 2011.

[23] J. Birui, “Lateral flow aptamer assay integrated smartphone-based portable device for simultaneous detection of multiple targets using upconversion nanoparticles,” Sensors and Actuators B: Chemical, vol. 276, pp. 48-56, 2018.

[24] N. Abbaspour, R. Hurrel, and R. Kelishadi, “Review on iron and its importance for human health,” J Res Med Sci, vol. 19, no. 2, pp. 164-174, 2014.

[25] D. Wallace, and N. Subramaniam, “The global prevalence of HFE and non-HFE hemochromatosis estimated from analysis of next-generation sequencing data,” Genetics in medicine, vol. 18, pp. 618-626, 2016.

[26] C. W. Siah, J. Ombiga, L. A. Adams, D. Trinder, and J. K. Olynyk, “Normal Iron Metabolism and the Pathophysiology of Iron Overload Disorders,” Clin Biochem Rev, vol. 27, no. 1, pp. 5, 2006.

[27] P. C. Adams, “Screening for iron overload: Lessons from the Hemochromatosis and iron Overload Screening (HeirS) Study,” Can J Gastroenterol, vol. 23, 2009.

[28] D. S. Gross, L. C. Gurrin, Bertalli A Nadine, and A. J. Katrina, “Clinical penetrance in hereditary hemochromatosis: estimates of the cumulative incidence of severe liver disease among HFE C282Y homozygotes,” Genetics in Medicine, vol. 20, pp. 383-389, 2018.

[29] M. J. Wood, R. Skoien, and L. W. Powell, “The global burden of iron overload,” Hepatol Int, vol. 3, no. 3, pp. 434-444, 2009.

[30] A. Dignass, K. Farrag, and J. Stein, “Limitations of Serum Ferritin in Diagnosing Iron Deficiency in Inflammatory Conditions,” International Journal of Chronic Diseases, 2018.

[31] J. Waalen, V. Felliti, T. Gelbart, N. J. Ho, and E. Beutler, “Penetrance of Hemochromatosis,” Blood Cells, Molecules and Diseases, vol. 29, no. 3, pp. 418-432, 2002.

[32] T. Honda, V. Pun, J. Manjourides, and H. Suh, “Anemia prevalence and hemoglobin levels are associated with long-term exposure to air pollution in an older population,” Environment International, 2017.

[33] C. Lutter K, “Iron Deficiency in Young Children in Low-Income Countries and New Approaches for Its Prevention,” Journal of nutrition, no. 12, pp. 2523-2528, 2008.

[34] W. H. Organization, "Worldwide prevalence of anaemia 1993–2005," 2008.

[35] J. Gabrilove, “Overview: erythropoiesis, anemia, and the impact of erythropoietin,” Semin Hematol, vol. 37, pp. 1, 2000.

[36] R. Galloway, E. Dusch, L. Elder, E. Achadi, R. Grajeda, E. Hurtado, M. Favin, S. Kanani, J. Marsaban, N. Meda, K. Moore, L. Morison, N. Raina, J. Rajartnam, J. Rodrquez, and C. Stephen, “Women's perceptions of iron deficiency and anemia prevention and control in eight developing countries,” Soc Sci Med, vol. 55, no. 4, 2002.

[37] J. L. Miller, “Iron Deficiency Anemia: A Common and Curable Disease,” Cold Spring Harbor Perspectives in Medicine, 2013.

[38] M. Capellini, K. Musallam, and A. Taher, “Iron deficiency anaemia revisited,” J intern Med, vol. 287, no. 2, pp. 153-170, 2020.

[39] A. Ogun, and A. Adeyinka, “Biochemistry, Transferrin,” 2020.

[40] H. Saito, “METABOLISM OF IRON STORES,” Nagoya J Med Sci, vol. 76, pp. 235-254, 2014.

[41] E. Nemeth, and T. Ganz, “The Role of Hepcidin in Iron Metabolism,” Acta Haematol, vol. 122, pp. 78-86, 2009.

[42] M. Kotze, D. van Velden, S. Van Rensburg, and R. Erasmus, “Pathogenic Mechanisms Underlying Iron Deficiency and Iron Overload: New Insights for Clinical Application,” EJIFCC, vol. 20, no. 2, pp. 108-123, 2009.

[43] A. J. Madua, and U. Donatus, Maduka “Anaemia of Chronic Disease: An In-Depth Review,” Med Princ Pract, vol. 26, pp. 1-9, 2017.

[44] R. Sarma, "Red Cell Indices," Clinical Methods: The History, Physical, and Laboratory Examinations. 3rd edition, H. Walker, W. Hall and J. Hurst, eds., 1990.

[45] C. A. Northrop-Clewes, and D. I. Thurnham, “Biomarkers for the differentiation of anemia and their clinical usefulness,” J. Blood Med, vol. 4, pp. 11-22, 2013.

[46] G. R. R. DOUGLAS J. HENNES, “Ferene - a new spectrophotometric reagent for iron,” Can. J. Chem, vol. 62, 1984.

[47] L. L. Stookey, “Ferrozine-A New Spectrophotometric Reagent for Iron,” Analytical Chemistry, vol. 42, no. 779-781, 1970.

[48] H. M. Eskelinen S, Räisänen S, “Ferene-S as the chromogen for serum iron determinations,” Scand J Clin Lab Invsest, vol. 43, no. 5, 1983.

[49] J. D. Artiss, S. Vinogradov, and B. Zak, “Spectrophotometric study of several sensitive reagents for serum iron,” Clinical Biochemistry, vol. 14, no. 6, 1981.

[50] P. Ponka, M. Tenenbien, and J. W. Eaton, Handbook on the Toxicology of Metals, p.^pp. 577-598, 2007.

[51] A. E. B. Mishtu Dey, "Isolation and Assays of Bacterial Dimethylsulfoniopropionate Lyases," Methods in Enzymology, 2018.

[52] W. Laboratories, “Fer-color,” 2000.

[53] C. Van Der Heu, H. G. Van Eijk, W. F. Wiltink, and W. Leijnse, “THE BINDING OF IRON TO TRANSFERRIN AND TO OTHER SERUM COMPONENTS AT DIFFERENT DEGREES OF SATURATION WITH IRON,” Clinica Chimica Acta, vol. 38, pp. 347-353, 1971.

[54] W. Ramsay, “The determination of the total iron-binding capacity of serum.1957.,” Clin Chim Acta, vol. 259, pp. 25-30, 1997.

[55] E. E. Gabbe , H. C. Heinrich, and F. Eagii, “Proposal for the standardization of the serum unsaturated iron binding capacity assay, and resultsin groups of subjects with normal iron stores and with prelatent, latent, and manifest iron deficiency,” Clinica Chimica Acta, vol. 119, pp. 51-63, 1982.

[56] H. Yamanishi, S. Iyama , Y. Yamaguchi, Y. Kanakura, and Y. Iwatani, “Total Iron-binding Capacity Calculated from Serum Transferrin Concentration or Serum Iron Concentration and Unsaturated Iron-binding Capacity,” Clinical Chemistry, vol. 49, no. 1, pp. 175-178, 2003.

[57] BioSystems, “UNSATURATED IRON BINDING CAPACITY (UIBC),” 2019.

[58] M. N. Al Hallak , W. Newman, and A. Al-Kali, “Transferrin Saturation (TS) Is a Surrogate Marker for Iron Deficiency Anemia (IDA),” Blood, vol. 118, no. 21, 2011.

[59] N. Asif, A. Ijaz, T. Rafi, Z. H. Haroon, S. Bashir, and M. Ayyub, “Diagnostic Accuracy of Serum Iron and Total Iron Binding Capacity (TIBC) in Iron Deficiency State,” 2015.

[60] A. El-Osta, M. Woringer, E. Pizzo, T. Verhoef, C. Dickie, M. Ni, J. Huddy R, M. Soljak, G. Hanna B, and A. Majeed, “Does use of point-of-care testing improve cost-effectiveness of the NHS Health Check programme in the primary care setting? A cost-minimisation analysis,” BMJ, vol. 8, 2017.

[61] S. K. Vashist, “Point-of-Care Diagnostics: Recent Advances and Trends,” biosensors, vol. 7, pp. 62, 2017.

[62] E. Macias, A. Suarez, and J. Lloret, “Mobile Sensing Systems,” Sensors, vol. 13, 2013.

[63] A. Shen Li, J. Hagen, and I. Papautsky, “Point-of-care colorimetric detection with a smartphone,” Lab on a Chip, vol. 12, pp. 4240-4243, 2012.

[64] V. Oncescu , D. O’Dell, and D. Erickson, “Smartphone based health accessory for colorimetric detection of biomarkers in sweat and saliva,” Lab on a Chip, vol. 13, 2013.

[65] R. C. Murdock, L. Shen, D. K. Griffin, N. Kelley-Loughnane, I. Papautsky, and J. A. Hagen, “Optimization of a Paper-Based ELISA for a Human Performance Biomarker,” Analytical Chemistry, vol. 85, pp. 11634-11642, 2013.

[66] C. F. Fronczek, T. San Park, D. K. Harshman, A. M. Nicolini, and J.-Y. Yoon, “Paper microfluidic extraction and direct smartphone-based identification of pathogenic nucleic acids from field and clinical samples,” Royal Society of Chemistry, vol. 4, 2014.

[67] X. Xu, X. Wang, J. Hu, Y. Gong, L. Wang, W. Zhou, X. Li, and F. Xu, “A smartphone-based on-site nucleic acid testing platform at point-of-care settings,” Electrophoresis, vol. 40, pp. 914-927, 2019.

[68] V. Oncescu, M. Mancuso, and D. Erickson, “Cholesterol testing on a smartphone,” Lab on a Chip, vol. 14, 2014.

[69] M. Serhan, D. Jackemeyer, M. Long, M. Sprowls, I. Perez Diez, M. Wolfgang, F. Chen, N. Tao, and E. Forzani, “Total iron measurement in human serum with a novel smartphone-based assay,” IEEE Journal of Translational Engineering in Health and Medicine, 2020.

[70] P. Kotecha, “Nutritional Anemia in Young Children with Focus on Asia and India,” Indian J Community Med, vol. 36, no. 1, pp. 8-16, 2011.

[71] S. ALI, “Healthcare in the Remote Developing World: Why healthcare is inaccessible and strategies towards improving current healthcare models,” 2016.

[72] M. JJ, “Iron deficiency in developed countries: prevalence, influence of lifestyle factors and hazards of prevention,” Eur J. Clin Nutr., vol. 51, 1997.

[73] R. Smith E, “The Clinical and Economic Burden of Anemia,” Am J Manag Care, vol. 16, 2010.

[74] J. L. Babitt, and Y. L. Herbert, “Mechanisms of Anemia in CKD,” JASN, vol. 23, no. 10, pp. 1631-1634, 2012.

[75] M. de Almeida, C. Saatkamp, A. Fernandes, and L. J. Silveira, “Estimating the concentration of urea and creatinine in the human serum of normal and dialysis patients through Raman spectroscopy,” Lasers in medical science, vol. 31, 2016.

[76] G. Dimeski, “Interference Testing,” The Clinical Biochemist Reviews, vol. 29, pp. 43-48, 2008.

[77] J. Wilkerson, S. Horvath, B. Gutin, S. Molnar, and F. Diaz, “Plasma electrolyte content and concentration during treadmill exercise in humans,” Journal of applied physiology: respiratory, environmental and excercise physiology, vol. 53, 1982.

[78] G. M, R. SA, and H. K, “What is a normal blood glucose?,” Archives of disease in childhood, vol. 6, pp. 569-574, 2016.

[79] GSMarena. "Applie iPhone 6s," https://www.gsmarena.com/apple_iphone_6s-7242.php.

[80] ASTM, “Standard Guide for Accelerated Aging of Sterile Barrier Systems for Medical Devices,” 2006.

[81] N. Saadati, M. P. Abdullah, Z. Zakaria, S. Sany, M. Rezayi, and H. Hassonizadeh, “Limit of detection and limit of quantification development procedures for organochlorine pesticides analysis in water and sediment matrices,” Chemistry Central Journal, vol. 7, pp. 63, 2013.

[82] A. Shrivastava, and V. B. Gupta, “Methods for the determination of limit of detection and limit of quantitation of the analytical methods,” Chronicles of Young Scientists, vol. 2, no. 1, 2015.

[83] D. Zhao, X. Xian, M. Terrera, R. Krishnan, D. Miller, D. Bridgeman, K. Tao, L. Zhang, F. Tsow, E. S. Forzani, and N. Tao, “A pocket-sized metabolic analyzer for assessment of resting energy expenditure,” Clinical Nutrition, vol. 33, pp. 341-347, 2014.

[84] I. Kucherenko S, D. Sanborn, B. Chen, N. Garland, M. Serhan, E. Forzani, C. Gomes, and C. J. Claussen, “Ion-Selective Sensors Based on Laser-Induced Graphene for Evaluating Human Hydration Levels Using Urine Samples,” Advanced Material Technologies, vol. 5, no. 6, 2020.

[85] P. S, S. Bains, G. A. Gupta N, and J. Bolodeoku, “Evaluating a Membrane Based Rapid Plasma Separation Device (RPSD) forImmunoassay Point-of-Care Testing (POCT) for Estimations of Cortisol, DDimer,Myoglobin and Thyroxine,” iMedPub Journals, 2017.

[86] S. Vemulapati, and D. Erickson, “H.E.R.M.E.S: rapid blood-plasma separation at the point-of-need,” Lab on a Chip, vol. 18, 2018.

[87] P. Ďurč, and F. Foret. Petr Kubáň, “Fast blood plasma separation device for point-of-care applications,” Talanta, vol. 183, 2018.

[88] S. Mukherjee, S. Kim, and Y. Chen, “Plasma Separation from Blood: The 'Lab-on-a-Chip' Approach,” Critical Reviews in Biomedical Engineering, 2009.

[89] T. EC, “Ferritin: structure, gene regulation, and cellular function in animals, plants, and microorganisms,” Annu Rev Biochem, vol. 56, pp. 289-315, 1987.

[90] N. L. Ritzert, S. S. Casella, and D. C. Zapien, “Surface-electrochemistry of ferritin adsorbed on 8-mercaptooctanoic acid-modified gold electrodes,” Electrochemistry Communications, vol. 11, pp. 827-830, 2009.

[91] W. W. Ting-Ting Song, Li-Li Meng, Yan Liu, Xiao-Bo Jia, Xun Mao, “Electrochemical detection of human ferritin based on gold nanorod reporter probe and cotton thread immunoassay device,” Chinese Chemical Letters, vol. 28, pp. 226-230, 2017.

[92] G. Bullard, F. Tassinari, C.-H. Ko, A. K. Mondal, R. Wang, S. Mishra, R. Naaman, and M. J. Therien, “Low-Resistance Molecular Wires Propagate Spin-Polarized Currents ” J. Am. Chem. Soc., vol. 141, pp. 14707-14711, 2019.

[93] C. W. Hsieh, Z. Bing, and S. Hsieh, “Ferritin protein imaging and detection by magnetic force microscopy,” Chem Commun (Camb.), vol. 46, no. 10, 2010.